Sound-Proof Models for Magnetic Buoyancy

John B. Moss

Thesis submitted for the degree of
Doctor of Philosophy

School of Mathematics, Statistics & Physics
Newcastle University
Newcastle upon Tyne
United Kingdom

September 2023

Acknowledgements

Firstly, I would like to thank my supervisors Toby Wood and Paul Bushby for their constant support and guidance throughout my PhD. I am particularly grateful for their patience, attention to detail and drive for excellence. Thank you for always making our work a priority and allowing my PhD experience to be as stress-free as possible.

Furthermore, I would like to thank the entire mathematics community at Newcastle University for making my time here so enjoyable. Throughout my time at Newcastle I have been fortunate enough to have encountered so many inspirational teachers and researchers from whom I learnt a great deal. Specifically, I would like to thank Anvar Shukurov, Carlo Barenghi, Nick Proukakis, Toby Wood, Paul Bushby, and Stefan Kolb. I am also grateful to my fellow PhD students and postdocs, with whom I have shared offices, lunches and seminars, for fostering such a welcoming and friendly environment as well as their thoughtful insight. I would particularly like to thank Craig Duguid and Fryderyk Wilczyński for their invaluable advice and knowledge. I found our regular meetings instilled a greater confidence in me and, especially during COVID lockdowns, were an important outlet. Thanks also go to my new employer – the Care Quality Commission – for allowing me the flexibility and time off to finish writing this thesis, as well as my friends and colleagues there for their kindness and providing some much needed relief.

I would like to thank my partner Hazel for her unwavering support, and also for allowing me to commandeer her dressing table to use as a desk for the past three years - maybe you'll get it back now. Finally, I would like to thank my mum. Thank you for your care, support and for always prioritising our education.

Abstract

Magnetic buoyancy is a phenomenon by which regions of strong magnetic field in a plasma can rise. In the Sun, magnetic buoyancy transports field from the deep interior to the surface, where it produces sunspots. This field is believed to originate in the solar tachocline, a thin layer of rotational shear beneath the convective envelope, wherein field lines are stretched azimuthally to produce a layer of strong horizontal field. A description of magnetic buoyancy and its role in the solar interior is provided in Chapters 1 - 2.

To model the magnetic buoyancy phenomenon, one typically solves the fully compressible fluid equations of magneto-hydrodynamics (MHD). This is because the presence of strong magnetic field affects both the density and the pressure of the fluid. However, the presence of fast acoustic waves in the fully compressible equations can present difficulties for analytical and numerical analyses. Therefore, several methods have been developed to filter out these waves, leading to various "sound-proof" models, including the Boussinesq, anelastic and pseudo-incompressible models. These sound-proof models are presented in Chapter 3, along with the assumptions under which they are derived. In Chapter 4 we assess the validity of each of these approximate models for describing magnetic buoyancy in the context of the solar interior. A general sound-proof model is introduced and compared to the fully compressible system in a number of asymptotic regimes, including both non-rotating and rotating cases. We obtain specific constraints that must be satisfied in order that the model captures the leading-order behaviour of the fully compressible system. We then discuss which of the existing sound-proof models satisfy these constraints, and in what parameter regimes. We find that the pseudo-incompressible model and a formulation of the anelastic model both reproduce the leading order behaviour of the fully compressible system in the most general parameter regimes we consider.

An alternative, and complementary, way to assess the validity of any model is to consider its mathematical properties, particularly conservation laws. An ideal magneto-hydrodynamic fluid is a Hamiltonian system, and conserves energy, momentum, and magnetic flux. However, sound-proof models are derived using approximations that may violate the Hamiltonian structure of the system. In Chapter 5, we compare the sound-proof models to the compressible system by considering the mathematical properties of the linearised equations. For a Hamiltonian system, the equations describing perturbations to any static state are guaranteed to be self-adjoint, a fact that is useful in obtaining stability criteria. We derive constraints under which our general linearised sound-proof system is self-adjoint. We show that there is a unique set of self-adjoint sound-proof equations, namely the pseudo-incompressible equations, that conserves the same energy as the fully compressible system.

The results presented in Chapters 4 and 5 neglect the effects of viscosity and magnetic diffusion. However, the presence of these diffusivities, as well as thermal diffusion, can lead to so-called double-diffusive instability, even in situations where the thermal and magnetic stratifications are individually stable. To date, this instability has only been extensively studied in the magneto-Boussinesq regime, which assumes very small vertical scales. In Chapter 6 we determine the behaviour of the double-diffusive instability outside of the Boussinesq regime by numerically solving the linearised fully compressible equations.

We conclude in Chapter 7 by summarising the key results as well as detailing some potential avenues for future work.

Contents

Chapter 1

The Sun

The Sun formed approximately 4.5 billion years ago and now exists in its main sequence phase, during which hydrogen is fused to helium in the core. The Sun has been an object of fascination and study for thousands of years. Records of solar observations date back to about 2000 BC when the Chinese recorded incidents of eclipses. Just under 2000 years later (approximately 300BC), the Chinese made the first recorded observations of sunspots — dark spots that appear on the surface of the Sun. The study of sunspots remains an active area of research to this day.

1.1 The solar structure

In order to discuss sunspots (and other phenomena) we first introduce the solar structure. The Sun is the largest body in the solar system, containing about 99.85% of the mass of the solar system, and is held together by its own gravity. It has a radius, $R_\odot$, of approximately 695.5Mm. We can divide the Sun into two parts; the solar interior and the solar atmosphere. The interface between these regions is the solar surface (or *photosphere*). Unlike with the surface of the Earth, it is not immediately obvious how the photosphere should be defined. In fact, we define the photosphere to be the outermost region that is fully opaque. This means that, by definition, the solar interior cannot be directly observed. However, the interior can still be studied by helioseismology — the study of the solar interior by observing oscillations at the surface. The solar atmosphere refers to layers of the Sun outside the photosphere. This project is primarily concerned with the solar interior.

The solar structure, with typical temperatures and densities in each region, is shown in Figure 1.1. At the centre of the Sun is the *core*, which extends to approximately $0.25R_\odot$. This is where nuclear fusion takes place and is the hottest part of the Sun. Outside the core is a *radiative zone*, so-called for the primary source of heat transfer — radiation — in

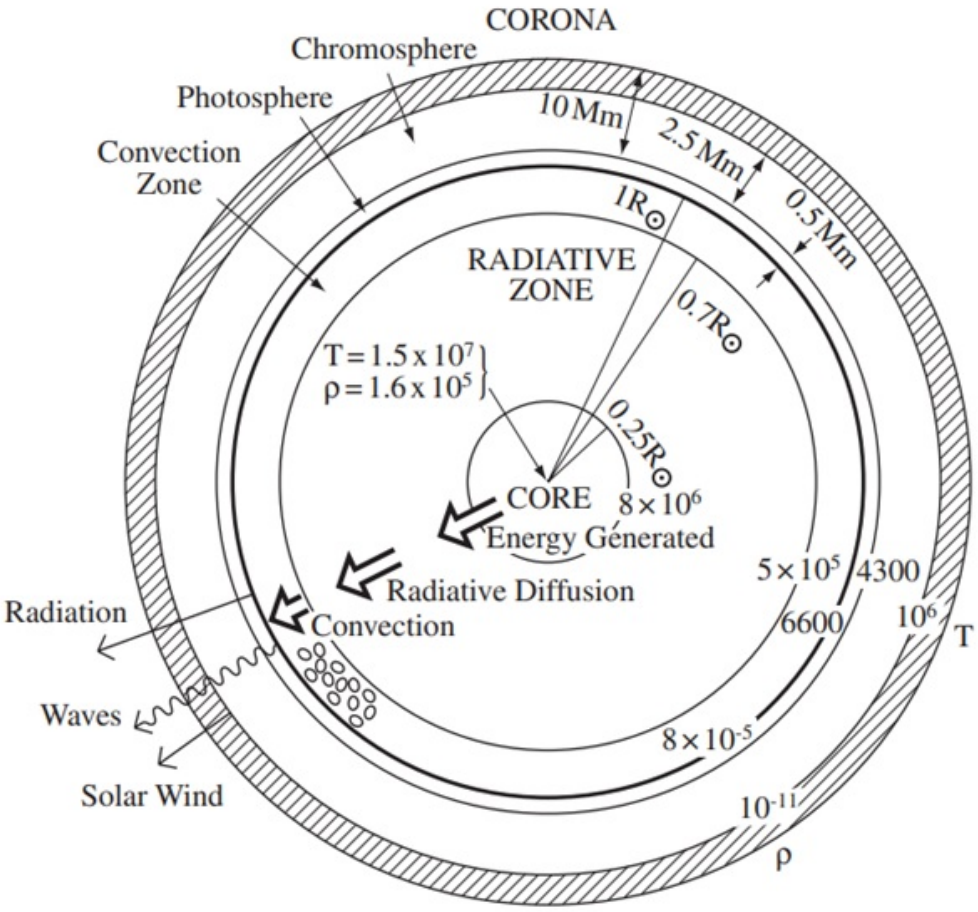

Figure 1.1: The structure of both the interior and exterior of the Sun. Temperatures (T) and densities (ρ) are given in K and kg m^{-3} respectively. Note that $R_\odot$ denotes the radius of the Sun. Figure from Priest (2014).

this region. The radiative zone extends out to approximately $0.7R_\odot$ and rotates almost uniformly as a solid body; see Figure 1.2. The *convective zone* extends from about $0.7R_\odot$ to the surface. In this region, intense fluid turbulence allows heat to be transferred from the base of the region to the *photosphere* by convection. This turbulence also redistributes angular momentum and therefore allows the convective zone to rotate differentially — with regions at the equator rotating faster than polar regions (Schou *et al.*, 1998) — see Figure 1.2. Spiegel & Zahn (1992) introduced the *tachocline*, from the Ancient Greek "tacho-" meaning speed or fast and "-cline" meaning slope or gradient, to define the transition region from uniform to differential rotation. This region is therefore located between the radiative and convective zones at approximately $0.7R_\odot$. This region is extremely thin (less than $0.04R_\odot$). Despite significant efforts (Hughes *et al.*, 2007), the tachocline is still not fully understood. However, some of its features are well-established by observations. For example, as a result of the transition from the solid-body rotation of the radiative zone to

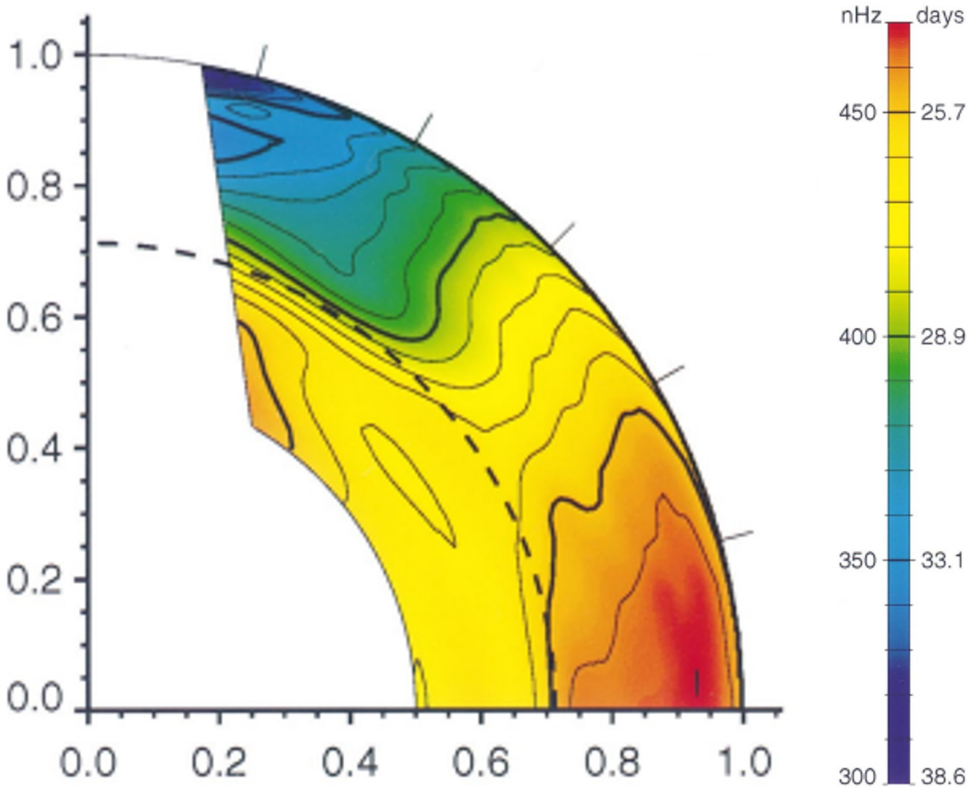

Figure 1.2: Colour map showing rotation rate in a slice of the solar interior. Both axes show distance from the centre of the Sun, measured in solar radii ($R_\odot$), such that the horizontal axis is the equator and the vertical axis is the pole. Red and blue colouring represents fast and slow rotation respectively. The dashed line at approximately $0.7R_\odot$ shows the location of the tachocline. Figure from Schou *et al.* (1998).

the differential rotation of the convective zone, the tachocline exhibits significant rotational shear. This rotational shear acts to generate and amplify magnetic field in this region and plays a crucial role in maintaining the large-scale solar magnetic field (see Section 1.3).

1.2 The solar cycle

1.2.1 Sunspots

Sunspots are darker regions of the Sun's surface of approximately 10–20 Mm in diameter. The first records of sunspots exist from approximately 300BC when they were seen by the naked eye through a thin cloud. The invention of the telescope in the 1600s led to more observations and in 1769 Alexander Wilson was able to deduce that a sunspot is a depression (of about 500 km) in the Sun's surface (Priest, 2014). Hale's paper in 1908 first determined that sunspots were magnetic in origin (Hale, 1908).

Sunspots are regions where strong magnetic field passes through the photosphere, hence

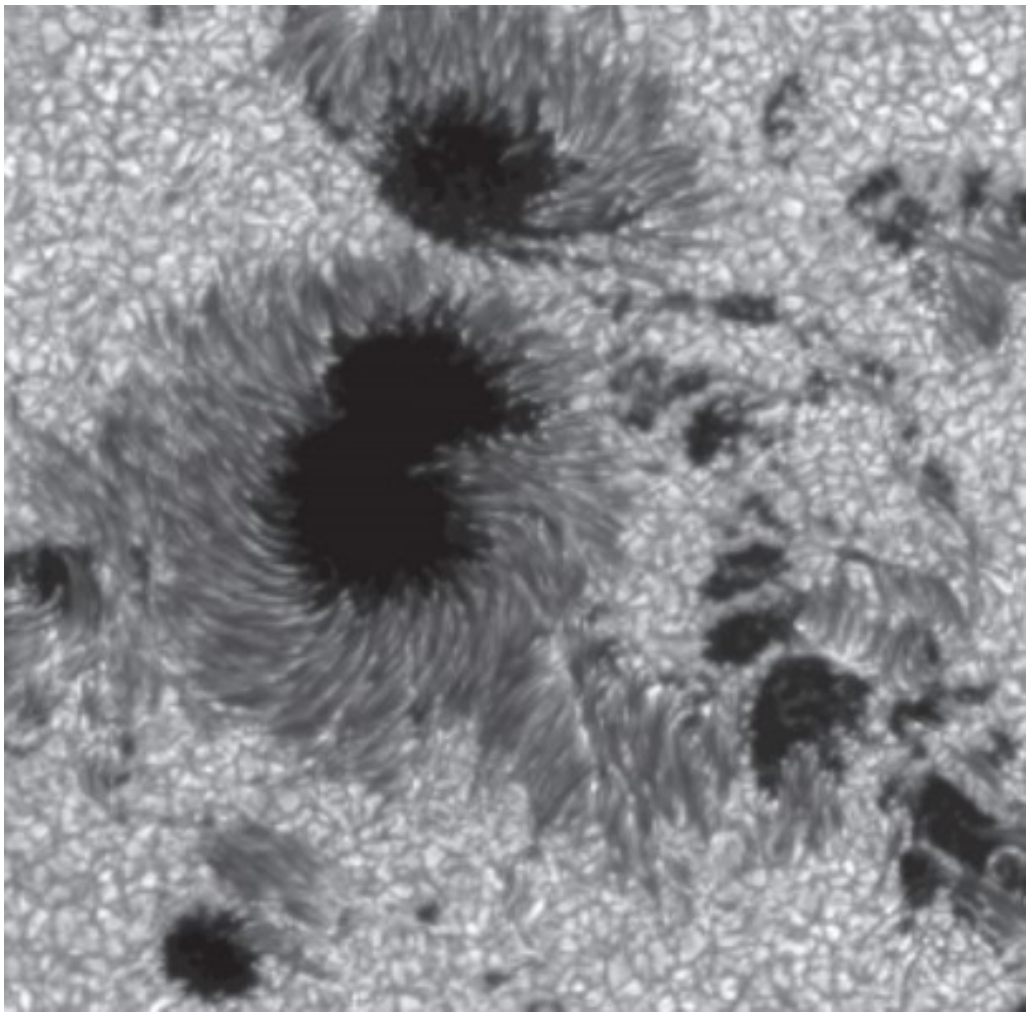

Figure 1.3: Image of a number of sunspots from the Swedish Solar Telescope (SST) on La Palma. Figure credit to Göran Scharmer from Priest (2014).

they appear in pairs — one where the field enters the atmosphere and another where the field returns to the solar interior. Sunspots appear darker than their surroundings because the strong magnetic field partially prevents normal energy transport. Sunspots have a darker central region known as the *umbra* with an almost entirely vertical magnetic field and a *penumbra* on the outside made of bright and dark filaments with a more-horizontal magnetic field (see Figures 1.3 and 1.4). The umbra of the sunspot is typically about 1000–2000 K cooler than the typical surface temperature, whereas the penumbra is about 200–400 K cooler. This is indicative of the fact that vertical magnetic field will inhibit convective heat transport. Sunspots' lifetimes are proportional to their area, so a sunspot of diameter 10Mm has an average lifetime of about 2–3 days whereas sunspots of diameter 60Mm last about 80–90 days (Priest, 2014).

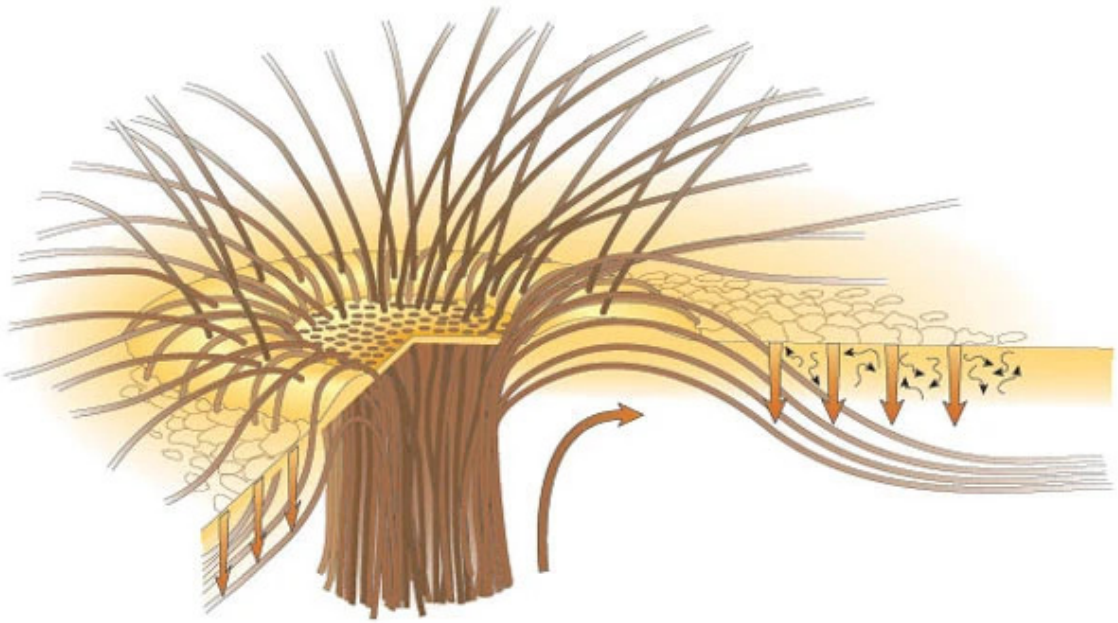

Figure 1.4: Illustration demonstrating the structure of a sunspot. Brown tubes represent magnetic flux tubes escaping the solar photosphere. We see that some flux tubes extend vertically out of the spot to form the umbra. On the other hand, some flux tubes immediately return to the interior and are near horizontal at the surface — these form the penumbra. Figure from Thomas *et al.* (2002).

1.2.2 The sunspot cycle

It is now well established that the emergence of sunspots follows a systematic pattern, known as the sunspot cycle. The sunspot cycle was first discovered by German astronomer Samuel Heinrich Schwabe through extended observations of sunspots. He first documented his discovery in his 1843 paper "*Sonnenbeobachtungen im Jahre 1843*" (which translates as "Observations of the sun in the year 1843") where one can find the extract "*Vergleicht man nun die Zahl der Gruppen und der flecken-freien Tage mit einander, so findet man, dass die Sonnenflecken eine Periode von ungefähr 10 Jahren hatten . . .* " which approximately translates as "If one compares the number of groups [of sunspots] and the sunspot-free days with one another, then one finds that the sunspots had a period of about 10 years . . . " (Schwabe, 1843). While Schwabe is credited with discovering the sunspot cycle — which is now accepted to be an 11 year cycle — a more vague statement about periodicity of the Sun's appearance was made by Danish astronomer Christian Horrebow almost 70 years earlier in 1776 (Hathaway, 2010).

Following Schwabe's discovery, Swiss astronomer Rudolf Wolf began more extensive study of sunspot numbers. He introduced a metric by which to record the number of sunspots which emphasises sunspot groups as opposed to individual sunspots. The Wolf

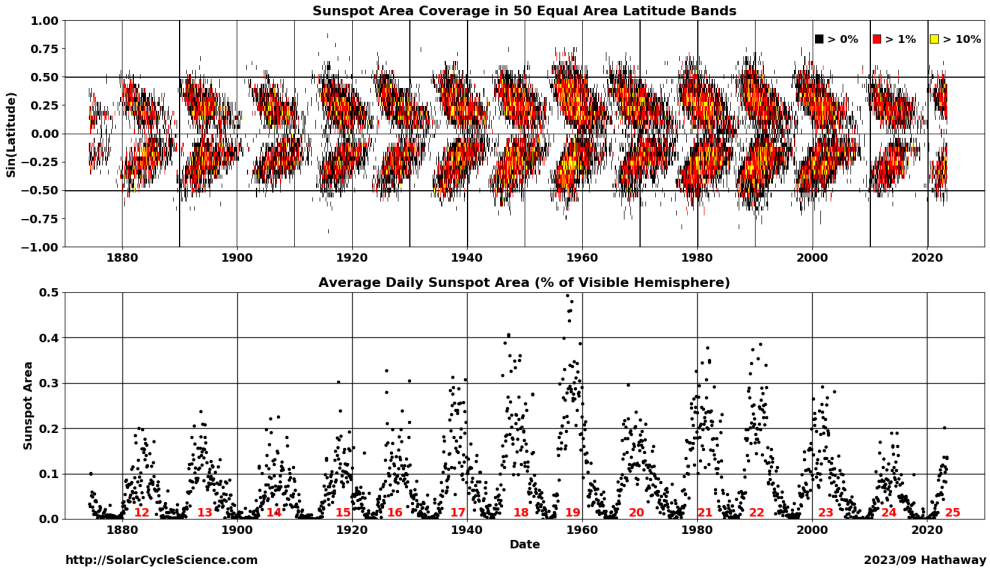

Figure 1.5: The "butterfly diagram" showing sunspot coverage, at each solar latitude, over time. Figure from Solar Cycle Science — http://www.solarcyclescience. com/solarcycle.html .

Sunspot Number, R, (also called Zurich or International Sunspot Number) is defined by

$$R = k(10g + n), \tag{1.1}$$

where g is the number of identified sunspot groups, n is the number of individual sunspots and k is a correction factor for the observer. The correction factor was a necessary part of the definition since different astronomers would have more/less stringent definitions of what constitutes a sunspot. The Wolf Sunspot Number has been obtained daily since 1849. In more recent times, R is calculated from a number of observers using averages weighted by k.

Figure 1.5 is the *butterfly diagram* which shows the distribution of sunspots over time. The diagram was first created by Annie and Walter Maunder in 1904. The diagram shows clearly the regularity of the 11-year cycle as well as an equator-ward shift in the sunspots as the cycle progresses.

1.2.3 Magnetic observations of the solar cycle

The sunspot cycle is often conflated with the related, yet distinct, solar cycle. The sunspot cycle is the 11-year cycle in which the number of sunspots rises and falls. However, the solar cycle refers to the 22-year period which covers two sunspot cycles. After the first sunspot cycle the magnetic field, which is responsible for the sunspots, reverses polarity, so it only after 22-years that we have truly completed a full cycle.

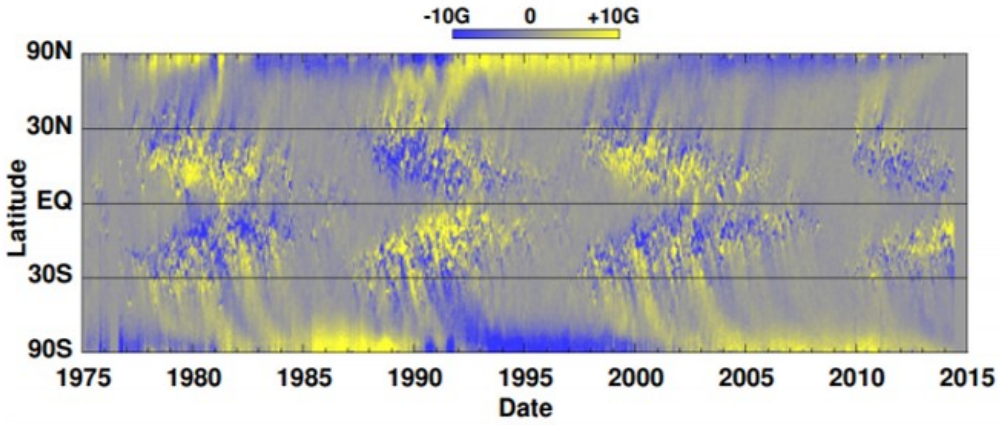

Figure 1.6: A "magnetic butterfly diagram" for the Sun's magnetic field; obtained by averaging radial magnetic field longitudinally. Data obtained from Kitt Peak National Observatory (Arizona, US) and the Solar and Heliospheric Observatory (SOHO) spacecraft. Figure from Hathaway (2010).

Clearly, magnetic field is intrinsically tied to the solar cycle. Hale *et al.* (1919) describe "Hale's polarity laws" which note that (a) the magnetic polarity of neighbouring sunspots are most commonly of opposing signs, (b) corresponding pairs of spots on the Northern hemisphere would be of opposite polarity to that of the Southern hemisphere, and (c) the polarity of leading spots in the current cycle are opposite to those of the previous cycle. As well as Hale's polarity laws, Hale *et al.* (1919) also states *Joy's Law* as *"The following spot of the pair tends to appear farther from the equator than the preceding spot, and the higher the latitude, the greater is the inclination of the axis to the equator"*. It was also noticed by Babcock (1959) that the polarity of the Sun's polar field appears to reverse every 11 years; in fact the reversal seems to occur approximately at the cycle maximum.

Figure 1.6 demonstrates much of the fundamental behaviour associated with the solar cycle. From Figure 1.6 we can see evidence of at least two of Hale's polarity laws; namely, it is evident that from one cycle to the next, regions of spots appearing to have predominantly positive magnetic field have switched to negative magnetic field and vice versa. Also, we see some approximate anti-symmetry about the equator where what we see in the northern hemisphere is roughly mirrored by what we see in the southern hemisphere but with a change in the polarity of the magnetic field. Finally, it is seen in Figure 1.6 that the fields of high latitude get transported to the poles, appearing to cause the switch in the polar field at around sunspot maximum.

1.3 The large-scale solar magnetic field

When discussing the large-scale magnetic field of the Sun, it is often useful to decompose the field into *poloidal* and *toroidal* components. We can decompose any divergence-free

vector field, say $\mathbf{B}$, into toroidal and poloidal components, $\mathbf{B}_t$ and $\mathbf{B}_p$, by

$$\mathbf{B} = \mathbf{B}_t + \mathbf{B}_p, \tag{1.2}$$

where both $\mathbf{B}_t$ and $\mathbf{B}_p$ are solenoidal. In spherical coordinates, we decompose as follows:

$$\mathbf{B}_t = \boldsymbol{\nabla} \times (J\widehat{\mathbf{r}}) \tag{1.3}$$

and

$$\mathbf{B}_p = \boldsymbol{\nabla} \times \boldsymbol{\nabla} \times (B\widehat{\mathbf{r}}), \tag{1.4}$$

where B and J are scalar fields and $\widehat{\mathbf{r}}$ is the unit vector in the radial direction (Glatzmaier, 1984). It can be seen that, in this decomposition, $\mathbf{B}_t$ has no radial component. If we were to assume an axisymmetric system, then the latitudinal component of $\mathbf{B}_t$ would also vanish and hence $\mathbf{B}_t$ would only have a component in the longitudinal direction, ϕ. Conversely, in an axisymmetric system, it can be seen that $\mathbf{B}_p$ has no ϕ component. In this axisymmetric geometry, toroidal field is oriented in an azimuthal sense, i.e. parallel, or anti-parallel, to the equator, and poloidal field is perpendicular to the toroidal field, i.e. in meridional planes.

The observations outlined in Section 1.2.3 point to the source of the sunspots being a large scale toroidal magnetic field. In order to explain Hale's Laws (see Section 1.2.3), the toroidal magnetic field must be antisymmetric about the equator — i.e. of the same strength but of opposite polarity, and must reverse every 11 years.

In order for there to be a self-sustaining solar dynamo, there will need to be a poloidal field that can generate the toroidal field (and vice versa). There is evidence of a weaker poloidal field in solar observations. This poloidal field can be established from observations of the corona where the weak field can result in large-scale magnetic structure.

The differential rotation profile of the Sun has a significant impact on magnetic fields. In the tachocline, where there is a velocity shear caused by the differential rotation profile (see Figure 1.2), poloidal field will be azimuthally stretched. This is because, as per Alfvén's theorem (Priest & Forbes, 2000), magnetic field in highly-conducting fluids will move with the flow. Hence the velocity shear will also shear out the magnetic field. In this way, in the tachocline, there is a mechanism for toroidal field to be generated from poloidal field. We call this mechanism the ω-effect (omega effect), as per Steenbeck & Krause (1969).

In order for the large-scale field of the Sun to be self-sustaining, there must also be a mechanism by which poloidal field can be generated from toroidal field. However, Cowling's theorem states that *An axisymmetric flow cannot sustain an axisymmetric magnetic field against resistive decay* (Cowling, 1933). This rules out the possibility of an axisym-

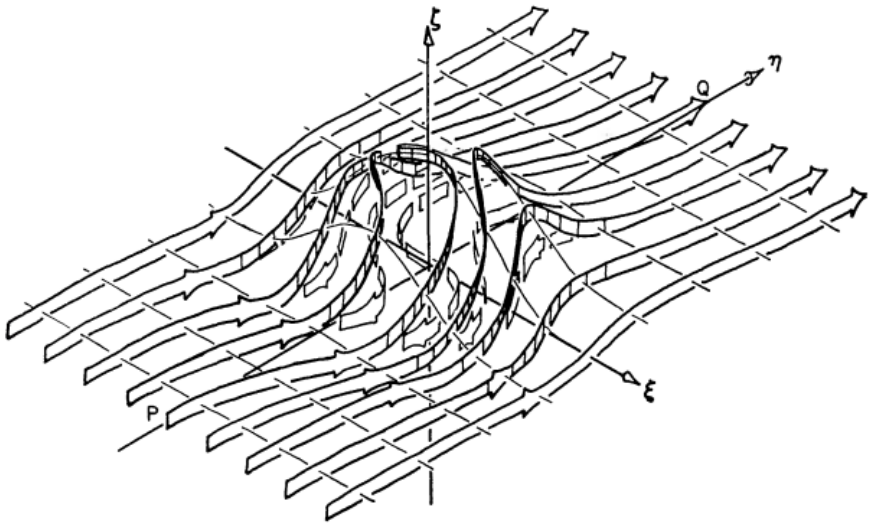

Figure 1.7: The "rise and twist" of toroidal field due to cyclonic convective motion. Figure from Parker (1955*b*).

metric dynamo and means that we cannot have a mechanism for generating poloidal field from toroidal field in an axisymmetric system. Parker (1955*b*) proposed a solution to this problem as a "rise and twist" of toroidal field; see Figure 1.7. Parker suggests that this would be due to the action of cyclonic convective upwellings on a toroidal field. Parker's proposal was later formalised mathematically by Steenbeck *et al.* (1966) and developed into what is now known as "mean field electrodynamics". Using mean field electrodynamics, where flow velocity and magnetic field are split into "mean field" and "small-scale fluctuation" parts, it can be shown that the mean magnetic field can depend on the *mean electromotive force* which only depends on small-scale fluctuation terms; i.e. small-scale effects contribute to the mean magnetic field, specifically poloidal field can be generated from toroidal field in the presence of small-scale turbulence (see, for example, Davidson (2001); Charbonneau (2010); Moffatt & Dormy (2019)). This mechanism of generating poloidal field from toroidal field is called the α-effect (alpha effect), as per Steenbeck & Krause (1969). Whilst small-scale turbulence is not the only process that could give rise to an alpha-effect (and there is still much debate in the literature regarding the details of the process), it is generally accepted that the large scale magnetic field of the Sun is the result of an $\alpha\omega$-dynamo whereby the poloidal field is regenerated by an α-effect and the toroidal field is regenerated by an ω-effect.

There are a number of different dynamo models, here we will briefly discuss only two, the *flux-transport* model and the *interface* model. Whilst there are many different dynamo models, no one model has been universally accepted (see Charbonneau (2010)).

One such model is the *flux-transport* model originally proposed by Babcock (1961) and further developed by Leighton (1964, 1969). Flux-transport is a model that arose as a potential explanation for surface observations of the Sun (for details one is referred to the review by Charbonneau (2010)). In this model, the ω-effect produces ropes of toroidal magnetic field. This magnetic field is transported through the convective zone to the surface (by magnetic buoyancy; see Chapter 2). As it traverses this region the ropes are twisted by the Coriolis force. This twist is reflected in the surface distribution of active regions (Joy's law), whereby the leading spot in a pair tends to be at a lower latitude (closer to the equator) than the proceeding one. The extent of the spreading is directly correlated with latitude, meaning that at higher latitudes an imaginary line connecting one spot to its pair is closer to vertical than at lower latitudes. The α-effect (in surface regions) is coupled to the ω-effect (in the tachocline) by a meridional flow, the details of which are still not well understood.

An alternative dynamo model is the *interface* model, which was proposed by Parker (1993). This model relies on the assumption that the solar dynamo is located at the tachocline — which we expect to be true for several reasons. The strength of active regions on the solar surface, coupled with the expected rise-times of magnetic field of the strength that is observed at the surface, determine that the magnetic field must be originating deep in the interior rather than the near the surface. Secondly, weak field in the convection zone will be preferentially pumped down by turbulence to gather at the tachocline (Tobias *et al.*, 2001). Then the strong shear, caused by differential rotation, in the tachocline can produce an ω-effect. In this context, Parker (1993) introduced a two-layer interface dynamo whereby there is an α-effect in the top layer, caused by cyclonic convection, and in the lower layer there is an ω-effect, caused by velocity shear. The separation of the alpha and omega regions gets round the so-called alpha-quenching problem, where strong magnetic fields inhibit the rise and twist of field required for an α-effect. In this setup, you get surface waves at the interface between the two layers. Now, turbulent diffusion allows for transfer of poloidal/toroidal field between the two layers. It has been shown (Parker, 1993; Tobias, 1996) that, under certain conditions, this can produce a solar-like dynamo.

While the precise dynamo mechanism is not widely agreed, a common thread of both the flux-transport and interface models is their reliance on a strong toroidal field at the tachocline. Observations of the Sun also confirm the presence of strong magnetic field, forming sunspots, at the surface. What is not yet fully understood is the process by which magnetic field is transported radially from the tachocline to the surface; we call this process magnetic buoyancy.

Parker (1955*a*) (see also Jensen, 1955) first argued that sunspots arise as strands of toroidal magnetic field which have been transported to the surface by magnetic buoyancy.

Once this origin of the sunspot is established, many properties of the solar cycle follow. Firstly, the fact that spots tend only to appear in at most middle latitudes corresponds to the fact that the toroidal field is not intensely amplified at higher altitudes. Secondly, the fact that we see this equatorial shift over time corresponds to the migration of the toroidal field towards the equator. Thirdly, the fact that the polarity appears to reverse every half-cycle corresponds to the alternation in sign of successive bands of toroidal field.

1.4 Thesis overview

This thesis will be concerned with dynamics of the solar interior. More specifically, we will be concerned with mathematical models approximating the dynamics, especially magnetic buoyancy, in the Sun. Magnetic buoyancy, and other processes and instabilities of interest, rely on changes in density. In the fully compressible system, these density perturbations produce sound (or acoustic) waves — fast density waves. For several reasons, including computational expense, it is often desirable to filter out sound waves. Therefore, a set of equations between the fully compressible and incompressible equations, where density perturbations cannot exist and therefore buoyancy and convection cannot take effect, are required. A number of such models already exist, namely Boussinesq, anelastic and pseudo-incompressible models, which we call *sound-proof* models. These models are derived to systematically filter out sound waves from the governing equations. These sound-proof models, and their applicability to magnetic buoyancy in the Sun, will be discussed and studied in this thesis.

The magneto-hydrodynamics of the Sun, discussed above, forms the physical motivation for our study. Specifically, we will be concerned with the dynamics of the solar interior. Chapter 2 describes magnetic buoyancy and introduces the underlying mathematics. Chapter 3 introduces sound-proof models. It is these sound-proof models which we shall be assessing against the fully compressible equations in Chapters 4 and 5. Chapter 4 compares these sound-proof models to the compressible equations by considering a number of asymptotic regimes and deriving leading-order dispersion relations. The majority of Chapter 4 comes from a paper co-written by myself, Toby Wood and Paul Bushby published in Physical Review Fluids (Moss *et al.*, 2022). Sections of this paper also appear in other areas of this thesis; specifically, Chapter 3 contains a derivation of a magnetic version of the pseudo-incompressible model which appears as an appendix in (Moss *et al.*, 2022). Chapter 5 compares sound-proof models to the fully compressible system by considering the energy conservation properties of the governing equations. The majority of this chapter also comes from a published paper co-written by myself, Toby Wood and Paul Bushby (Moss *et al.*, 2023). Chapter 6 discusses the double-diffusive instability which had been neglected to this point in the thesis. The final chapter contains a summary of the

key findings and discussion of potential future work.

Chapter 2

Magnetic Buoyancy

In this chapter we will introduce the concept of magnetic buoyancy by considering a parcel argument. We will then formally introduce the fully compressible equations of magnetohydrodynamics (MHD), which will allow us to more rigorously derive conditions for magnetic buoyancy instability. For an introductory overview of MHD and magnetoconvection one is referred to Weiss & Proctor (2014). We will then consider the effects of thermal diffusion and rotation on magnetic buoyancy.

2.1 Basic concepts

As noted in Chapter 1, magnetic buoyancy is a phenomenon that was first described by Parker (1955*a*) and Jensen (1955). The term "magnetic buoyancy" in fact refers to multiple related, but distinct, processes. Firstly, as initially described by Parker (1955*a*) and Jensen (1955), "magnetic buoyancy" is used to describe a non-equilibrium phenomenon where an isolated flux tube will rise. To describe this process we begin by considering a horizontal magnetic flux tube in thermal equilibrium with its non-magnetic surroundings. The total pressure (i.e. gas plus magnetic pressure ; see equation (2.17) and surrounding text for the definition of magnetic pressure) within the tube must be in pressure balance with the non-magnetic fluid surrounding it, therefore the gas pressure within the tube must be lower than that of its surroundings and hence the tube will tend to be buoyant. Secondly, "magnetic buoyancy" is also used to refer to an instability mechanism whereby regions of strong magnetic field become unstable and rise. To demonstrate this instability we consider a fluid parcel argument (Acheson, 1979; Wilczyński *et al.*, 2022). Consider an ideal fluid in magneto-static equilibrium, in the absence of diffusion, with a horizontal magnetic field that only depends on height (z-direction) with fluid properties that also are only functions of height. We write this equilibrium as a balance between the gradient of

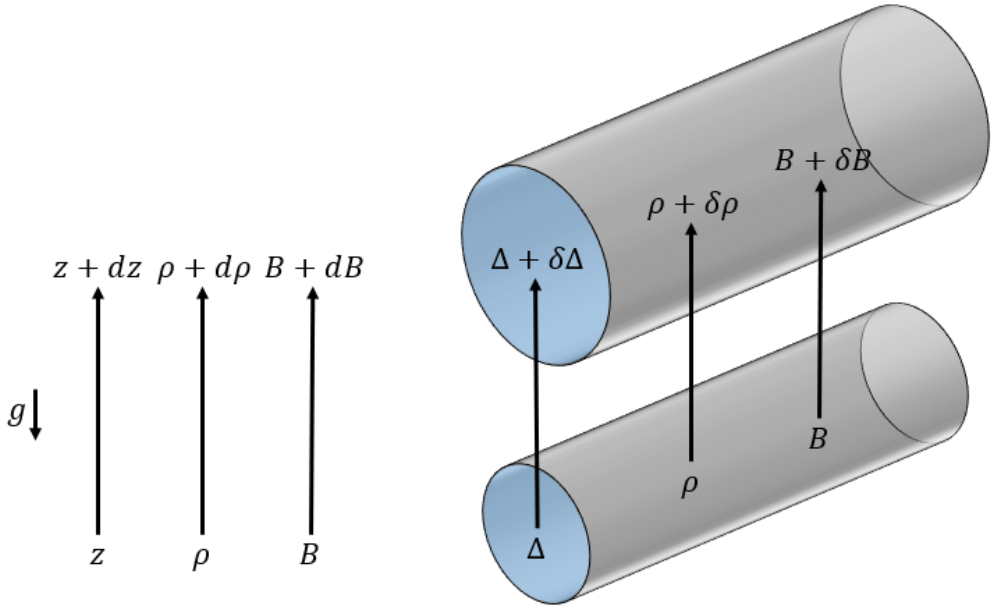

Figure 2.1: Schematic of a magnetic flux tube before and after displacement.

the total pressure and the gravity,

$$\frac{\mathrm{d}}{\mathrm{d}z}(p + \tfrac{1}{2}\mu_0^{-1}B^2) = -\rho g\,, \tag{2.1}$$

where B represents the horizontal magnetic field (in the x-direction), ρ the fluid density, p the fluid pressure, μ_0 the constant magnetic permeability and g is a uniform gravitational acceleration (directed downwards). Note that here, and throughout, we will be using SI units.

We consider a magnetic flux tube which we displace from vertical position z to $z + \mathrm{d}z$, without bending the field lines (note that here, and throughout most of the thesis, we adopt a co-ordinate system with z to be positive upwards; i.e. in the opposite direction to gravity). If we denote the initial cross sectional area of the flux tube (at position z) to be Δ, then we can write the mass per unit length as $\rho\Delta$ and the magnetic flux as $B\Delta$. For any property of the flux tube at z, say ϕ, we denote the value in the tube at $z + \mathrm{d}z$ by $\phi + \delta\phi$, whereas we will denote the local value at $z + \mathrm{d}z$ by $\phi + \mathrm{d}\phi$ (see Figure 2.1).

We can utilise the conservation of magnetic flux to write

$$B\Delta = (B + \delta B)(\Delta + \delta\Delta) \implies \frac{B + \delta B}{B} = \frac{\Delta}{\Delta + \delta\Delta}\,, \tag{2.2}$$

and similarly, by conservation of mass per unit length of the flux tube we have

$$\rho\Delta = (\rho + \delta\rho)(\Delta + \delta\Delta) \implies \frac{\rho + \delta\rho}{\rho} = \frac{\Delta}{\Delta + \delta\Delta}\,. \tag{2.3}$$

We can now eliminate $\Delta/(\Delta + \delta\Delta)$ to yield the result

$$\frac{B + \delta B}{B} = \frac{\rho + \delta\rho}{\rho} \implies \frac{\delta B}{B} = \frac{\delta\rho}{\rho}\,. \tag{2.4}$$

Note that this demonstrates that the quantity B/ρ is conserved.

Since we have assumed that there is no diffusion, specific entropy, s, is conserved and we have $s = s + \delta s$. See the next section for brief discussion of the thermodynamics assumed throughout this thesis. For an ideal gas we have

$$s = c_v \ln(p\rho^{-\gamma})\,, \tag{2.5}$$

where $\gamma = \frac{c_p}{c_v}$ is the ratio of specific heats and c_p and c_v are the specific heat capacity at constant pressure and volume respectively. Therefore,

$$\begin{aligned} c_v[\ln(p) - \gamma\ln(\rho)] &= c_v[\ln(p + \delta p) - \gamma\ln(\rho + \delta\rho)] \\ \implies p\rho^{-\gamma} &= (p + \delta p)(\rho + \delta\rho)^{-\gamma} \\ \implies 1 + \frac{\delta p}{p} &= \left(1 + \frac{\delta\rho}{\rho}\right)^{\gamma} \\ \implies \frac{\delta p}{p} &\approx \gamma\frac{\delta\rho}{\rho}\,, \end{aligned} \tag{2.6}$$

where we have used the binomial expansion to approximate

$$\left(1 + \frac{\delta\rho}{\rho}\right)^{\gamma} \approx 1 + \gamma\frac{\delta\rho}{\rho}. \tag{2.7}$$

Under the assumption that the tube moves sufficiently slowly that the total pressure (gas pressure plus magnetic pressure) equilibrium between the inside and outside of the tube is preserved then we can write

$$p + \delta p + \frac{1}{2\mu_0}(B + \delta B)^2 = p + \mathrm{d}p + \frac{1}{2\mu_0}(B + \mathrm{d}B)^2\,,$$

where μ_0 is the magnetic permeability. This, at first order, reduces to

$$\delta p + \frac{1}{\mu_0}B\delta B = \mathrm{d}p + \frac{1}{\mu_0}B\mathrm{d}B\,. \tag{2.8}$$

We can use equations (2.4) and (2.6) to write equation (2.8) as

$$\left(v^2 + c^2\right)\delta\rho = \mathrm{d}p + \frac{1}{\mu_0}B\mathrm{d}B\,. \tag{2.9}$$

where $c^2 = \gamma p/\rho$ and $v^2 = B^2/(\mu_0\rho)$ are the square of the adiabatic sound speed and the

Alfvén speed respectively. Now, if we have $\delta\rho < \mathrm{d}\rho$, i.e. the density of the fluid within the displaced tube is less than the density of the surrounding fluid, then the tube will continue to rise and hence we have instability. By equation (2.9), we have instability if

$$\mathrm{d}p + \frac{1}{\mu_0} B \mathrm{d}B < (v^2 + c^2)\mathrm{d}\rho\,. \tag{2.10}$$

To manipulate this instability criterion into a more familiar form, we divide through by $\mathrm{d}z$ (positive by construction) and rearrange as follows;

$$\begin{aligned}
\frac{\mathrm{d}p}{\mathrm{d}z} + \frac{B}{\mu_0}\frac{\mathrm{d}B}{\mathrm{d}z} &< (v^2 + c^2)\frac{\mathrm{d}\rho}{\mathrm{d}z} \\
\implies \frac{1}{p}\frac{\mathrm{d}p}{\mathrm{d}z} + \frac{B^2}{\mu_0 p}\frac{1}{B}\frac{\mathrm{d}B}{\mathrm{d}z} &< \left(\gamma + \frac{B^2}{\mu_0 p}\right)\frac{1}{\rho}\frac{\mathrm{d}\rho}{\mathrm{d}z} \\
\implies \frac{B^2}{\mu_0 p}\left(\frac{1}{B}\frac{\mathrm{d}B}{\mathrm{d}z} - \frac{1}{\rho}\frac{\mathrm{d}\rho}{\mathrm{d}z}\right) &< -\left(\frac{1}{p}\frac{\mathrm{d}p}{\mathrm{d}z} - \gamma\frac{1}{\rho}\frac{\mathrm{d}\rho}{\mathrm{d}z}\right) \\
\implies \frac{B^2}{\mu_0 p}\frac{\mathrm{d}}{\mathrm{d}z}\ln\left(\frac{B}{\rho}\right) &< -\frac{\mathrm{d}}{\mathrm{d}z}\ln\left(\frac{p}{\rho^\gamma}\right).
\end{aligned} \tag{2.11}$$

This instability condition was first derived by Newcomb (1961) by considering energy arguments, which we present in Section 2.3. Inequality (2.11) can be viewed as a modified Schwarzchild criterion — the stability condition for convection. In this derivation we have considered so-called *interchange* modes — that is, where the magnetic flux tube is displaced without bending — i.e. the field lines are interchanged. Inequality (2.11) demonstrates that the destabilising gradient in B/ρ (the left hand side of (2.11)) must overcome the stabilising effect of the entropy gradient (the right hand side of (2.11)) in order to get an instability. Note that in our co-ordinate system, with z positive vertically upwards, or radially outwards of a star for example, a destabilising field gradient would be negative — with stronger field at the bottom of the domain.

Above, we considered $2D$-interchange modes. However, if we were to consider $3D$ effects — so-called *undular* modes, where we account for the bending of the magnetic field lines — then we get a different stability criterion. In the same notation as above, we find that a necessary condition for instability in the $3D$ case is

$$\frac{B^2}{\mu_0 p}\frac{\mathrm{d}}{\mathrm{d}z}\ln(B) < -\frac{\mathrm{d}}{\mathrm{d}z}\ln\left(\frac{p}{\rho^\gamma}\right), \tag{2.12}$$

where we have looked for the preferred mode of instability that has a long wavelength in the direction parallel to the field; i.e. $k_x \to 0$ where k_x represents the wavenumber in the x-direction. This was originally derived by Newcomb (1961) and Thomas & Nye (1975), and is derived in Section 2.3 by considering energy conservation arguments; in fact, by

considering energy conservation, it is shown that (2.12) is a necessary *and* sufficient condition. We notice that in this case instability requires a sufficient gradient in B, rather than in B/ρ. It is perhaps surprising that, despite now having to do work against magnetic tension, undular modes are more easily destabilised than interchange modes. The reasoning for this is explained in Hughes & Cattaneo (1987) and Hughes (2007). Essentially, in the interchange case, density perturbations are created by doing work against pressure — this includes both gas pressure and magnetic pressure. However, in the $3D$ case, it is possible — by having a long wavelength in the direction of the field — to minimise the work done against magnetic pressure. Therefore undular modes can be destabilised more easily than the interchange modes.

2.2 Fully compressible equations

Before pursuing a more rigorous discussion of magnetic buoyancy in the next section, we first introduce the fully compressible equations of magnetohydrodynamics (MHD). In writing these equations, we are making some thermodynamic assumptions. Whilst the Sun consists of several different elements (primarily Hydrogen and Helium), here we neglect variations in composition and assume a fluid of fully ionised Hydrogen. We also assume that collisions within the fluid conserve energy and momentum, and hence we can treat the fluid as a continuum and the hydrodynamic equations apply (see, for example, Choudhuri (1998).) With uniform angular velocity $\boldsymbol{\Omega}$, these equations are

$$\rho\frac{\mathrm{D}\mathbf{u}}{\mathrm{D}t} + 2\rho\,\boldsymbol{\Omega}\times\mathbf{u} = -\boldsymbol{\nabla}p - g\rho\,\widehat{\mathbf{z}} + \frac{1}{\mu_0}(\boldsymbol{\nabla}\times\mathbf{B})\times\mathbf{B} + \mu\boldsymbol{\nabla}\cdot\tau\,, \tag{2.13}$$

$$\frac{\partial\mathbf{B}}{\partial t} = \boldsymbol{\nabla}\times(\mathbf{u}\times\mathbf{B}) + \eta\nabla^2\mathbf{B}\,, \tag{2.14}$$

$$\frac{\mathrm{D}\rho}{\mathrm{D}t} + \rho\boldsymbol{\nabla}\cdot\mathbf{u} = 0\,, \tag{2.15}$$

$$\rho T\frac{\mathrm{D}s}{\mathrm{D}t} = Q\,, \tag{2.16}$$

where $\boldsymbol{\nabla}\cdot\tau$ is the divergence of the symmetric deviatoric rate-of-strain tensor (the effects of which will be ignored for the majority of this thesis). Many of these quantities have already been defined but for ease of reference we will repeat these definitions now. The fluid velocity is given by $\mathbf{u} = (u_x, u_y, u_z)$, $\mathbf{B} = (B_x, B_y, B_z)$ represents the magnetic field, ρ is the fluid density, p is the pressure, s is the specific entropy, T is the temperature, Q represents the sum of all diabatic heating processes, such as thermal diffusion, μ is the dynamic viscosity, η is the magnetic diffusivity, $\mathrm{D}/\mathrm{D}t \equiv \partial/\partial t + \mathbf{u}\cdot\boldsymbol{\nabla}$ is the material derivative, μ_0 is the magnetic permeability, and $-g\widehat{\mathbf{z}}$ is the gravitational acceleration, assumed to be uniform. The equations are closed using an equation of state. Since we assume a single-species fluid, we can express specific entropy, s, as a function of any two

independent thermodynamic variables, e.g. density, ρ, and pressure, p. Specifically for an ideal gas, the equation of state is simple (and also a reasonable approximation for the solar interior) and we have $p = R\rho T$ and $s = c_v \ln(p\rho^{-\gamma})$, where γ is the ratio of specific heats and the gas constant, R, and the heat capacity at constant volume, c_v, are related by $R = (\gamma - 1)c_v$. Note that the Lorentz force can be decomposed as

$$\frac{1}{\mu_0}(\boldsymbol{\nabla} \times \mathbf{B}) \times \mathbf{B} = -\frac{1}{2\mu_0}\boldsymbol{\nabla}|\mathbf{B}|^2 + \frac{1}{\mu_0}(\mathbf{B} \cdot \boldsymbol{\nabla})\mathbf{B}. \tag{2.17}$$

Notice that the first term on the right-hand side acts on the fluid in the same way as the pressure term $(-\boldsymbol{\nabla}p)$, and hence is referred to as the *magnetic pressure*. We can then define the total pressure, π, to be the sum of the gas pressure and the magnetic pressure, i.e. $\pi \equiv p + |\mathbf{B}|^2/(2\mu_0)$. The final term in (2.17) represents the magnetic tension. Then, in the absence of viscosity, equation (2.13) becomes

$$\rho\frac{\mathrm{D}\mathbf{u}}{\mathrm{D}t} + 2\rho\,\boldsymbol{\Omega} \times \mathbf{u} = -\boldsymbol{\nabla}\pi - g\rho\,\widehat{\mathbf{z}} + \frac{1}{\mu_0}(\mathbf{B} \cdot \boldsymbol{\nabla})\mathbf{B}\,. \tag{2.18}$$

Throughout much of this thesis we will neglect viscosity and magnetic diffusion; in general these are expected to play only a minor role in magnetic buoyancy under solar conditions (although they can result in double-diffusive-type instabilities, e.g., Hughes & Weiss (1995)). We will include viscosity and magnetic diffusion, and consider their effect, in Chapter 6. In the tachocline, the magnitudes of the three diffusivities are as follows: magnetic diffusivity $\eta \approx 4.1\times10^2$ cm^{2}s^{-1}, kinematic viscosity $\nu = 2.7\times10^1$ cm^{2}s^{-1} (related to dynamic viscosity by $\mu = \nu\rho$), thermal diffusivity $\kappa = 1.4 \times 10^7$ cm^{2}s^{-1} (Hughes *et al.*, 2007). As such, the dominant diabatic process is usually thermal diffusion, which will therefore be retained in much of the subsequent analysis.

Within the tachocline, beneath the solar convection zone, there is strong rotational shear that is expected to generate strong toroidal magnetic field. Into our local Cartesian model we will therefore introduce a layer of magnetic field oriented in the x-direction, representing azimuth, whose strength varies with altitude, z. We will consider linear perturbations to a background state in magneto-hydrostatic balance in order to determine the conditions under which this magnetic layer becomes buoyantly unstable. From previous studies (e.g., Gilman, 1970; Acheson, 1979; Hughes, 2007) we expect the growth rate of the instability to be of the order of weeks or longer, whereas the acoustic timescale in the solar interior is of the order of minutes. Moreover, the Alfvén speed, $v \equiv |\mathbf{B}|/\sqrt{\mu_0\rho}$, is expected to be only a very small fraction of the sound speed, c, given by $c^2 \equiv (\partial p/\partial\rho)_s$, which suggests that the instability ought to be captured to high accuracy by some form of *sound-proof model* (which we will introduce and discuss in Chapter 3). This suggestion forms the motivation for the present study.

2.2.1 Linearised compressible equations

We begin by taking the fully compressible equations (2.13)–(2.16), where we neglect viscosity and magnetic diffusion, and consider linear perturbations to a static background state containing a horizontal layer of magnetic field oriented in the x-direction, $\mathbf{B} = B_0(z)\widehat{\mathbf{x}}$. Each quantity, say f, is expanded as $f = f_0(z) + f_1(x, y, z, t)$, where f_0 is the background value and f_1 is the linear perturbation. As noted previously, in Section 2.1, the background state is in magneto-hydrostatic balance, i.e.

$$\frac{\mathrm{d}\pi_0}{\mathrm{d}z} = \frac{\mathrm{d}}{\mathrm{d}z}\left(p_0 + \frac{B_0^2}{2\mu_0}\right) = -g\rho_0\,. \tag{2.19}$$

This implies a relation between the scale heights of density, entropy and magnetic field,

$$g = c^2 H_\rho^{-1} - c^2 H_s^{-1} + v^2 H_B^{-1}\,, \tag{2.20}$$

where (as before) c is the adiabatic sound speed and v is the Alfvén speed, both defined in terms of the background state. For a general equation of state, the scale heights in equation (2.20) are defined as:

$$H_\rho^{-1} \equiv -\frac{\mathrm{d}}{\mathrm{d}z}\ln\rho_0\,, \tag{2.21}$$

$$H_s^{-1} \equiv -\left(\frac{\partial \ln\rho}{\partial s}\right)_p \frac{\mathrm{d}s_0}{\mathrm{d}z}\,, \tag{2.22}$$

$$H_B^{-1} \equiv -\frac{\mathrm{d}}{\mathrm{d}z}\ln B_0\,, \tag{2.23}$$

where the partial derivative is evaluated in the background state. These scale heights provide a measure of the distance over which the background variables vary; i.e. can provide a measure of stratification. In future chapters we will introduce scaling assumptions that will relate these distances to that of the perturbed quantities. Note that, for an ideal gas, the entropy scale height (2.22) reduces to $H_s^{-1} = -\mathrm{d}/\mathrm{d}z\left(\ln(\rho/p^{1/\gamma})\right)$, which is clearly a combination of pressure and density scale heights. Note that in many studies of magnetic buoyancy, the Brunt-Väisälä frequency, N, is defined as

$$N^2 = -g\left(\frac{\partial \ln\rho}{\partial s}\right)_p \frac{\mathrm{d}s_0}{\mathrm{d}z} = gH_s^{-1}\,. \tag{2.24}$$

The Brunt-Väisälä frequency is the frequency at which a displaced parcel will oscillate (in a stably-stratified system). However, in the presence of a magnetic field this physical interpretation of N would no longer hold, so to avoid mis-interpretation we prefer to work with H_s instead. Note that, provided that pressure, density and magnetic field strength increases with depth, the scale heights defined above will be positive quantities.

Having taken account of the background state, the linearised fully compressible equations are

$$\rho_0 \frac{\partial}{\partial t}\mathbf{u} + 2\rho_0 \boldsymbol{\Omega} \times \mathbf{u} = -g\rho_1 \widehat{\mathbf{z}} - \boldsymbol{\nabla}\pi_1 + \frac{1}{\mu_0}\mathbf{B}_0 \cdot \boldsymbol{\nabla}\mathbf{B}_1 + \frac{1}{\mu_0}\mathbf{B}_1 \cdot \boldsymbol{\nabla}\mathbf{B}_0 \,, \tag{2.25}$$

$$\frac{\partial}{\partial t}\mathbf{B}_1 = \boldsymbol{\nabla} \times (\mathbf{u} \times \mathbf{B}_0) \,, \tag{2.26}$$

$$\frac{\partial}{\partial t}\rho_1 = -\boldsymbol{\nabla} \cdot (\rho_0 \mathbf{u}) \,, \tag{2.27}$$

$$\left(\frac{\partial \rho}{\partial s}\right)_p \frac{\partial}{\partial t} s_1 - \rho_0 H_s^{-1} u_z = \left(\frac{\partial \rho}{\partial T}\right)_p \frac{Q_1}{\rho_0 c_p}, \tag{2.28}$$

$$\pi_1 = p_1 + \frac{1}{\mu_0}\mathbf{B}_0 \cdot \mathbf{B}_1 \,, \tag{2.29}$$

$$\left(\frac{\partial \rho}{\partial T}\right)_p T_1 = \left(\frac{\partial \rho}{\partial s}\right)_p s_1 - \frac{\gamma - 1}{c^2} p_1 \,, \tag{2.30}$$

$$\rho_1 = \left(\frac{\partial \rho}{\partial s}\right)_p s_1 + \frac{1}{c^2} p_1 \,, \tag{2.31}$$

where γ is the adiabatic index and π_1 is the perturbation to the total (i.e. gas plus magnetic) pressure. In equation (2.28), Q_1 represents perturbations to the diabatic heating. Ordinarily, for thermal diffusion, this would take the form of a Laplacian acting on T_1 (with diffusivity κ). Here, we simplify things by replacing diffusion with Newtonian cooling and setting

$$Q_1 = -\rho_0 c_p \alpha T_1 \tag{2.32}$$

where α is a specified constant. This simplification assumes that temperature perturbations will decay linearly to the background state, with rate α. While, in general, Newtonian cooling will not closely approximate thermal diffusion, in the limits of very fast or slow/no diffusion we can choose α to be such that Newtonian cooling is a sufficient approximation, i.e. will not alter the leading-order dynamics. Note that these equations are valid for an arbitrary equation of state. The form of equations (2.30)–(2.31) has been chosen so that the temperature and entropy perturbations, T_1 and s_1, have the same prefactors as in equation (2.28), which simplifies the subsequent algebra. Equations (2.28), (2.30), and (2.31) are derived in Appendix A.

2.3 Energy considerations

The parcel argument outlined in Section 2.1 can be made more rigorous by considering an energy argument. Newcomb (1961) utilised Bernstein's energy principle to derive the stability criteria of the previous section. One consequence of the Bernstein *et al.* (1958)

energy principle is that one can derive stability properties by considering the total potential energy of a system. It has been shown (Bernstein *et al.*, 1958) that the linearised MHD equations of motion (2.25 – 2.31), in the absence of diffusion and rotation, can be written in terms of Lagrangian displacement $\boldsymbol{\xi}$, given by $\mathbf{r} = \mathbf{r}_0 + \boldsymbol{\xi}$ where $\mathbf{r}$ is a position vector and $\mathbf{r}_0$ is the initial position vector, to yield

$$\rho_0 \frac{\partial^2 \boldsymbol{\xi}}{\partial t^2} = \mathbf{F}[\boldsymbol{\xi}]\,, \tag{2.33}$$

where $\mathbf{F}$ is a self-adjoint operator given by (Bernstein *et al.*, 1958)

$$\begin{aligned}\mathbf{F}[\boldsymbol{\xi}] = \boldsymbol{\nabla}\left(\rho_0(c^2+v^2)\boldsymbol{\nabla}\cdot\boldsymbol{\xi} - \rho_0 v^2\frac{\partial \xi_x}{\partial x} - g\rho_0\xi_z\right)\\ + \rho_0 v^2\frac{\partial^2\boldsymbol{\xi}}{\partial x^2} - \rho_0 v^2\frac{\partial}{\partial x}(\boldsymbol{\nabla}\cdot\boldsymbol{\xi})\widehat{\mathbf{x}} + g\boldsymbol{\nabla}\cdot(\rho_0\boldsymbol{\xi})\,\widehat{\mathbf{z}}\,,\end{aligned} \tag{2.34}$$

where we assume a static background that varies only with height z subject to a horizontal magnetic field, i.e. $p_0 = p_0(z)$, $\mathbf{B}_0 = B_0(z)\widehat{\mathbf{x}}$ etc. With this formulation we can calculate the potential energy, $\mathcal{W}$, given by

$$\mathcal{W} = -\frac{1}{2}\int \boldsymbol{\xi}\cdot\mathbf{F}[\boldsymbol{\xi}]\,\mathrm{d}^3\mathbf{x} \tag{2.35}$$

(Bernstein *et al.*, 1958). By conservation of energy, stability criteria can be inferred from $\mathcal{W}$. Specifically, if $\mathcal{W}$ is positive, for all $\boldsymbol{\xi}$, then the system is stable — since the associated kinetic energy cannot increase. We now calculate $\mathcal{W}$ as

$$\begin{aligned}\mathcal{W} = -\frac{1}{2}\int_V \Bigg[2g\rho_0\xi_z(\boldsymbol{\nabla}\cdot\boldsymbol{\xi}) + 2\rho_0 v^2\frac{\partial\xi_x}{\partial x}(\boldsymbol{\nabla}\cdot\boldsymbol{\xi}) + g\frac{\mathrm{d}\rho_0}{\mathrm{d}z}\xi_z^2\\ - \rho_0(c^2+v^2)(\boldsymbol{\nabla}\cdot\boldsymbol{\xi})^2 - \rho_0 v^2\left(\frac{\partial\boldsymbol{\xi}}{\partial x}\right)^2\Bigg]\mathrm{d}^3\mathbf{x}\,.\end{aligned} \tag{2.36}$$

If we now consider interchange modes — 2D modes without bending of the field lines — we can make the simplification that $\partial\boldsymbol{\xi}/\partial x = \mathbf{0}$. The integrand, which we now denote by w, hence becomes

$$w = 2g\rho_0\xi_z\left(\frac{\partial\xi_y}{\partial y} + \frac{\partial\xi_z}{\partial z}\right) + g\frac{\mathrm{d}\rho_0}{\mathrm{d}z}\xi_z^2 - \rho_0(c^2+v^2)\left(\frac{\partial\xi_y}{\partial y} + \frac{\partial\xi_z}{\partial z}\right)^2. \tag{2.37}$$

Following Hughes & Cattaneo (1987), without loss of generality we assume that the perturbations have the form

$$\xi_y = \hat{\xi}_y(z)\sin(k_y y) \qquad \text{and} \qquad \xi_z = \hat{\xi}_z(z)\cos(k_y y) \tag{2.38}$$

(recall we have already assumed there is no dependence on x). Equation (2.37) can then be written as

$$w = \left[2g\rho_0\hat{\xi}_z \left(\hat{\xi}_y k_y + \frac{\partial \hat{\xi}_z}{\partial z} \right) + g\frac{\mathrm{d}\rho_0}{\mathrm{d}z}\hat{\xi}_z^2 - \rho_0(c^2+v^2) \left(\hat{\xi}_y k_y + \frac{\partial \hat{\xi}_z}{\partial z} \right)^2 \right] \cos^2(k_y y) \,. \quad (2.39)$$

We have now split our integrand into a y-dependent part (the $\cos^2(k_y y)$ term) and a z-dependent part. If we integrate over y, then we are left with the large bracketed term, with a multiplicative constant, which we will minimise with respect to $\hat{\xi}_y$. We differentiate w, ignoring the $\cos^2(k_y y)$ term, and set this to zero to get

$$\frac{\partial w}{\partial \hat{\xi}_y} = -2g\rho_0\hat{\xi}_z k_y + \rho_0(c^2+v^2) \left(2k_y\hat{\xi}_y + 2\frac{\partial \hat{\xi}_z}{\partial z} \right) k_y = 0 \quad (2.40)$$

$$\implies \qquad k_y\hat{\xi}_y = \frac{g\hat{\xi}_z}{(c^2+v^2)} - \frac{\partial \hat{\xi}_z}{\partial z} \,. \quad (2.41)$$

We can now substitute this minimum value of $\hat{\xi}_y$ into equation (2.36) (recall we have also assumed that $\partial\boldsymbol{\xi}/\partial x = \mathbf{0}$) to determine if there can be a situation where $\mathcal{W}$ is negative. When we make this substitution we arrive at

$$\begin{aligned} \mathcal{W} &= -\frac{1}{2}\int \cos^2(k_y y)\,\mathrm{d}y \int g\left[\frac{\rho_0 g}{(c^2+v^2)} + \frac{\mathrm{d}\rho_0}{\mathrm{d}z} \right] \hat{\xi}_z^2 \,\mathrm{d}z \\ &= -\frac{A}{2}\int g\left[\frac{\rho_0 g}{(c^2+v^2)} + \frac{\mathrm{d}\rho_0}{\mathrm{d}z} \right] \hat{\xi}_z^2 \,\mathrm{d}z \,, \end{aligned} \quad (2.42)$$

where $A = \int \cos^2(k_y y)\,\mathrm{d}y$ is a (positive) constant. Clearly, $\mathcal{W}$ can be negative if the integrand is positive. We claim that, in general, if $\mathcal{W}$ is negative at any point then we will necessarily have stability. Clearly, this is a necessary condition for instability — if $\mathcal{W}$ is positive everywhere, then the system is stable since the associated kinetic energy cannot increase. To show that $\mathcal{W}$ being negative somewhere is a sufficient condition for instability is less obvious. If we suppose we had such a point where $\mathcal{W}$ can be negative, then we can choose $\boldsymbol{\xi}$ to be zero everywhere except in the vicinity of this point. We will then necessarily have instability (Newcomb, 1961). Therefore, in this example, we will have instability if

$$\frac{\rho_0 g}{(c^2+v^2)} + \frac{\mathrm{d}\rho_0}{\mathrm{d}z} > 0 \quad (2.43)$$

is satisfied anywhere in the domain. We rearrange this, using the magneto-hydrostatic condition (2.20) to eliminate g, to get

$$\frac{B_0^2}{\mu_0 p_0}\frac{\mathrm{d}}{\mathrm{d}z}\ln\left(\frac{B_0}{\rho_0}\right) < -\frac{\mathrm{d}}{\mathrm{d}z}\ln\left(\frac{p_0}{\rho_0^\gamma}\right) \tag{2.44}$$

which is exactly equation (2.11) from the previous section.

Following similar methodology, one can formally derive equation (2.12) for undular modes. For undular modes we no longer assume that $\boldsymbol{\xi}$ has no x-dependence. We begin with expression (2.36), where we let

$$\xi_x = \hat{\xi}_x(z)\cos(k_x x)\cos(k_y y)\,, \tag{2.45}$$

$$\xi_y = \hat{\xi}_y(z)\sin(k_x x)\sin(k_y y)\,, \tag{2.46}$$

$$\xi_z = \hat{\xi}_z(z)\sin(k_x x)\cos(k_y y) \tag{2.47}$$

(Hughes & Cattaneo, 1987). The result is

$$\mathcal{W} = \frac{1}{2}\int\left[\mu_0^{-1}B_0^2\left[k_x^2(\hat{\xi}_y^2+\hat{\xi}_z^2)+\left(k_y\hat{\xi}_y+\frac{\mathrm{d}\hat{\xi}_z}{\mathrm{d}z}\right)^2\right]+\gamma p_0\left(-k_x\hat{\xi}_x+k_y\hat{\xi}_y+\frac{\mathrm{d}\hat{\xi}_z}{\mathrm{d}z}\right)^2\right.$$
$$\left.-2g\rho_0\hat{\xi}_z\left(-k_x\hat{\xi}_x+k_y\hat{\xi}_y+\frac{\mathrm{d}\hat{\xi}_z}{\mathrm{d}z}\right)-g\frac{\mathrm{d}\rho_0}{\mathrm{d}z}\hat{\xi}_z^2\right]\mathrm{d}z\,, \tag{2.48}$$

where, since they will have no effect for this stability analysis, we have neglected the integral over x and y.

Whereas for interchange modes we minimised the integrand with respect to $\hat{\xi}_y$, we now minimise with respect to both $\hat{\xi}_x$ and $\hat{\xi}_y$. We'll begin with $\hat{\xi}_x$. Differentiating the integrand in (2.48), which again we'll call w, with respect to $\hat{\xi}_x$ and setting this to 0 we get

$$\frac{\partial w}{\partial\hat{\xi}_x} = -2\gamma p_0 k_x\left(-k_x\hat{\xi}_x+k_y\hat{\xi}_y+\frac{\mathrm{d}\hat{\xi}_z}{\mathrm{d}z}\right)+2g\rho_0 k_x\hat{\xi}_z = 0\,, \tag{2.49}$$

$$\implies \hat{\xi}_x = \frac{1}{k_x}\left(-\frac{g\rho_0}{\gamma p_0}\hat{\xi}_z+k_y\hat{\xi}_y+\frac{\mathrm{d}\hat{\xi}_z}{\mathrm{d}z}\right)\,. \tag{2.50}$$

We substitute this minimal value of $\hat{\xi}_x$ back in to the integrand to get an expression for

w in terms of only $\hat{\xi}_y$ and $\hat{\xi}_z$,

$$w = \mu_0^{-1} B_0^2 \left[k_x^2 (\hat{\xi}_y^2 + \hat{\xi}_z^2) + \left(k_y \hat{\xi}_y + \frac{\mathrm{d}\hat{\xi}_z}{\mathrm{d}z} \right)^2 \right] - \frac{g^2 \rho_0^2}{\gamma p_0} \hat{\xi}_z^2 - g \frac{\mathrm{d}\rho_0}{\mathrm{d}z} \hat{\xi}_z^2 \,. \tag{2.51}$$

We now repeat the same procedure again but for $\hat{\xi}_y$

$$\frac{\partial w}{\partial \hat{\xi}_y} = \mu_0^{-1} B_0^2 \left[2k_x^2 \hat{\xi}_y + 2k_y \left(k_y \hat{\xi}_y + \frac{\mathrm{d}\hat{\xi}_z}{\mathrm{d}z} \right) \right] = 0 \,, \tag{2.52}$$

$$\implies \hat{\xi}_y = -\frac{k_y}{(k_x^2 + k_y^2)} \frac{\mathrm{d}\hat{\xi}_z}{\mathrm{d}z} \,, \tag{2.53}$$

which, when we substitute back in, gives us

$$\mathcal{W} = \frac{1}{2} \int \left[\left(k_x^2 \frac{B_0^2}{\mu_0} - g \frac{\mathrm{d}\rho_0}{\mathrm{d}z} - \frac{g^2 \rho_0^2}{\gamma p_0} \right) \hat{\xi}_z^2 + \frac{B_0^2}{\mu_0} \frac{k_x^2}{(k_x^2 + k_y^2)} \left(\frac{\mathrm{d}\hat{\xi}_z}{\mathrm{d}z} \right)^2 \right] \mathrm{d}z \,. \tag{2.54}$$

This result agrees with the equivalent result in Hughes & Cattaneo (1987). Clearly, (2.54) will become negative most easily in the limit where $k_x \to 0$ and $k_y \to \infty$. In this limit, (2.54) becomes

$$\mathcal{W} = \frac{1}{2} \int \left[\left(-g \frac{\mathrm{d}\rho_0}{\mathrm{d}z} - \frac{g^2 \rho_0^2}{\gamma p_0} \right) \hat{\xi}_z^2 \right] \mathrm{d}z \,. \tag{2.55}$$

Therefore we will have instability when

$$-g \frac{\mathrm{d}\rho_0}{\mathrm{d}z} - \frac{g^2 \rho_0^2}{\gamma p_0} < 0 \tag{2.56}$$

is satisfied somewhere in the domain. We recall our magneto-hydrostatic condition (2.20) and that, for an ideal gas,

$$H_s^{-1} = \frac{1}{\gamma} \frac{\mathrm{d}}{\mathrm{d}z} \ln \left(\frac{p_0}{\rho_0^\gamma} \right). \tag{2.57}$$

We can then write

$$\frac{B_0^2}{\mu_0 p_0} \frac{\mathrm{d}}{\mathrm{d}z} \ln B_0 < -\frac{\mathrm{d}}{\mathrm{d}z} \ln \left(\frac{p_0}{\rho_0^\gamma} \right) \tag{2.58}$$

which is exactly (2.12).

2.4 Effect of thermal diffusion

In the previous section we have (by necessity) only considered a diffusionless setup. Here, we will investigate the effect of a fast thermal diffusion, i.e. with large thermal diffusivity, κ. One would intuitively assume that magnetic buoyancy instability would prefer large thermal diffusion, to erode the stabilising entropy gradient. We will follow the methodology of Gilman (1970) to consider the large κ limit. We begin with the full linearised magneto-hydrodynamic (MHD) equations (2.25 – 2.31), where we once again ignore rotation. For the sake of easy comparison with Gilman (1970) we will assume a perfect gas, i.e. an equation of state of

$$p = R\rho T \tag{2.59}$$

where R is the gas constant per unit mass. Hence we arrive at equations (2.25 – 2.27) and the energy equation and equation of state become

$$\frac{\partial}{\partial t}s_1 + \mathbf{u}\cdot\boldsymbol{\nabla}s_0 = -\frac{1}{T_0}\kappa\nabla^2 T_1\,, \tag{2.60}$$

$$\frac{p_1}{p_0} = \frac{T_1}{T_0} + \frac{\rho_1}{\rho_0}\,, \tag{2.61}$$

where we have substituted $Q_1 = -\rho_0\kappa\nabla^2 T_1$.

We now assume we have perturbations of the form $f_1 = \tilde{f}_1(z)\exp\left(ik_x x + ik_y y + \sigma t\right)$. For ease of notation the tildes will subsequently be ignored. We will now also take the large diffusion limit, i.e. $\kappa \to \infty$. This will have the effect that all temperature perturbations will vanish and hence equation (2.60) will become redundant. The governing equations then reduce to

$$\sigma u_x = -\frac{ik_x}{\rho_0}\pi_1 + v^2 ik_x\frac{B_{1x}}{B_0} - v^2 H_B^{-1}\frac{B_{1z}}{B_0}\,, \tag{2.62}$$

$$\sigma u_y = -\frac{ik_y}{\rho_0}\pi_1 + v^2 ik_x\frac{B_{1y}}{B_0}\,, \tag{2.63}$$

$$\sigma u_z = -\frac{1}{\rho_0}\frac{\partial\pi_1}{\partial z} - \frac{g}{\rho_0}\rho_1 + v^2 ik_x\frac{B_{1z}}{B_0}\,, \tag{2.64}$$

$$\sigma B_{1x} = -B_0 ik_y u_y - B_0\frac{\partial u_z}{\partial z} + B_0 H_B^{-1}u_z\,, \tag{2.65}$$

$$\sigma B_{1y} = B_0 ik_x u_y\,, \tag{2.66}$$

$$\sigma B_{1z} = B_0 ik_x u_z\,, \tag{2.67}$$

$$\sigma\frac{\rho_1}{\rho_0} = -ik_x u_x - ik_y u_y - \frac{\partial u_z}{\partial z} + H_\rho^{-1}u_z\,, \tag{2.68}$$

$$\frac{p_1}{p_0} = \frac{\rho_1}{\rho_0}\,, \tag{2.69}$$

where $\mathbf{B}_1 = (B_{1x}, B_{1y}, B_{1z})$ and we recall

$$H_\rho^{-1} = -\frac{1}{\rho_0}\frac{\mathrm{d}\rho_0}{\mathrm{d}z}\,, \qquad H_B^{-1} = -\frac{1}{B_0}\frac{\mathrm{d}B_0}{\mathrm{d}z}\,, \qquad v^2 = \frac{B_0^2}{\mu_0\rho_0}\,. \tag{2.70}$$

Following Gilman (1970), we now only consider perturbations which are extremely narrow in the y-direction, i.e. we take the limit $k_y \to \infty$. Under this limit, upon review of equation (2.63), we determine that we must have

$$\pi_1 = p_1 + \frac{B_0}{\mu_0}B_{1x} = 0. \tag{2.71}$$

The reduced set of equations can now be written as

$$\sigma u_x = v^2 i k_x \frac{B_{1x}}{B_0} - v^2 H_B^{-1}\frac{B_{1z}}{B_0}\,, \tag{2.72}$$

$$\sigma u_z = -\frac{g}{\rho_0}\rho_1 + v^2 i k_x \frac{B_{1z}}{B_0}\,, \tag{2.73}$$

$$\sigma B_{1z} = B_0 i k_x u_z\,, \tag{2.74}$$

$$\frac{p_1}{p_0} = \frac{\rho_1}{\rho_0}\,, \tag{2.75}$$

$$p_1 + \frac{B_0}{\mu_0}B_{1x} = 0\,, \tag{2.76}$$

$$\sigma\left(\frac{B_{1x}}{B_0} - \frac{\rho_1}{\rho_0}\right) = i k_x u_x + (H_B^{-1} - H_\rho^{-1})u_z\,, \tag{2.77}$$

where equation (2.77) comes from combining equations (2.65) and (2.68) by eliminating k_y. We see that the derivative terms from these equations also cancel, and hence we are left with purely algebraic expressions; i.e. our set of equations contains no derivatives. Since we have algebraic expressions it is simple enough to eliminate u_x, u_z, B_{1x}, B_{1z}, ρ_1, p_1 to derive the following dispersion relation,

$$\left(s^2 + v^2\right)\sigma^4 + v^2\left(\left(2s^2 + v^2\right)k_x^2 - g(H_B^{-1} - H_\rho^{-1})\right)\sigma^2 + v^4 k_x^2\left(s^2 k_x^2 - g H_B^{-1}\right) = 0\,, \tag{2.78}$$

where $s^2 = p_0/\rho_0$ is the square of the *isothermal* sound speed; note this differs by a factor of γ from the adiabiatic sound speed which we commonly use, denoted by c. This dispersion relation was first derived by Gilman (1970). Note that Gilman's notation for the growth rate, ω, differs from our σ by a factor of $-i$ and hence there is a minus sign difference in the σ^2 term of equation (2.78). Note that equation (2.78) is a depth-dependent dispersion relation. In a physical system, this cannot be true since you can't have a different growth rate at each depth since any unstable eigenmode will necessarily have a finite size in z. Mizerski *et al.* (2013) discusses Gilman's depth-dependent dispersion relation and provides a mathematical explanation by reconciling with the two-point boundary value problem of

the Gilman system.

One can examine this dispersion relation to determine stability conditions. Note that in the absence of a magnetic field we have $v = 0$, and hence the only solution of (2.78) is $\sigma = 0$ and therefore there cannot be instability; i.e. all instabilities must be caused by the magnetic field. It is easy to see that the stability boundary for direct (non-oscillatory) instability, which occurs when $\sigma = 0$, is given by

$$k_x^2 = \frac{g}{s^2} H_B^{-1} = -g \frac{\rho_0}{p_0} \frac{\mathrm{d}}{\mathrm{d}z} \ln B_0 \,. \tag{2.79}$$

i.e. there will be instability if $k_x^2 < g H_B^{-1}/s^2$. This means that, for any magnetic field which decreases with height — and hence H_B^{-1} is positive — there is a wavenumber k_x such that direct instability will take effect, provided that you are in such a situation whereby the assumption of $k_y \to \infty$ is valid.

The inclusion of magnetic diffusion and viscosity can, in certain circumstances, lead to some unexpected behaviour. Specifically, in the presence of magnetic diffusion and viscosity, certain regimes which otherwise would be stable to both magnetic buoyancy and convection can produce a new instability (so-called double-diffusive instability). This is discussed in Chapter 6.

2.5 Rotation

Another important element that has thus far been neglected is rotation. The solar rotation period is approximately 30 days (depending on precisely where you measure). An estimate of the growth time of magnetic buoyancy instability (from the tachocline to the surface) is also approximately 30 days (Hughes, 2007). Since these two timescales are comparable, we would expect rotation to have a significant effect on magnetic buoyancy instability in the solar interior. When rotation is included the system can become far more complicated. Firstly, if we consider a rapidly rotating fluid in the presence of a magnetic field, but ignore any effects of stratification, we will get magneto-Coriolis (MC) waves. Generally MC waves can be divided into two distinct branches, fast MC waves and slow MC waves. Lehnert (1954) considered the situation where the magnetic field and axis of rotation are aligned. This situation makes description of the physical processes easier and while in general the axis of rotation will not be parallel to the magnetic field — this is certainly not the case in much of the Sun — the physical picture remains useful. Simply put, fast MC waves occur when the Lorentz force and Coriolis force act together, whereas slow MC waves occurs when Lorentz force acts against the Coriolis force. This is most easily understood by studying the dispersion relation.

We will derive the MC wave equation for an incompressible fluid at constant angular

frequency $\boldsymbol{\Omega}$ and magnetic field $\mathbf{B} = \mathbf{B}_0 + \mathbf{B}_1$ for background $\mathbf{B}_0$ in the absence of gravity and diffusion. Whilst the majority of this thesis is concerned with magnetic buoyancy, and therefore compressible fluids, we consider an incompressible fluid here to provide the mathematically simplest example to illustrate how MC waves emerge in the presence of rotation. The background is assumed to be uniform and static, and therefore $\mathbf{B}_0$ is constant. We do not make any assumption about the directions of these vectors at this stage. The linearised momentum and induction equations (2.25 – 2.26) in this case can be written as

$$\rho_0 \frac{\partial \mathbf{u}}{\partial t} + 2\rho_0(\boldsymbol{\Omega} \times \mathbf{u}) = -\boldsymbol{\nabla}\pi_1 + \frac{1}{\mu_0}(\mathbf{B}_0 \cdot \boldsymbol{\nabla})\mathbf{B}_1 \,, \tag{2.80}$$

$$\frac{\partial \mathbf{B}_1}{\partial t} = (\mathbf{B}_0 \cdot \boldsymbol{\nabla})\mathbf{u} \,. \tag{2.81}$$

We take the curl of these equations and define the vorticity to be $\boldsymbol{\omega} = \boldsymbol{\nabla} \times \mathbf{u}$ to yield,

$$\rho_0 \frac{\partial \boldsymbol{\omega}}{\partial t} - 2\rho_0(\boldsymbol{\Omega} \cdot \boldsymbol{\nabla})\mathbf{u} = \frac{1}{\mu_0}(\mathbf{B}_0 \cdot \boldsymbol{\nabla})(\boldsymbol{\nabla} \times \mathbf{B}_1) \,, \tag{2.82}$$

$$\frac{\partial}{\partial t}(\boldsymbol{\nabla} \times \mathbf{B}_1) = (\mathbf{B}_0 \cdot \boldsymbol{\nabla})\boldsymbol{\omega} \,. \tag{2.83}$$

We combine these two, by taking the time derivative of equation (2.82) and eliminating $\partial/\partial t(\boldsymbol{\nabla} \times \mathbf{B}_1)$ to get

$$\rho_0 \frac{\partial^2 \boldsymbol{\omega}}{\partial t^2} - 2\rho_0(\boldsymbol{\Omega} \cdot \boldsymbol{\nabla})\frac{\partial \mathbf{u}}{\partial t} = \frac{1}{\mu_0}(\mathbf{B}_0 \cdot \boldsymbol{\nabla})^2 \boldsymbol{\omega} \,. \tag{2.84}$$

We take the curl of this equation to yield

$$-2(\boldsymbol{\Omega} \cdot \boldsymbol{\nabla})\frac{\partial \boldsymbol{\omega}}{\partial t} = \left(\frac{\partial^2}{\partial t^2} - \frac{1}{\mu_0 \rho_0}(\mathbf{B}_0 \cdot \boldsymbol{\nabla})^2 \right) \nabla^2 \mathbf{u} \,, \tag{2.85}$$

where we have recognised that, since $\mathbf{u}$ is incompressible and hence $\boldsymbol{\nabla} \cdot \mathbf{u} = 0$, we can write $\boldsymbol{\nabla} \times \boldsymbol{\omega} = \boldsymbol{\nabla} \times (\boldsymbol{\nabla} \times \mathbf{u}) = -\nabla^2 \mathbf{u}$. To eliminate $\boldsymbol{\omega}$ from this equation we can take the time-derivative of equation (2.84) to derive an equation written entirely in terms of $\mathbf{u}$,

$$-4(\boldsymbol{\Omega} \cdot \boldsymbol{\nabla})^2 \frac{\partial^2 \mathbf{u}}{\partial t^2} = \left(\frac{\partial^2}{\partial t^2} - \frac{1}{\mu_0 \rho_0}(\mathbf{B}_0 \cdot \boldsymbol{\nabla})^2 \right)^2 \nabla^2 \mathbf{u} \,. \tag{2.86}$$

This equation is known as the MC wave equation (Lehnert, 1954; Acheson & Hide, 1973).

To derive a dispersion relation we consider perturbations of the form $\mathbf{u} = \tilde{\mathbf{u}} \exp(i\mathbf{k} \cdot \mathbf{r} + i\omega t)$

(note that ω here is unrelated to the vorticity $\boldsymbol{\omega}$ used earlier), which yields

$$\left(-\omega^2 + \frac{1}{\mu_0\rho_0}(\mathbf{B}_0\cdot\mathbf{k})^2\right)^2 |\mathbf{k}|^2 - 4\omega^2(\boldsymbol{\Omega}\cdot\mathbf{k})^2 = 0\,. \tag{2.87}$$

This is a 4th-order polynomial in ω, so we will get four solutions for ω. However, since it is a biquadratic we can easily solve for ω^2. Rearranging (2.87) for ω^2 we get

$$-\omega^2 + \frac{1}{\mu_0\rho_0}(\mathbf{B}_0\cdot\mathbf{k})^2 = \pm 2\omega\frac{(\boldsymbol{\Omega}\cdot\mathbf{k})}{|\mathbf{k}|}\,. \tag{2.88}$$

We now have two quadratics in ω (one for each sign of the $\pm$) which we can solve with the quadratic formula to get

$$\omega = \pm\frac{(\boldsymbol{\Omega}\cdot\mathbf{k})}{|\mathbf{k}|} \pm \sqrt{\frac{(\boldsymbol{\Omega}\cdot\mathbf{k})^2}{|\mathbf{k}|^2} + \frac{(\mathbf{B}_0\cdot\mathbf{k})^2}{\mu_0\rho_0}}\,. \tag{2.89}$$

Note that the two $\pm$ signs are independent and hence the equation represents four solutions. If we were to consider a situation where the Coriolis effect is much greater than that induced by the magnetic field then we should expect that the result is inertial waves. If we take this limit in equation (2.89) we get

$$\omega = \pm\frac{(\boldsymbol{\Omega}\cdot\mathbf{k})}{|\mathbf{k}|} \pm \frac{(\boldsymbol{\Omega}\cdot\mathbf{k})}{|\mathbf{k}|}\,, \tag{2.90}$$

which is exactly our expected frequency (when we have same-signs in the $\pm$) for inertial waves (Davidson, 2001). We will denote half this quantity by ω_C, i.e.

$$\omega_C^2 = (\boldsymbol{\Omega}\cdot\mathbf{k})^2/|\mathbf{k}|^2. \tag{2.91}$$

Conversely, in a magnetic-dominant situation we would expect (2.89) to recover the Alfvén wave solution. Indeed, in that limit we would get

$$\omega = \pm\frac{1}{\sqrt{\mu_0\rho_0}}(\mathbf{B}_0\cdot\mathbf{k})\,. \tag{2.92}$$

which is exactly the solution of the Alfvén wave dispersion relation (Davidson, 2001). We will denote this frequency by ω_M, defined by

$$\omega_M^2 = \frac{(\mathbf{B}_0\cdot\mathbf{k})^2}{\mu_0\rho_0}. \tag{2.93}$$

Reassuringly, we have seen that in the limits where one of the Coriolis or Lorentz force dominates the other, equation (2.89) recovers the expected solutions. It is in the

intermediate regime where neither force is completely dominant that MC waves occur. If we assume that we are in a sufficiently rapidly rotating system, such that $\omega_C^2 \gg \omega_M^2$, then we can perform a Taylor expansion on the square root term in equation (2.89). Expanding this term and keeping only the first terms we get

$$\omega = \pm\frac{(\mathbf{\Omega}\cdot\mathbf{k})}{|\mathbf{k}|} \pm \frac{(\mathbf{\Omega}\cdot\mathbf{k})}{|\mathbf{k}|}\sqrt{1+\frac{|\mathbf{k}|^2(\mathbf{B}_0\cdot\mathbf{k})^2}{\mu_0\rho_0(\mathbf{\Omega}\cdot\mathbf{k})^2}} \tag{2.94}$$

$$\approx \pm\frac{(\mathbf{\Omega}\cdot\mathbf{k})}{|\mathbf{k}|} \pm \frac{(\mathbf{\Omega}\cdot\mathbf{k})}{|\mathbf{k}|}\left(1+\frac{|\mathbf{k}|^2(\mathbf{B}_0\cdot\mathbf{k})^2}{2\mu_0\rho_0(\mathbf{\Omega}\cdot\mathbf{k})^2}\right). \tag{2.95}$$

It can now be seen how the distinct fast and slow modes come about. If we take the opposing signs in each of the $\pm$ we get slow MC waves with frequency ω_{slow}, given by

$$\omega_{\text{slow}} = \pm\frac{|\mathbf{k}|(\mathbf{B}_0\cdot\mathbf{k})^2}{2\mu_0\rho_0(\mathbf{\Omega}\cdot\mathbf{k})}. \tag{2.96}$$

Otherwise, where each $\pm$ takes the same sign we get fast MC waves with frequency ω_{fast}, given by

$$\omega_{\text{fast}} = \pm\frac{2(\mathbf{\Omega}\cdot\mathbf{k})}{|\mathbf{k}|}\left(1-\frac{|\mathbf{k}|^2(\mathbf{B}_0\cdot\mathbf{k})^2}{4\mu_0\rho_0(\mathbf{\Omega}\cdot\mathbf{k})^2}\right). \tag{2.97}$$

It can be seen from this expression for ω_{fast} that, at least in this rapid rotation regime, we can think of fast MC waves as magnetic-affected inertial waves where the magnetic effect is to slightly alter the frequency of the wave. Slow MC waves are entirely different to both inertial and Alfvén waves — they are slower than both — and only occur in the prescence of both rotation and magnetic field. Slow MC waves have been significantly studied in the field of geophysical fluid dynamics.

In the description outlined above, the effects of density stratification are ignored. When these effects are included the resulting waves are called magnetic Archimedes Coriolis (MAC) waves. Even in the simplest example possible we now have three conflicting sources for waves; we have waves caused by pressure/density gradient (sound/acoustic waves), waves caused by magnetic tension (Alfvén waves), and waves caused by the Coriolis force from rotation (inertial waves). The nature of the resulting MAC waves will vary depending on the particular setup and the relative magnitudes and directions of the three effects.

Chapter 3

Sound-proof models

Throughout fluid dynamics, especially astrophysical fluid dynamics, study of instability is abundant. Many of these instabilities, including convection and magnetic buoyancy, rely on changes in density. For this reason, incompressible equations are unsuitable for study of these instabilities — incompressible equations do not allow for any changes in density. On the other hand, using the compressible equations, those which do allow density perturbations, can also be unsuitable. An unavoidable consequence of using the fully compressible equations is *sound waves* (or *acoustic waves*). Sound waves are density waves (so do not appear in incompressible systems).

As a result, several sound-proof models have been developed to study these systems by removing the sound waves. Specifically, a sound-proof model is one that removes the systems ability to oscillate acoustically. It does this by recognising that sound waves operate on a timescale that is much faster to the dynamics of interest (i.e. convection, magnetic buoyancy, etc.). In practice, there cannot be a model that does this perfectly since there will always be some regime where the assumption that the sound waves are much faster than all dynamics of interest somewhat breaks down. Mathematically, sound-proof models are generally derived by some asymptotic assumptions that justify the neglect of terms in the governing (MHD) equations. This is done in such a way that sound-waves cannot exist. That is that, even in a very simple set-up (no gravity, uniform density and uniform pressure) with the fluid initially at rest, solutions with pressure perturbations oscillating with high frequency do not emerge.

3.1 Sound waves in compressible fluids

To illustrate the problem we will now consider the simplest possible setting in which it is possible to derive sound waves. We start with the fully compressible equations (2.25-2.31), but without any diffusivities (i.e. $Q_1 = 0$), rotation ($\mathbf{\Omega} = \mathbf{0}$), magnetic field ($\mathbf{B} = \mathbf{0}$),

gravity ($g = 0$), or density stratification ($H_s^{-1} \to 0$). Hence, all background quantities are constant. We are left with

$$\rho_0 \frac{\partial}{\partial t}\mathbf{u} = -\boldsymbol{\nabla} p_1 \,, \tag{3.1}$$

$$\frac{\partial}{\partial t}\rho_1 = -\rho_0 \boldsymbol{\nabla}\cdot\mathbf{u} \,, \tag{3.2}$$

$$\rho_1 = \frac{1}{c^2} p_1 \,. \tag{3.3}$$

Let each variable, say f_1, have the form $f_1 = \tilde{f}_1(x, y, z)\exp(i\omega t)$, then we have

$$\rho_0 i\omega\mathbf{u} = -\boldsymbol{\nabla} p_1 \,, \tag{3.4}$$

$$i\omega\rho_1 = -\rho_0 \boldsymbol{\nabla}\cdot\mathbf{u} \tag{3.5}$$

$$\rho_1 = \frac{1}{c^2} p_1 \,, \tag{3.6}$$

where we have immediately omitted tildes. Finally, we eliminate $\mathbf{u}$ and p_1 to get

$$-\omega^2\rho_1 = c^2\boldsymbol{\nabla}\cdot(\boldsymbol{\nabla}\rho_1) = c^2\nabla^2\rho_1 \,, \tag{3.7}$$

which is precisely the wave equation, whose solution will be waves of speed c.

For many astrophysically relevant regimes, including the solar interior which we are interested in here, sound-waves are significantly faster than the dynamics of interest — e.g. convection, magnetic buoyancy etc. We expect that the expected rise-time for a magnetic flux tube to traverse the convection zone by magnetic buoyancy is approximately 30 days, i.e. an average speed of approximately 8×10^3cm s^{-1}, whereas we expect a sound wave to travel at approximately 2×10^7cm s^{-1} (in the tachocline) (Gough, 2007). These fast waves cause issues for computational analysis. Any numerical scheme would track the propagation of sound waves through each cell in the computational grid. Therefore, if the sound speed is faster than other characteristic velocities then a lot of computational work will be spent on resolving waves that likely will not affect the resulting dynamics.

Therefore, a number of so-called *sound-proof* models have been developed. That is, mathematical models that do not allow sound waves to exist. We will discuss and derive a number of these such models, namely the Boussinesq, anelastic and pseudo-incompressible models, in the coming sections.

In general, these models are derived by making some asymptotic assumption about the regime of interest and determining that some terms in the governing equations are negligible. These simplified equations can then be used to study situations where the fully compressible or incompressible equations are unsuitable. However, since each model is derived under strict asymptotic assumptions, they are only strictly valid in that asymptotic

limit. For example, anelastic models are derived by assuming that the background state has almost uniform entropy. Hence, one can only expect anelastic models to be accurate provided they are being used in regimes with almost uniform entropy. However, we often need to be able to describe fluid flows in situations where these asymptotic conditions are not satisfied. This begs the question, when can one actually use these models and when do they produce the "correct" answer — i.e. the same solution as the compressible system. This key question is the primary motivator for this work, applied to the magnetic buoyancy instability in the solar interior. It was previously not known how well these sound-proof models reproduced the linear behaviour of the compressible system for magnetic buoyancy.

We now briefly review the most commonly-used sound-proof models for astrophysical applications: the Boussinesq, anelastic, and pseudo-incompressible models. (We do not consider the family of quasi-hydrostatic models often used to model shallow atmospheres (e.g., Miller & White, 1984; Arakawa & Konor, 2009; Dubos & Voitus, 2014), because these are not suited to describing buoyancy processes with a small horizontal scale, which are the motivation for the present study). We will restrict our discussion to the linear regime and will be neglecting viscosity and magnetic diffusion in all cases. Here, we will present each of these models in the form that they are usually found in the literature; in Section 4.2 we will introduce a very general, linearised sound-proof model for which each of these models arises as a special or limiting case. Throughout this chapter we will be assuming a depth-dependent horizontal background magnetic field, i.e. $\mathbf{B}_0 = B_0(z)\widehat{\mathbf{x}}$.

3.2 Boussinesq approximation

The Boussinesq model was first introduced by Oberbeck (1879) and Boussinesq (1903), and later formalised by Jeffreys (1930). The approximation amounts to assuming that, on small length-scales, pressure variations do not produce significant changes in density. This allows pressure perturbations to be neglected in the relations between other thermodynamic variables, and density variations are neglected everywhere except in the buoyancy force (Spiegel & Veronis, 1960; Mihaljan, 1962; Gray & Giorgini, 1976). As a result, the pressure perturbation effectively acts as a Lagrange multiplier that enforces a zero-divergence constraint on the fluid velocity, i.e. incompressibility. The simplest way to extend the Boussinesq model to include a magnetic field is simply to add the Lorentz force to the momentum equation, and simultaneously solve the magnetic induction equation in its usual MHD form, i.e. equation (2.14). However, this alone does not capture the effects of magnetic buoyancy since, in this formulation, density perturbations can only be brought about by change in temperature. Spiegel & Weiss (1982) extended the Boussinesq model to include magnetic buoyancy by (a) assuming small variations to the *total* (i.e. gas plus magnetic) pressure, and (b) allowing for density variations in the induction equation.

This magneto-Boussinesq approximation was later re-derived more rigorously by Corfield (1984). Crucially, the magneto-Boussinesq model allows for magnetic pressure to play a significant role. In the original magnetic Boussinesq model (or, *Boussinesq equations of magneto-convection*) both the gas pressure and magnetic pressure are individually negligible. In the magneto-Boussinesq equations however, gas pressure and magnetic pressure are not individually small but are of similar size such that their sum is small; i.e. they cancel at leading order.

We will now derive the magneto-Boussinesq equations, starting from the linearised equations (2.25 – 2.31). We follow Corfield's derivation by introducing two small parameters, ϵ_1 and ϵ_2, and assuming the following hierarchy of length-scales,

$$\epsilon_1 \boldsymbol{\nabla}_\perp \sim k_x \sim H_\rho^{-1} \sim H_B^{-1} \sim \frac{\epsilon_1}{\epsilon_2} H_s^{-1}, \tag{3.8}$$

where the subscript $\perp$ refers to the components perpendicular to the magnetic field $\mathbf{B}_0 = B_0(z)\widehat{\mathbf{x}}$ and k_x represents the wavenumber in the x-direction. We also assume that the timescale is set by the buoyancy frequency, i.e.

$$\frac{\partial}{\partial t} \sim N = \sqrt{g H_s^{-1}}\,, \tag{3.9}$$

and that the ratio of Alfvén speed to sound speed satisfies

$$\frac{v^2}{c^2} \sim \frac{\epsilon_2}{\epsilon_1}\,. \tag{3.10}$$

The magneto-Boussinesq model is obtained by adopting the ordering $\epsilon_2 \ll \epsilon_1 \ll 1$, which implies that $v^2 \ll c^2$. With these scalings in mind we can re-write the continuity equation (2.27) as

$$\begin{aligned} \frac{\partial \rho_1}{\partial t} &= -\boldsymbol{\nabla}\cdot(\rho_0 \mathbf{u}) \\ \implies \quad -\frac{1}{\rho_0}\frac{\partial \rho_1}{\partial t} &= \boldsymbol{\nabla}\cdot\mathbf{u} + \frac{1}{\rho_0}\frac{\mathrm{d}\rho_0}{\mathrm{d}z} u_z \\ \implies \quad \underbrace{\boldsymbol{\nabla}_\perp \cdot \mathbf{u}_\perp}_{O(1)} &= \underbrace{H_\rho^{-1} u_z - \mathrm{i}k_x u_x}_{O(\epsilon_1)} - \underbrace{\frac{1}{\rho_0}\frac{\partial \rho_1}{\partial t}}_{O(\epsilon_2)}\,, \end{aligned} \tag{3.11}$$

and the induction equation (2.26) as

$$\begin{aligned} \frac{\partial}{\partial t}\mathbf{B}_1 &= \boldsymbol{\nabla}\times(\mathbf{u}\times\mathbf{B}_0) \\ \implies \frac{\partial}{\partial t}\mathbf{B}_1 &= (\mathbf{B}_0\cdot\boldsymbol{\nabla})\mathbf{u} - (\boldsymbol{\nabla}\cdot\mathbf{u})\mathbf{B}_0 - \frac{\mathrm{d}B_0}{\mathrm{d}z}u_z\widehat{\mathbf{x}} \\ \implies \underbrace{(\boldsymbol{\nabla}_\perp\cdot\mathbf{u}_\perp)\mathbf{B}_0}_{O(1)} &= \underbrace{(\mathbf{B}_0\cdot\boldsymbol{\nabla})\mathbf{u} + (H_B^{-1}u_z - \mathrm{i}k_x u_x)\mathbf{B}_0 - \frac{\partial\mathbf{B}_1}{\partial t}}_{O(\epsilon_1)}, \end{aligned} \tag{3.12}$$

where the relative magnitudes of $\mathbf{u}$, ρ_1 and $\mathbf{B}_1$ are inferred from the momentum equation (2.25). At leading order, these two equations contain the same information, and so it is necessary to consider the terms of order ϵ_1. This can be done by eliminating the $O(1)$ terms, resulting in

$$\boldsymbol{\nabla}_\perp\cdot\mathbf{u}_\perp = 0, \tag{3.13}$$

$$\frac{\partial\mathbf{B}_1}{\partial t} = (\mathbf{B}_0\cdot\boldsymbol{\nabla})\mathbf{u} + (H_B^{-1} - H_\rho^{-1})u_z\mathbf{B}_0. \tag{3.14}$$

Therefore the fields $\mathbf{u}_\perp$ and $\mathbf{B}_{1\perp}$ are solenoidal under this approximation, but not the full fields $\mathbf{u}$ and $\mathbf{B}_1$. If we compare the relative magnitudes of, for example, $g\rho_1\widehat{\mathbf{z}}$ with $\boldsymbol{\nabla}p_1$, in equation (2.25), then we determine that $g\rho_1\widehat{\mathbf{z}} \sim \epsilon_1\boldsymbol{\nabla}p_1$ (where the relative magnitudes of ρ_1 and p_1 are determined by equation (2.31)). By similar comparisons with the other terms in equation (2.25) we determine that both $\boldsymbol{\nabla}p_1$ and $\boldsymbol{\nabla}(1/\mu_0)\mathbf{B}_0\cdot\mathbf{B}_1$ are a factor of ϵ_1 larger than the other terms. Therefore, in order for the pressure term, $\boldsymbol{\nabla}\pi$, not to dominate over the other terms in (2.25), the total pressure perturbation, π_1, must be smaller than both the individual perturbations of gas pressure, p_1, and magnetic pressure, $(1/\mu_0)\mathbf{B}_0\cdot\mathbf{B}_1$, by a factor of ϵ_1. In other words, these two contributions to the total pressure must cancel at leading order, with

$$p_1 + \frac{1}{\mu_0}\mathbf{B}_0\cdot\mathbf{B}_1 = 0. \tag{3.15}$$

This means that π_1 simply becomes a Lagrange multiplier in the magneto-Boussinesq model, and is mathematically independent of the other perturbed quantities.

The resulting equations can then be written as

$$\rho_0 \frac{\partial}{\partial t}\mathbf{u} + 2\rho_0 \boldsymbol{\Omega} \times \mathbf{u} = -g\rho_1 \widehat{\mathbf{z}} - \boldsymbol{\nabla}_\perp \pi_1 + \frac{1}{\mu_0}\mathbf{B}_0 \cdot \boldsymbol{\nabla}\mathbf{B}_1 - \frac{1}{\mu_0} H_B^{-1} B_{1z}\mathbf{B}_0 \,, \tag{3.16}$$

$$\frac{\partial}{\partial t}\mathbf{B}_1 = (\mathbf{B}_0 \cdot \boldsymbol{\nabla})\mathbf{u} + (H_B^{-1} - H_\rho^{-1}) u_z \mathbf{B}_0 \,, \tag{3.17}$$

$$\boldsymbol{\nabla}_\perp \cdot \mathbf{u} = 0 \,, \tag{3.18}$$

$$\frac{\partial}{\partial t} s_1 + \mathbf{u} \cdot \boldsymbol{\nabla} s_0 = \frac{Q_1}{\rho_0 T_0}, \tag{3.19}$$

$$p_1 + \frac{1}{\mu_0}\mathbf{B}_0 \cdot \mathbf{B}_1 = 0 \,, \tag{3.20}$$

in addition to the thermodynamic relations (2.30)–(2.31) — except that the coefficients in these equations are usually taken to be constant. Here, ρ_0, T_0 and $\mathbf{B}_0$ are taken to be constant, and where the subscript $\perp$ represents components that are perpendicular to $\mathbf{B}_0$. The $\perp$ subscript is required in equation (3.16) since, as per our scaling assumption (see equation 3.8), the x-derivative is significantly smaller than the other components and therefore is neglected. The usual solenoidality condition for the magnetic field is replaced by $\boldsymbol{\nabla}_\perp \cdot \mathbf{B}_1 = 0$. Here, despite π_1 cancelling at leading order, as per equation (3.20), it is retained in the momentum equation as a Lagrange multiplier (which is independent of other quantities) and enforces the zero-divergence constraint on the velocity. The fact that the orientation of the magnetic field must be known *a priori* makes the magneto-Boussinesq model unsuitable for numerical simulations with complex field geometries.

For later convenience we present an alternative formulation of equations (3.16 – 3.20) now:

$$\rho_0 \frac{\partial}{\partial t}\mathbf{u} + 2\rho_0 \boldsymbol{\Omega} \times \mathbf{u} = -\left[\frac{1}{c^2} p_1 + \left(\frac{\partial \rho}{\partial s}\right)_p s_1\right] g\widehat{\mathbf{z}} - \boldsymbol{\nabla}_\perp \pi_1 + \frac{1}{\mu_0}\mathbf{B}_0 \cdot \boldsymbol{\nabla}\mathbf{B}_1 + \frac{1}{\mu_0}\mathbf{B}_1 \cdot \boldsymbol{\nabla}\mathbf{B}_0 \,, \tag{3.21}$$

$$\frac{\partial}{\partial t}\mathbf{B}_1 = \boldsymbol{\nabla} \times (\mathbf{u} \times \mathbf{B}_0) \,, \tag{3.22}$$

$$\boldsymbol{\nabla} \cdot \mathbf{u} = H_\rho^{-1} u_z \,, \tag{3.23}$$

$$\left(\frac{\partial \rho}{\partial s}\right)_p \frac{\partial}{\partial t} s_1 - \rho_0 H_s^{-1} u_z = \left(\frac{\partial \rho}{\partial T}\right)_p \frac{Q_1}{\rho_0 c_p}, \tag{3.24}$$

$$p_1 + \frac{1}{\mu_0}\mathbf{B}_0 \cdot \mathbf{B}_1 = 0 \,, \tag{3.25}$$

$$\left(\frac{\partial \rho}{\partial T}\right)_p T_1 = \left(\frac{\partial \rho}{\partial s}\right)_p s_1 - \frac{\gamma - 1}{c^2} p_1 \,. \tag{3.26}$$

Equation (3.16) is easily recovered from (3.21) by re-introducing ρ_1 by $\rho_1 = (1/c^2)p_1 + (\partial\rho/\partial s)_p\, s_1$ (equation 2.31) and by recalling the definition of H_B^{-1} — equation (2.23).

Equation (3.17) is recovered from (3.22) by expanding $\boldsymbol{\nabla} \times (\mathbf{u} \times \mathbf{B}_0) = (\mathbf{B}_0 \cdot \boldsymbol{\nabla})\mathbf{u} - (\boldsymbol{\nabla} \cdot \mathbf{u})\mathbf{B}_0 - (\mathrm{d}B_0/\mathrm{d}z)u_z\widehat{\mathbf{x}}$, eliminating $\boldsymbol{\nabla} \cdot \mathbf{u}$ by (3.23), and introducing H_B^{-1} by (2.23). Equation (3.24) is a re-scaling of (3.19) where we have also introduced H_s^{-1} by (2.22). Recall that the fields $\mathbf{u}_\perp$ and $\mathbf{B}_{1\perp}$ are solenoidal under this approximation, but not the full fields $\mathbf{u}$ and $\mathbf{B}_1$. This inherent anisotropy makes the magneto-Boussinesq approximation unsuitable for many practical applications, and here we have retained all components of $\mathbf{u}$ and $\mathbf{B}_1$ in the velocity constraint and induction equation.

3.3 Anelastic models

The anelastic model was first introduced by Ogura & Phillips (1962), extending earlier work by Batchelor (1954). They showed that the small length-scale assumption, which allows density perturbations to be neglected everywhere except in the buoyancy term in the Boussinesq model, can be dropped provided that the fluid has almost uniform specific entropy. Their model formally assumes small (though nonlinear) perturbations to a background state with exactly uniform entropy, i.e. adiabatic stratification. Such a state is rarely achieved in any physical system, however, and many subsequent works have therefore adapted the anelastic model to allow the specific entropy to be a slowly varying function of altitude (e.g. Gough, 1969; Gilman & Glatzmaier, 1981; Lipps & Hemler, 1982). These different formulations are equivalent only in the asymptotic limit of adiabatic stratification. Generally, the term "anelastic" is used to refer to any fluid model in which the continuity equation (2.15) is replaced with a velocity constraint

$$\boldsymbol{\nabla} \cdot (\rho_0 \mathbf{u}) = 0, \tag{3.27}$$

where $\rho_0(z)$ represents the density of the background state (Braginsky & Roberts, 2007). While anelastic models were first derived in the absence of magnetic fields, they can be easily extended to include a magnetic field, provided that $v \ll c$; the only change is that the Lorentz force now appears in the momentum equation (Glatzmaier, 1984). The induction equation retains its flux-conservative form (2.14), so $\boldsymbol{\nabla} \cdot \mathbf{B}$ remains exactly zero.

Here, we will consider two particular formulations of the anelastic model. Following Wood & Bushby (2016), we refer to these as GGG (after Gough (1969); Gilman & Glatzmaier (1981)) and LBR (after Lantz (1992); Braginsky & Roberts (1995)). These two versions of the anelastic model will be derived in the following subsections.

In the coming chapters we will study how accurately the anelastic approximation captures magnetic buoyancy. Fan (2001) verified that the anelastic model has the correct stability properties in the asymptotic limit in which it is formally valid, i.e. for $v \ll c$ and adiabatic stratification. However, since Fan's analysis only considered the ideal equations it does not differentiate between the GGG and LBR implementations. Berkoff *et al.*

(2010) have compared these two formulations of the anelastic approximation, finding that while both produce consistent results for a background state of nearly uniform entropy, they differ under more general conditions. Wilczyński *et al.* (2022) studied, amongst others, a similar question to one that we consider in this thesis — under what constraints does the anelastic model accurately capture the effects of magnetic buoyancy instability? They found that the anelastic model agrees well with the fully compressible result under the theoretical conditions for the anelastic model — i.e. nearly adiabatic stratification and magnetic pressure is small. If these conditions are violated then Wilczyński *et al.* found that agreement breaks down and then anelastic model no longer captures the fully compressible result well.

3.3.1 Gough, Gilman & Glatzmaier anelastic

As with the Boussinesq model, we begin with the linearised fully compressible equations (2.25 – 2.31). For the GGG anelastic model, all (non-magnetic) terms are retained apart from the left-hand side of the continuity equation (2.27), which therefore reduces to the "anelastic equation",

$$\boldsymbol{\nabla} \cdot (\rho_0 \mathbf{u}) = 0 \,. \tag{3.28}$$

This approximation can be justified by assuming that the perturbations have a length-scale that is comparable to the density scale height, H_ρ, and a timescale, τ, that is much longer than the acoustic timescale, H_ρ/c. Under these assumptions, and assuming that the buoyancy force is of the same order as the fluid acceleration in equation (2.25), the left-hand side of equation (2.27) is found to be of order M^2, where $M \equiv H_\rho/(c\tau) \ll 1$ is the Mach number. However, in order for both terms on the left-hand side of equation (2.28) to be of the same order, the timescale must be of order $\tau \sim \sqrt{H_s/g} \equiv 1/N$, where N is the buoyancy frequency. For consistency, we therefore require that $H_s \sim H_\rho/M^2 \gg H_\rho$, i.e. the background state must have nearly uniform entropy. Moreover, in the anelastic approximation the background state is usually taken to be non-magnetic, with the entire magnetic field regarded as a small perturbation. This requires that the total magnetic pressure force is negligible in comparison with gravity, i.e. that $g \gg v^2/H_B$. Therefore, at leading order, equation (2.20) becomes simply

$$g = c^2/H_\rho \,. \tag{3.29}$$

Although the anelastic approximation is formally valid only when $H_s \gg H_\rho$, it is quite often used in situations where this condition does not apply (which partly motivates the present study).

For later convenience, we present a formulation of the GGG anelastic equations as

$$\rho_0 \frac{\partial}{\partial t}\mathbf{u} + 2\rho_0 \boldsymbol{\Omega} \times \mathbf{u} = -\left[\frac{1}{c^2}p_1 + \left(\frac{\partial \rho}{\partial s}\right)_p s_1\right] g\widehat{\mathbf{z}} - \boldsymbol{\nabla}\pi_1 + \frac{1}{\mu_0}\mathbf{B}_0 \cdot \boldsymbol{\nabla}\mathbf{B}_1 + \frac{1}{\mu_0}\mathbf{B}_1 \cdot \boldsymbol{\nabla}\mathbf{B}_0\,, \tag{3.30}$$

$$\frac{\partial}{\partial t}\mathbf{B}_1 = \boldsymbol{\nabla} \times (\mathbf{u} \times \mathbf{B}_0)\,, \tag{3.31}$$

$$\boldsymbol{\nabla} \cdot \mathbf{u} = H_\rho^{-1} u_z\,, \tag{3.32}$$

$$\left(\frac{\partial \rho}{\partial s}\right)_p \frac{\partial}{\partial t} s_1 - \rho_0 H_s^{-1} u_z = \left(\frac{\partial \rho}{\partial T}\right)_p \frac{Q_1}{\rho_0 c_p}, \tag{3.33}$$

$$\pi_1 = p_1 + \frac{1}{\mu_0}\mathbf{B}_0 \cdot \mathbf{B}_1\,, \tag{3.34}$$

$$\left(\frac{\partial \rho}{\partial T}\right)_p T_1 = \left(\frac{\partial \rho}{\partial s}\right)_p s_1 - \frac{\gamma - 1}{c^2} p_1\,, \tag{3.35}$$

where we have eliminated ρ_1 by $\rho_1 = (\partial\rho/\partial s)_p\, s_1 + (1/c^2)p_1$, and replaced the full continuity equation by the anelastic equation (3.28).

3.3.2 Lantz, Braginsky & Roberts anelastic

The LBR model makes an additional approximation, to that of GGG anelastic, by replacing temperature diffusion with entropy diffusion. Without approximation, the pressure and gravity terms in the momentum equation (2.25) can be re-written as

$$-\rho_1 g\widehat{\mathbf{z}} - \boldsymbol{\nabla} p_1 = \rho_0 \left(-\boldsymbol{\nabla}\left(\frac{p_1}{\rho_0}\right) + \frac{1}{\rho_0}\left[H_\rho^{-1} - \frac{g}{c^2}\right] p_1 \widehat{\mathbf{z}} - \frac{1}{\rho_0}\left(\frac{\partial \rho}{\partial s}\right)_p s_1 g\widehat{\mathbf{z}}\right). \tag{3.36}$$

Under the conditions inherent in the anelastic approximation, i.e. equation (3.29), the term involving $\left[H_\rho^{-1} - g/c^2\right]$ is negligible. With this term neglected, the equations have a very similar mathematical form to the Boussinesq equations, except that ρ_0 is not constant. In particular, in the absence of diabatic processes (i.e. with $Q_1 = 0$) the pressure perturbation p_1 appears only in the gradient term in the momentum equation, meaning that it does not need to be calculated explicitly. However, this analogy with the Boussinesq approximation breaks down when thermal relaxation is included (i.e. with $Q_1 \neq 0$), because the temperature perturbation, T_1, depends on p_1 via equation (2.30). If the p_1 term in equation (2.30) is neglected, the analogy with the Boussinesq equations is restored. This point was independently discovered by Lantz (1992) and Braginsky & Roberts (1995), so we refer to the resulting equations as the LBR approximation. Whereas Lantz considered this merely as a mathematical convenience, Braginsky & Roberts justified it by arguing that, in a convective system, it is entropy gradients rather than temperature gradients that drive

the flow of heat; in this sense, omitting the p_1 term in equation (2.30), and thus replacing temperature diffusion with entropy diffusion, can be regarded as a mean-field prescription for the heat transport by small-scale convection. More recently, Pauluis (2008) has shown that this approximation is also necessary for "thermodynamic consistency", i.e. to make the anelastic equations consistent with the laws of thermodynamics.

In fact, a system of equations mathematically identical to the LBR model was earlier obtained by Lipps & Hemler (1982) under slightly different assumptions. Lipps & Hemler (1982) carried out a scale analysis in the context of deep moist convection in the atmosphere. They assumed that the timescale is set by the buoyancy frequency (as in the Boussinesq approximation) and assumed that the background potential temperature was a slowly varying function of height/depth. They considered perturbations with a length-scale $\ll H_\rho \sim H_s$, but retained some next-to-leading-order terms in the resulting equations. Under these conditions it can be shown that the p_1 term in equation (2.30) is negligible, much as in the Boussinesq approximation.

If the anelastic approximation is used in circumstances where the background state is not close to adiabatic, then the neglect of the $\left[H_\rho^{-1} - g/c^2\right]$ term in equation (3.36) makes a material difference to the results.

The LBR equations have the benefit that they can be solved without explicitly calculating either pressure or temperature, and for this reason the LBR model has become the standard implementation in astrophysical applications (Jones *et al.*, 2011).

We will present the LBR equations here for future reference,

$$\rho_0 \frac{\partial}{\partial t}\mathbf{u} + 2\rho_0 \boldsymbol{\Omega} \times \mathbf{u} = -\left[\frac{H_\rho^{-1}}{g} p_1 + \left(\frac{\partial \rho}{\partial s}\right)_p s_1\right] g\widehat{\mathbf{z}} - \boldsymbol{\nabla}\pi_1 + \frac{1}{\mu_0}\mathbf{B}_0 \cdot \boldsymbol{\nabla}\mathbf{B}_1 + \frac{1}{\mu_0}\mathbf{B}_1 \cdot \boldsymbol{\nabla}\mathbf{B}_0\,, \tag{3.37}$$

$$\frac{\partial}{\partial t}\mathbf{B}_1 = \boldsymbol{\nabla} \times (\mathbf{u} \times \mathbf{B}_0)\,, \tag{3.38}$$

$$\boldsymbol{\nabla} \cdot \mathbf{u} = H_\rho^{-1} u_z\,, \tag{3.39}$$

$$\left(\frac{\partial \rho}{\partial s}\right)_p \frac{\partial}{\partial t} s_1 - \rho_0 H_s^{-1} u_z = \left(\frac{\partial \rho}{\partial T}\right)_p \frac{Q_1}{\rho_0 c_p}, \tag{3.40}$$

$$\pi_1 = p_1 + \frac{1}{\mu_0}\mathbf{B}_0 \cdot \mathbf{B}_1\,, \tag{3.41}$$

$$\left(\frac{\partial \rho}{\partial T}\right)_p T_1 = \left(\frac{\partial \rho}{\partial s}\right)_p s_1\,, \tag{3.42}$$

where we have made use of equation (3.36) in the momentum equation and neglected the $\left[H_\rho^{-1} - g/c^2\right]$ term. We have also replaced the full continuity equation by the anelastic equation (3.28), and neglected the p_1 term in the T_1 equation (3.42) — for reasons explained in the text following equation (3.36). Recall that Q_1 represents perturbations to

the diabatic heating, which would ordinarily include temperature diffusion. Given our form of equation (3.42) this could be re-written as entropy diffusion.

3.4 Pseudo-incompressible model

The pseudo-incompressible model was originally derived by Durran (1989) as an improvement upon the anelastic model, although it can also be viewed as a generalisation of earlier "low Mach number" models to include stratification (Rehm & Baum, 1978). Anelastic models do not allow density perturbations to effect the mass-balance. However, the pseudo-incompressible model accounts for density perturbations, arising from changes in temperature, to effect the mass-balance. This means that the fluid expands in response to heating. (In the anelastic model, by contrast, the expansion of fluid elements is dictated by the density of their surroundings, ρ_0.) The pseudo-incompressible approximation was derived, in the absence of magnetic field, with atmospheric flows in mind. Specifically, Durran (1989) advocates for using the pseudo-incompressible model in strongly stable regions where the pseudo-incompressible is more accurate than the anelastic model. Similar to the anelastic model, the pseudo-incompressible model is asymptotically valid in the limit where the background state is adiabatically stratified, but it retains terms that are formally negligible in this limit. A detailed discussion on the asymptotic validity of the anelastic and pseudo-incompressible models can be found in Klein *et al.* (2010). A key feature of the pseudo-incompressible model is that the velocity satisfies an inhomogeneous constraint of the form

$$\boldsymbol{\nabla}\cdot\mathbf{u} = \frac{g}{c^2}u_z - \left(\frac{\partial\rho}{\partial T}\right)_p \frac{Q}{\rho^2 c_p}\,, \tag{3.43}$$

where we have used the same notation as in Section 2.2.1.

A generalisation of the pseudo-incompressible model that exactly obeys the laws of thermodynamics was presented by Klein & Pauluis (2012). Subsequently, Vasil *et al.* (2013) showed that the pseudo-incompressible approximation can be derived very efficiently using Lagrangian dynamics, either by imposing a constraint on the fluid pressure or, equivalently, by linearising the fluid action in the pressure variable. This derivation can be generalised to include non-ideal physics (Gay-Balmaz, 2019) and a time-dependent background state (Snodin & Wood, 2022). Vasil *et al.* also obtained an MHD extension of the pseudo-incompressible model, by imposing a constraint on the total (i.e. gas plus magnetic) pressure. The resulting momentum equation has the form

$$\rho\frac{\mathrm{D}\mathbf{u}}{\mathrm{D}t} + 2\rho\,\boldsymbol{\Omega}\times\mathbf{u} = -\boldsymbol{\nabla}(\pi_0+\pi_1) - g\rho\widehat{\mathbf{z}} + \mathbf{B}\cdot\boldsymbol{\nabla}\mathbf{H} + \frac{\pi_1\boldsymbol{\nabla}\pi_0}{\rho(c^2+v^2)}\,, \tag{3.44}$$

where $\pi_0(\mathbf{x})$ is the total background pressure and where

$$\mathbf{H} \equiv \left(1 + \frac{\pi_1}{\rho(c^2 + v^2)}\right) \frac{\mathbf{B}}{\mu_0}\,. \tag{3.45}$$

The form of equation (3.44) can be derived by considering a variational derivation of the governing equations subject to the constraint that total pressure is small; see Vasil *et al.* (2013). This must be solved together with a complicated velocity constraint. In the absence of diabatic terms (i.e. for $Q = 0$), this constraint is

$$\rho(c^2 + v^2)\boldsymbol{\nabla} \cdot \mathbf{u} + \mathbf{u} \cdot \boldsymbol{\nabla}\pi_0 = \frac{1}{\mu_0}(\mathbf{B} \cdot \boldsymbol{\nabla}\mathbf{u}) \cdot \mathbf{B}\,. \tag{3.46}$$

In the absence of magnetic field (i.e. with $\mathbf{B} = \mathbf{0}$, $v = 0$ and $\pi = p$) these equations reduce to the pseudo-incompressible model of Klein & Pauluis (2012).

The main advantage of this model is that, owing to its variational derivation, it is guaranteed to conserve energy. However, the complexity of the equations makes solving them difficult, and the asymmetric form of the Lorentz force in equation (3.44) has no simple physical explanation.

The derivation performed by Vasil *et al.* does not make any assumption about the relative magnitudes of the sound speed, c, and the Alfvén speed, v, but in the solar interior we expect that $v \ll c$. In the following subsection, we show that this extra condition can be explicitly incorporated into the variational derivation, ultimately leading to a pseudo-incompressible MHD model in which the Lorentz force retains its usual form, i.e. we have the momentum equation,

$$\rho\frac{\mathrm{D}\mathbf{u}}{\mathrm{D}t} + 2\rho\,\boldsymbol{\Omega} \times \mathbf{u} = -\boldsymbol{\nabla}(p_0 + p_1) - g\rho\widehat{\mathbf{z}} + \frac{1}{\mu_0}(\boldsymbol{\nabla} \times \mathbf{B}) \times \mathbf{B} + \frac{p_1}{\rho c^2}\boldsymbol{\nabla}p_0\,, \tag{3.47}$$

and the velocity constraint takes the same form as equation (3.43). It is this version of the pseudo-incompressible equations that we will consider in our study.

3.4.1 Variational derivation of MHD pseudo-incompressible Model

To our knowledge, there has not been a formal (i.e. rigorous asymptotic) derivation of the pseudo-incompressible model that includes magnetic fields. An MHD version has been derived by Vasil *et al.* (2013) using variational methods, but this resulted in a non-standard form of the Lorentz force. The derivation of Vasil *et al.* (2013) assumed that perturbations to the total magnetic pressure remain small, but made no explicit assumption about the magnitude of the Alfvén speed, v, relative to the sound speed, c. Here we will present a variational derivation of the MHD pseudo-incompressible model in which the smallness of v/c is used to further simplify the action. By making use of variational methods we

necessarily neglect any diabatic processes, such as diffusion. For simplicity we will also neglect rotation.

We begin by deriving the governing equations describing a fully compressible fluid under the MHD approximation by considering the action

$$\mathcal{S} = \iint \left[\tfrac{1}{2}\rho|\mathbf{u}|^2 - \rho\Phi - \frac{|\mathbf{B}|^2}{2\mu_0} - \rho U(\rho, s) \right] \mathrm{d}^3\mathbf{x}\,\mathrm{d}t\,, \tag{3.48}$$

where $\Phi(\mathbf{x})$ is the gravitational potential, which we take to be fixed, and U is the specific internal energy, expressed in terms of its natural variables, ρ and s. To derive the equations of motion we apply Hamilton's principle of stationary action, expressing the variations in ρ, s, $\mathbf{u}$ and $\mathbf{B}$ in terms of the Lagrangian displacement, $\boldsymbol{\xi}$:

$$\delta\rho = -\boldsymbol{\nabla}\cdot(\rho\boldsymbol{\xi})\,, \quad \delta s = -\boldsymbol{\xi}\cdot\boldsymbol{\nabla} s\,, \quad \delta\mathbf{u} = \frac{\partial\boldsymbol{\xi}}{\partial t} + \mathbf{u}\cdot\boldsymbol{\nabla}\boldsymbol{\xi} - \boldsymbol{\xi}\cdot\boldsymbol{\nabla}\mathbf{u}\,, \quad \delta\mathbf{B} = \boldsymbol{\nabla}\times(\boldsymbol{\xi}\times\mathbf{B}) \tag{3.49}$$

(Newcomb, 1962; Lundgren, 1963). After integrating by parts, and neglecting surface contributions, the first variation of the action $\mathcal{S}$ is found to be

$$\delta\mathcal{S} = \iint \left[-\frac{\partial}{\partial t}(\rho\mathbf{u}) - \boldsymbol{\nabla}\cdot(\rho\mathbf{u}\otimes\mathbf{u}) - \boldsymbol{\nabla} p - \rho\boldsymbol{\nabla}\Phi + \frac{1}{\mu_0}(\boldsymbol{\nabla}\times\mathbf{B})\times\mathbf{B} \right] \cdot\boldsymbol{\xi}\,\mathrm{d}^3\mathbf{x}\,\mathrm{d}t\,, \tag{3.50}$$

where $p \equiv \rho^2\partial U/\partial\rho$ is the fluid pressure, and where $\otimes$ represents the tensor product. Hamilton's principle requires that $\delta\mathcal{S} = 0$ for all possible displacements $\boldsymbol{\xi}$, and hence we deduce the momentum equation for the fluid. Moreover, the form of expressions (3.49) builds in the conservation of mass, entropy and magnetic flux in their usual forms. (Because the relations (3.49) do not contain any explicit time dependence, we can simply replace $\delta \to \partial/\partial t$ and $\boldsymbol{\xi} \to \mathbf{u}$.) We thus arrive at the fully compressible MHD equations:

$$\rho\frac{\mathrm{D}\mathbf{u}}{\mathrm{D}t} = -\boldsymbol{\nabla} p - \rho\boldsymbol{\nabla}\Phi + \frac{1}{\mu_0}(\boldsymbol{\nabla}\times\mathbf{B})\times\mathbf{B}\,, \tag{3.51}$$

$$\frac{\partial\mathbf{B}}{\partial t} = \boldsymbol{\nabla}\times(\mathbf{u}\times\mathbf{B})\,, \tag{3.52}$$

$$\frac{\mathrm{D}\rho}{\mathrm{D}t} + \rho\boldsymbol{\nabla}\cdot\mathbf{u} = 0\,, \tag{3.53}$$

$$\frac{\mathrm{D}s}{\mathrm{D}t} = 0\,, \tag{3.54}$$

where $\mathrm{D}/\mathrm{D}t \equiv \partial/\partial t + \mathbf{u}\cdot\boldsymbol{\nabla}$ is the material derivative.

Vasil *et al.* (2013) showed that, in the non-magnetic case, the pseudo-incompressible model can be derived by first making a Legendre transformation (that is, a mathematical transformation on a convex function, which here amounts to transforming from one variable to a conjugate variable — for the mathematical theory underpinning Legendre transforms see, for example, Rockafellar (1970)) from specific internal energy, $U(\rho, s)$,

to enthalpy, $H(p,s) \equiv U + p/\rho$, while introducing the pressure, $p \equiv \rho^2\,\partial U/\partial\rho$, as an additional independent variable, and then linearising the action about a fixed reference pressure, $p_0(\mathbf{x})$. To generalise this argument to a magnetised fluid, we must first recognise that it is perturbations to the *total* pressure, π, that are expected to be small. We therefore begin by introducing π as an additional variable in the action, by making an appropriate Legendre transformation. Generalising the thermodynamic definition of p, we can write

$$\pi \equiv \rho^2 \frac{\partial \tilde{U}}{\partial \rho}\,, \tag{3.55}$$

where $\tilde{U}(\rho, s, s_B)$ is the effective internal energy,

$$\tilde{U}(\rho, s, s_B) = U(\rho, s) + \rho\, s_B\,, \tag{3.56}$$

and

$$s_B \equiv \frac{|\mathbf{B}|^2}{2\mu_0\rho^2} \tag{3.57}$$

is the "magnetic entropy", note that s_B has different units from specific entropy — s_B has units of (specific) energy per unit denisty rather than the usual (specific) energy per unit temperature. The second derivative of $\tilde{U}$ with respect to $1/\rho$ is readily found to be $\rho^2(c^2 + v^2)$, which is strictly positive, and so $\tilde{U}$ is a convex function of $1/\rho$. We can therefore define the effective enthalpy via the Legendre transformation

$$\tilde{H}(\pi, s, s_B) \equiv \tilde{U}(\rho, s, s_B) + \pi/\rho\,, \tag{3.58}$$

by analogy with the non-magnetic case. We note that, in general, it is not possible to express the function $\tilde{H}(\pi, s, s_B)$ analytically, even when the equation of state $U(\rho, s)$ is known, but nonetheless this function is well-defined. With these definitions, we can now write the Lagrangian density as

$$\mathcal{L} = \tfrac{1}{2}\rho|\mathbf{u}|^2 - \rho\Phi - \rho\tilde{H}(\pi, s, s_B) + \pi\,. \tag{3.59}$$

We emphasize that, up to this point, no approximation has been made; if we apply Hamilton's principle to this action, regarding π as an independent variable, then we eventually obtain the fully compressible equation of motion as well as the equation of state,

$$\frac{1}{\rho} = \frac{\partial \tilde{H}}{\partial \pi}\,. \tag{3.60}$$

We can now reproduce the pseudo-incompressible MHD model of Vasil *et al.* (2013) by writing the total pressure in equation (3.59) as $\pi = \pi_0(\mathbf{x}) + \pi_1$, where $\pi_0(\mathbf{x})$ is a fixed reference pressure, and neglecting terms that are nonlinear in π_1. However, with this

approach the contributions to the pressure from the fluid and from the magnetic field are treated on an equal footing, whereas in reality we expect the magnetic pressure to be only a small perturbation to a non-magnetic reference state; this is equivalent to the assumption that $v \ll c$. We will therefore make a double approximation in which we write $\pi = p_0(\mathbf{x}) + \pi_1$ and then neglect terms that are nonlinear in π_1 or s_B. The Lagrangian density then becomes

$$\mathcal{L} = \tfrac{1}{2}\rho|\mathbf{u}|^2 - \rho\Phi - \rho\tilde{H}(p_0, s, 0) - \pi_1\rho\frac{\partial\tilde{H}}{\partial\pi}(p_0, s, 0) - s_B\rho\frac{\partial\tilde{H}}{\partial s_B}(p_0, s, 0) + p_0 + \pi_1\,. \quad (3.61)$$

Using the definitions given above, this can be rewritten in the form

$$\mathcal{L} = \tfrac{1}{2}\rho|\mathbf{u}|^2 - \rho\Phi - \rho H(p_0, s) + p_0 - \frac{\rho^\star}{\rho}\frac{|\mathbf{B}|^2}{2\mu_0} + \pi_1(1 - \rho/\rho^\star)\,, \quad (3.62)$$

where

$$\rho^\star(p_0, s) \equiv 1 \Big/ \frac{\partial H}{\partial p}(p_0, s) \quad (3.63)$$

is the density given by the usual equation of state, but with p replaced by p_0. When we apply Hamilton's principle to this action, the pressure perturbation π_1 serves as a Lagrange multiplier that enforces the approximate equation of state $\rho = \rho^\star(p_0, s)$. The equation of motion is eventually found to be

$$\rho\frac{\mathrm{D}\mathbf{u}}{\mathrm{D}t} = -\rho\boldsymbol{\nabla}\Phi - \boldsymbol{\nabla}p_0 + \frac{1}{\mu_0}(\boldsymbol{\nabla}\times\mathbf{B})\times\mathbf{B} - \boldsymbol{\nabla}p_1 + \frac{p_1}{\rho c^2}\boldsymbol{\nabla}p_0\,, \quad (3.64)$$

where $p_1 \equiv \pi_1 - |\mathbf{B}|^2/2\mu_0$ and $1/c^2 = \partial\rho^\star(p_0, s)/\partial p$. Thus we finally arrive at the same set of pseudo-incompressible equations as in the non-magnetic case, except that the Lorentz force is now included in the momentum equation in its usual form, and the induction equation also appears in its usual form (as guaranteed by the definition of $\delta\mathbf{B}$ in equation (3.49)). From the action given by equation (3.62), we deduce that this system conserves the same energy,

$$\int\left[\tfrac{1}{2}\rho|\mathbf{u}|^2 + \rho\Phi + \rho U(\rho, s) + \frac{|\mathbf{B}|^2}{2\mu_0}\right]\mathrm{d}^3\mathbf{x}, \quad (3.65)$$

as the fully compressible system. The fact that the equations can be obtained from an action also implies that the linearised equations are self-adjoint (in the absence of rotation).

In order to include diabatic processes in the model, it is necessary to relate the temperature to the other thermodynamic variables. However, since the density is now given by the approximate equation of state (3.63), the correct definition of temperature is not obvious. In fact, there is a unique definition that preserves the laws of thermodynamics

(Klein & Pauluis, 2012):

$$T = T^\star(p_0, s) + p_1 \frac{\partial T^\star}{\partial p}(p_0, s)\,, \tag{3.66}$$

where $T^\star(p, s) \equiv \dfrac{\partial H}{\partial s}(p, s)$ is the usual equation of state. This is the definition that we have used in our results; in its linearised form, it is identical to the fully compressible relation (2.30).

For future convenience, we will present the linearised pseudo-incompressible equations here,

$$\rho_0 \frac{\partial}{\partial t}\mathbf{u} + 2\rho_0 \boldsymbol{\Omega} \times \mathbf{u} = -\left[\frac{1}{c^2} p_1 + \left(\frac{\partial \rho}{\partial s}\right)_p s_1\right] g\widehat{\mathbf{z}} - \boldsymbol{\nabla}\pi_1 + \frac{1}{\mu_0}\mathbf{B}_0 \cdot \boldsymbol{\nabla}\mathbf{B}_1 + \frac{1}{\mu_0}\mathbf{B}_1 \cdot \boldsymbol{\nabla}\mathbf{B}_0\,, \tag{3.67}$$

$$\frac{\partial}{\partial t}\mathbf{B}_1 = \boldsymbol{\nabla} \times (\mathbf{u} \times \mathbf{B}_0)\,, \tag{3.68}$$

$$\boldsymbol{\nabla} \cdot \mathbf{u} = H_\rho^{-1} u_z - \left(\frac{\partial \rho}{\partial T}\right)_p \frac{Q_1}{\rho_0^2 c_p}\,, \tag{3.69}$$

$$\left(\frac{\partial \rho}{\partial s}\right)_p \frac{\partial}{\partial t} s_1 - \rho_0 H_s^{-1} u_z = \left(\frac{\partial \rho}{\partial T}\right)_p \frac{Q_1}{\rho_0 c_p}, \tag{3.70}$$

$$\pi_1 = p_1 + \frac{1}{\mu_0}\mathbf{B}_0 \cdot \mathbf{B}_1\,, \tag{3.71}$$

$$\left(\frac{\partial \rho}{\partial T}\right)_p T_1 = \left(\frac{\partial \rho}{\partial s}\right)_p s_1 - \frac{\gamma - 1}{c^2} p_1\,, \tag{3.72}$$

where we have replaced the full continuity equation by equation (3.43).

Chapter 4

Asymptotic approach to linear problem

The majority of this chapter comes from a paper published in Physical Review Fluids, co-written by myself, Toby Wood and Paul Bushby (Moss *et al.*, 2022).

4.1 Introduction

To model buoyancy-driven flows, in many astrophysical and geophysical contexts it is essential to include effects of compressibility and stratification. However, in many cases the dynamics of interest occur on a timescale that is much longer than the acoustic timescale, i.e. the time taken for a sound wave to traverse the fluid. Most models, whether theoretical or numerical, therefore make some kind of sound-proof approximation (e.g., Boussinesq or anelastic) in which sound waves are filtered out of the governing equations. However, each of these approximations is derived under certain assumptions that may not hold in the system of interest. In particular, the Boussinesq approximation is derived under the assumption of small length-scales, and the anelastic approximation is derived assuming small perturbations to a state with uniform entropy.

Magnetic buoyancy — the tendency for regions of strong magnetic flux to be less dense than their surroundings — potentially provides a stringent test problem for any sound-proof model, because it involves significant perturbations to the fluid pressure and density, on length-scales that are typically long in the direction of the magnetic field but short in the other directions. Yet there has been relatively little work done to compare how accurately different sound-proof models describe the magnetic buoyancy instability, outside of specific asymptotic regimes. The main scientific interest in the magnetic buoyancy instability comes from the solar interior, where buoyant magnetic structures rise through the Sun's convective envelope and emerge at the surface. These buoyant structures are

believed to originate in the tachocline below the convection zone, where strong magnetic fields are generated by differential rotation. In the lower part of the tachocline the temperature gradient is strongly subadiabatic, inhibiting the magnetic buoyancy instability until the field becomes sufficiently strong. Most global numerical studies of the solar interior have employed the anelastic approximation. However, it is unclear how accurately the anelastic approximation captures the onset of instability in the presence of such large entropy variations. Indeed, under these conditions the meaning of the anelastic approximation becomes somewhat ambiguous, because there are different formulations that only become equivalent in the asymptotic limit of adiabatic stratification (e.g., Berkoff *et al.*, 2010).

Our goal in this chapter is to determine which sound-proof models accurately describe the magnetic buoyancy instability, and in precisely which parameter regimes. Our approach is similar to that of Berkoff *et al.* (2010), who numerically solved the linearised equations describing perturbations to specific background states, and compared the growth rates they obtained using the anelastic and fully compressible models. However, here we consider several asymptotic parameter regimes in order to obtain analytical solutions for more general background states. This allows us to identify more precisely the conditions under which different sound-proof approximations reproduce the fully compressible results. Note that we will only be considering sound-*proof* models — that is, models in which sound waves are removed from the governing equations — rather than alternative models that slow down sound waves (Iijima *et al.*, 2019) or damp them using implicit timestepping (Goffrey *et al.*, 2017).

Whilst the relative merits of the different sound-proof approximations have been extensively studied in the context of various hydrodynamic problems (Bannon, 1995; Lilly, 1996; Davies *et al.*, 2003; Brown *et al.*, 2012; Wood & Bushby, 2016), there are still a number of important open questions regarding the applicability of such approximations in the context of magnetohydrodynamics. It is one of these open questions (i.e. the extent to which such approximations can be used to describe magnetic buoyancy) that provides the motivation for this chapter. Recent work by Wilczyński *et al.* (2022) presents a similar analysis focused on the analestic model, and restricted to nearly-adiabatic parameter regimes, for which the anelastic model is asymptotically valid. Recent work by Wilczyński *et al.* (2022) addressed some questions in this area. Firstly, they show that both the Boussinesq and anelastic approximations can be generalised to include magnetic fields in such a way that magnetic buoyancy is included. Secondly, Wilczyński *et al.* (2022) consider a linear stability analysis to show that, under the asymptotic conditions of the anelastic model, the anelastic model can accurately describe the magnetic buoyancy instability. Here, we will take a similar approach to the latter, and will carry out a linear stability analysis which will consider each of the models discussed in Chapter 3 under wide parameter ranges.

We will be making use of the linearised equations presented in Section 2.2, which also defines the geometry and essential notation for the problem. Section 4.2 introduces a general linearised sound-proof model that includes several adjustable coefficients. This general model includes each of the sound-proof models discussed in Chapter 3 as special cases. In Section 4.3 we compare the linear stability properties of our sound-proof model with the fully compressible system in the absence of rotation; Section 4.4 presents a similar analysis for the rotating fluid. In each case we consider several asymptotic regimes and identify the leading-order dynamics, i.e. the dynamics governed by the dominant terms, in both the fully compressible system and our general sound-proof model, both with and without thermal relaxation. Comparison between these two systems yields constraints on the coefficients in our model which in turn tell us which models are applicable in which regimes. A summary and discussion of these results is presented in Section 4.5.

4.1.1 Fully compressible linearised equations

In Chapter 3 we discussed how each of the sound proof models we will be considering can be derived and written in the form that they appear in our general sound proof model (introduced in the next section).

For ease of reference we paste the linearised compresssible equations (2.25)–(2.31) here

$$\rho_0 \frac{\partial}{\partial t}\mathbf{u} + 2\rho_0 \boldsymbol{\Omega} \times \mathbf{u} = -g\rho_1 \widehat{\mathbf{z}} - \boldsymbol{\nabla}\pi_1 + \frac{1}{\mu_0}\mathbf{B}_0 \cdot \boldsymbol{\nabla}\mathbf{B}_1 + \frac{1}{\mu_0}\mathbf{B}_1 \cdot \boldsymbol{\nabla}\mathbf{B}_0\,, \tag{4.1}$$

$$\frac{\partial}{\partial t}\mathbf{B}_1 = \boldsymbol{\nabla} \times (\mathbf{u} \times \mathbf{B}_0)\,, \tag{4.2}$$

$$\frac{\partial}{\partial t}\rho_1 = -\boldsymbol{\nabla} \cdot (\rho_0 \mathbf{u})\,, \tag{4.3}$$

$$\left(\frac{\partial \rho}{\partial s}\right)_p \frac{\partial}{\partial t} s_1 - \rho_0 H_s^{-1} u_z = \left(\frac{\partial \rho}{\partial T}\right)_p \frac{Q_1}{\rho_0 c_p}, \tag{4.4}$$

$$\pi_1 = p_1 + \frac{1}{\mu_0}\mathbf{B}_0 \cdot \mathbf{B}_1\,, \tag{4.5}$$

$$\left(\frac{\partial \rho}{\partial T}\right)_p T_1 = \left(\frac{\partial \rho}{\partial s}\right)_p s_1 - \frac{\gamma - 1}{c^2} p_1\,, \tag{4.6}$$

$$\rho_1 = \left(\frac{\partial \rho}{\partial s}\right)_p s_1 + \frac{1}{c^2} p_1\,, \tag{4.7}$$

where in the background we have

$$g = c^2 H_\rho^{-1} - c^2 H_s^{-1} + v^2 H_B^{-1}\,. \tag{4.8}$$

A more thorough description and derivation of these equations is provided in Section 2.2.1.

When comparing results from the fully compressible equations with results from any sound-proof model, care must be taken in the interpretation of the background state. In

particular, most sound-proof models first introduce a non-magnetic background state in hydrostatic balance, and regard the entire magnetic field as a perturbation to this. For consistency, we will therefore only consider background states that are weakly magnetised, in the sense that the magnetic pressure force is negligible in comparison with gravity. This means that the final term in equation (4.8) can be neglected, at least in a leading-order analysis.

In much of what follows we will introduce Newtonian cooling, with $Q_1 = \rho c_p \alpha (T_0 - T)$ (where $T_0(z)$ is the equilibrium temperature profile and α is the cooling rate) as an alternative to thermal diffusion. This simplifies the analysis by reducing the number of vertical derivatives in the linearised equations. In what follows, we are mostly concerned with the limits $\alpha \to 0$ and $\alpha \to \infty$, the latter of which reproduces the "fast thermal relaxation" regime considered by Gilman (1970), in which temperature perturbations are vanishingly small. In both of these limits, the exact mechanism of thermal relaxation becomes irrelevant.

4.2 General sound-proof model

To ascertain how well each of the sound-proof models discussed in Chapter 3 describes magnetic buoyancy, we consider a general linearised sound-proof model that includes each of the sound-proof models, namely the magneto-Boussinesq, anelastic and pseudo-incompressible models, as special cases. This is a more efficient approach than simply analysing each individual model in turn.

Our general sound-proof model is given by the following set of linearised equations:

$$\rho_0 \frac{\partial}{\partial t}\mathbf{u} + 2\rho_0 \boldsymbol{\Omega} \times \mathbf{u} = -\left[\frac{D}{c^2} p_1 + \left(\frac{\partial \rho}{\partial s}\right)_p s_1\right] g\hat{\mathbf{z}} - \boldsymbol{\nabla}\pi_1 + \frac{1}{\mu_0}\mathbf{B}_0 \cdot \boldsymbol{\nabla}\mathbf{B}_1 + \frac{1}{\mu_0}\mathbf{B}_1 \cdot \boldsymbol{\nabla}\mathbf{B}_0 \,, \tag{4.9}$$

$$\frac{\partial}{\partial t}\mathbf{B}_1 = \boldsymbol{\nabla} \times (\mathbf{u} \times \mathbf{B}_0) \,, \tag{4.10}$$

$$\left(\frac{\partial \rho}{\partial s}\right)_p \frac{\partial}{\partial t} s_1 - \rho_0 H_s^{-1} u_z = \left(\frac{\partial \rho}{\partial T}\right)_p \frac{Q_1}{\rho_0 c_p} \,, \tag{4.11}$$

$$\boldsymbol{\nabla} \cdot \mathbf{u} = C \frac{g}{c^2} u_z - F \left(\frac{\partial \rho}{\partial T}\right)_p \frac{Q_1}{\rho_0^2 c_p} \,, \tag{4.12}$$

$$J\pi_1 = p_1 + \frac{B_0}{\mu_0} B_{1x} \,, \tag{4.13}$$

$$\left(\frac{\partial \rho}{\partial T}\right)_p T_1 = \left(\frac{\partial \rho}{\partial s}\right)_p s_1 - G \frac{\gamma - 1}{c^2} p_1 \,, \tag{4.14}$$

where we have used the same notation as for the fully compressible equations (4.1)–(4.7). The coefficients C, D, F, G, J are assumed to be known functions of altitude, z; different

choices for these coefficients correspond to different sound-proof approximations. For example, in the pseudo-incompressible approximation all of these coefficients are equal to 1. We will therefore assume that all the coefficients are of order unity. Table 4.1 shows the values of these coefficients for each of the models discussed in Chapter 3. This general model is constructed to be as general as possible and, in theory, contain every sound-proof model as a special case. The sound-proof models that we will be considering, and are present in Table 4.1, are first introduced and discussed in Chapter 3. Each subsection of Chapter 3 ends by presenting the linearised equations for the relevant model. By comparing these equations, i.e. (3.16)–(3.26), (3.30)–(3.35), (3.37)–(3.42), (3.67)–(3.72), to equations (4.9)–(4.14) the values for each of the coefficients C, D, F, G, J for each model will be clear. However, there are other models, which we do not consider here, for which it would be unclear whether or not they fit within our framework; e.g. Quasi-hydrostatic model (e.g., Miller & White, 1984). The Quasi-hydrostatic model, for example, is written in pressure coordinates (i.e. pressure in place of a vertical, z, coordinate), as such it would not be obvious how one could easily add magnetic fields to such a model. Furthermore, given that it is in written in terms of pressure coordinates, it is unclear whether or not it would fit into our framework; that is not to say that it doesn't, but just that significant manipulation of the equations would be required to find out.

Note that in our sound-proof model we have deliberately not included a density perturbation, ρ_1. This is because there is often ambiguity in how density should be defined in a sound-proof system. For example, Durran (1989) defined two quantities called ρ and ρ^*, one that satisfies the equation of state and one that satisfies the continuity equation. Note that in many implementations of the anelastic approximation (e.g., Ogura & Phillips, 1962; Lipps & Hemler, 1982; Lantz, 1992; Braginsky & Roberts, 1995) an expression for density is not explicitly needed because the equations are written in terms of pressure and entropy. Combining equations (4.11) and (4.12), we find that

$$\frac{\partial}{\partial t} F \left(\frac{\partial \rho}{\partial s} \right)_p s_1 = \left[F H_s^{-1} + C \frac{g}{c^2} - H_\rho^{-1} \right] \rho_0 u_z - \boldsymbol{\nabla} \cdot (\rho_0 \mathbf{u}) \,, \tag{4.15}$$

which has the same form as the continuity equation (4.3) if we define

$$\rho_1 \equiv F \left(\frac{\partial \rho}{\partial s} \right)_p s_1 \tag{4.16}$$

and if the coefficients C and F are chosen such that

$$F H_s^{-1} + C \frac{g}{c^2} = H_\rho^{-1} \,. \tag{4.17}$$

However, this definition of ρ_1 does not satisfy the equation of state (4.7), and nor, in

Coefficient \ Model	LBR anelastic	GGG anelastic	Pseudo-incompressible	Magneto-Boussinesq
C	$\frac{c^2}{g}H_\rho^{-1}$	$\frac{c^2}{g}H_\rho^{-1}$	1	$\frac{c^2}{g}H_\rho^{-1}$
D	$\frac{c^2}{g}H_\rho^{-1}$	1	1	1
F	0	0	1	0
G	0	1	1	1
J	1	1	1	0

Table 4.1: Values for each of the coefficients in our sound-proof model needed to reproduce the models summarised in Chapter 3.

general, is it the same quantity that appears in the buoyancy term of equation (4.9). For this reason, we will later refer to the quantity

$$\rho_{\mathrm{k}} \equiv F\left(\frac{\partial \rho}{\partial s}\right)_p s_1 \tag{4.18}$$

as the "kinematic density".

4.3 Non-rotating case

Our goal now is to solve the linearised equations arising from the fully compressible and sound-proof models. In both cases, since the background state depends only on altitude, z, we can seek solutions in the form $f_1 = \tilde{f}_1(z)\exp(\sigma t + \mathrm{i}k_x x + \mathrm{i}k_y y)$, where f represents any of the perturbed variables. The linearised equations then reduce to a second-order system of linear ordinary differential equations (ODEs) in z. In general this system cannot be solved analytically, so to make progress we will consider several asymptotic limits of relevance to the interior of the Sun and other stars. Throughout the remainder of this chapter we will approximate thermal diffusion by introducing Newtonian cooling, i.e. $Q_1 = \rho c_p \alpha(T_0(z) - T)$.

4.3.1 Fast thermal relaxation

We first consider the case with no rotation and $\alpha \to \infty$. In this limit, the temperature perturbation vanishes (Gilman, 1970). The specific asymptotic regime we consider is given

by

$$v \ll c\,, \tag{4.19}$$

$$H_B \sim H_\rho \sim H_s\,, \tag{4.20}$$

$$k_y, \tfrac{\mathrm{d}}{\mathrm{d}z} \gtrsim k_x, H_\rho^{-1}\,, \tag{4.21}$$

$$\alpha \to \infty\,, \tag{4.22}$$

$$\sigma \sim v/H_\rho\,. \tag{4.23}$$

By adopting the scalings $k_y, \mathrm{d}/\mathrm{d}z \gtrsim k_x, H_\rho^{-1}$ we can initially assume that all length-scales are equal, before subsequently assuming smaller length-scales in the directions perpendicular to the magnetic field, if desired. The scaling for the growth rate, σ, is justified by the results, and is the expected timescale for magnetic buoyancy instability based on previous studies. We apply this scaling regime to our fully compressible equations (4.1)–(4.7) and retain only the leading-order terms. The equations can then be reduced to a pair of coupled ODEs:

$$\left(\frac{\mathrm{d}}{\mathrm{d}z} + \frac{\gamma g}{c^2}\frac{\sigma^2}{q}\right)\pi_1 = -\frac{1}{\sigma}\left(q + \gamma g \frac{v^2}{c^2}\left(\frac{\sigma^2}{q}H_\rho^{-1} - H_B^{-1}\right)\right)\rho_0 u_z\,, \tag{4.24}$$

$$\left(\frac{\mathrm{d}}{\mathrm{d}z} - H_\rho^{-1}\frac{\sigma^2}{q}\right)u_z = -\frac{\sigma}{q}(k_x^2 + k_y^2)\frac{\pi_1}{\rho_0}\,, \tag{4.25}$$

where we have defined

$$q \equiv \sigma^2 + v^2 k_x^2\,. \tag{4.26}$$

Since we have neglected viscosity and magnetic diffusion, the most unstable modes are found in the limit $k_y \to \infty$. In this limit the total pressure perturbation, π_1, and hence the left-hand side of equation (4.24), becomes negligible, and we are left with a local dispersion relation:

$$(\sigma^2 + v^2 k_x^2)^2 + \gamma g \frac{v^2}{c^2} H_B^{-1}\left(\sigma^2\left(\frac{H_B}{H_\rho} - 1\right) - v^2 k_x^2\right) = 0\,, \tag{4.27}$$

which exactly matches the result of Gilman (1970). In the case of interchange motions (i.e. for $k_x = 0$) we have instability if and only if $H_B^{-1} > H_\rho^{-1}$. If instead we have $k_x^2 > 0$, i.e. undular modes, we can maximise with respect to k_x^2. When we do this, by differentiating (4.27) and setting to zero, we find that the fastest growing mode occurs with

$$k_x^2 = \frac{\gamma g}{2c^2 H_B}\left(1 - \frac{H_\rho}{2H_B}\right) \tag{4.28}$$

at a growth rate given by

$$\sigma^2 = \frac{\gamma g}{4}\frac{v^2}{c^2}\frac{H_\rho}{H_B^2}\,. \tag{4.29}$$

Note that, since we require $k_x^2 > 0$ we must have $0 < H_B^{-1} < 2H_\rho^{-1}$.

If we apply the same analysis to the general sound-proof model (4.9)–(4.14), we again eventually obtain a pair of coupled ODEs:

$$\left(\frac{\mathrm{d}}{\mathrm{d}z} + (D + G(\gamma-1))\frac{g}{c^2}\left(J - \frac{v^2k_x^2}{q}\right)\right)\pi_1 =$$
$$-\frac{1}{\sigma}\left(q + (D + G(\gamma-1))\frac{gv^2\sigma^2}{qc^2}\left(C\frac{g}{c^2} + FH_s^{-1} - \frac{q}{\sigma^2}H_B^{-1}\right)\right)\rho_0 u_z\,, \tag{4.30}$$
$$\left(\frac{\mathrm{d}}{\mathrm{d}z} - \left(C\frac{g}{c^2} + FH_s^{-1}\right)\frac{\sigma^2}{q}\right)u_z = -\frac{\sigma}{q}(k_x^2 + k_y^2)\frac{\pi_1}{\rho_0}\,. \tag{4.31}$$

Hence we can reproduce the fully compressible result (4.24)–(4.25) provided that

$$J \simeq 1\,, \tag{4.32}$$
$$D + G(\gamma - 1) \simeq \gamma\,, \tag{4.33}$$
$$C\frac{g}{c^2} + FH_s^{-1} \simeq H_\rho^{-1}\,. \tag{4.34}$$

Note that we use "$\simeq$" here because we require these results to hold only at leading order, for the particular asymptotic regime we have considered. It is perhaps surprising that the sound-proof model can perfectly reproduce (at leading-order) the results of a fully compressible system. This demonstrates that the terms neglected in the sound-proof model, including sound waves, have no impact on the leading-order dynamics.

Referring to the particular sound-proof models listed in Table 4.1, we see immediately that the GGG anelastic model satisfies all of these constraints. The same is true of the pseudo-incompressible model, when we recall that the final term in equation (4.8) is negligible under our scaling assumptions. However, the LBR anelastic model does not satisfy these constraints, and therefore does not correctly describe the wavelength or growth rate of the magnetic buoyancy instability in this regime. It is perhaps surprising that GGG satisfies all the constraints when LBR doesn't considering they are derived under the same assumptions; certainly this wouldn't have been predicted beforehand. The reason for this will be that, in GGG anelastic, the assumptions amount to neglecting just one term, the time-derivative term in the continuity equation, whereas, in LBR anelastic, additional approximations are made. Given that the GGG equations have reproduced the result of the fully compressible equations, it must be the case that the neglect of the time-derivative term in the continuity equation is justified — but just not for the reasons that are used to justify its neglect in the anelastic approximation. LBR on the other hand makes additional approximations which are no longer valid in the regime we consider here; which should not be surprising since we are not in the regime of validity of the anelastic model. The magneto-Boussinesq approximation has $J = 0$, and therefore

does not satisfy constraint (4.32). However, on smaller scales in y and/or z (which was the regime considered by Spiegel & Weiss (1982)) the term involving J on the left-hand side of equation (4.30) is negligible. This is because, for small scales in z, the z-derivative term dominates the left-hand side of equation (4.30). For small scales in y, the perturbation π_1 becomes vanishingly small, and so the entire left-hand side of equation (4.30) is negligible. In particular, the condition $J \simeq 1$ is not required in order to correctly reproduce the fastest growing mode (which, in the absence of viscosity and resistivity, has $k_y \to \infty$).

Interestingly, equation (4.34) is exactly the result (4.17) required to achieve a form of mass conservation in the sound-proof model. Here we have arrived at the same result on purely dynamical grounds, without any explicit reference to mass conservation.

4.3.2 No thermal relaxation

We now consider the ideal limit, with $\alpha = 0$. We also reduce the strength of the (stabilising) thermal stratification, which otherwise overwhelms the destabilising effect of magnetic buoyancy in the absence of thermal relaxation. Specifically, we now assume that $H_s^{-1} \sim (v^2/c^2)H_\rho^{-1} \ll H_\rho^{-1}$. Note that this means the background state now has $g \simeq c^2/H_\rho$, since both the H_s and H_B terms are negligible in the magneto-hydrostatic equation (4.8). The complete regime is given by

$$v \ll c\,, \tag{4.35}$$

$$H_B \sim H_\rho \sim (v^2/c^2)H_s\,, \tag{4.36}$$

$$k_y, \tfrac{\mathrm{d}}{\mathrm{d}z} \gtrsim k_x\,, H_\rho^{-1}\,, \tag{4.37}$$

$$\sigma \sim v/H_\rho\,, \tag{4.38}$$

$$\alpha = 0\,. \tag{4.39}$$

Again, we apply this scaling regime to the fully compressible equations (4.1)–(4.7) and retain only the leading-order terms. This leads to

$$\left(\frac{\mathrm{d}}{\mathrm{d}z} + H_\rho^{-1}\frac{\sigma^2}{q}\right)\pi_1 = -\frac{1}{\sigma}\left(q + c^2 H_\rho^{-1}H_s^{-1} + v^2 H_\rho^{-1}\left(\frac{\sigma^2}{q}H_\rho^{-1} - H_B^{-1}\right)\right)\rho_0 u_z\,, \tag{4.40}$$

$$\left(\frac{\mathrm{d}}{\mathrm{d}z} - H_\rho^{-1}\frac{\sigma^2}{q}\right)u_z = -\frac{\sigma}{q}\left(k_x^2 + k_y^2\right)\frac{\pi_1}{\rho_0}\,. \tag{4.41}$$

The fastest growing mode is again found in the limit $k_y \to \infty$, for which $\pi_1 \to 0$, resulting in a local dispersion relation similar to (4.27):

$$(\sigma^2 + v^2k_x^2)^2 + v^2H_\rho^{-1}\left(\sigma^2\left(H_\rho^{-1} - H_B^{-1} + \frac{c^2}{v^2}H_s^{-1}\right) + v^2k_x^2\left(\frac{c^2}{v^2}H_s^{-1} - H_B^{-1}\right)\right) = 0\,. \tag{4.42}$$

We can directly translate the results from the previous section by replacing $c^2/\gamma \to c^2 = gH_\rho$ and then replacing $H_B^{-1} \to H_B^{-1} - (c^2/v^2)H_s^{-1}$. This shows that, in the absence of fast thermal relaxation, the isothermal sound speed $c/\sqrt{\gamma}$ is replaced by the adiabatic sound speed c, and the entropy gradient opposes the destabilising field gradient.

When we apply the same analysis to our sound-proof model (4.9)–(4.14), we obtain

$$\left(\frac{\mathrm{d}}{\mathrm{d}z} + DH_\rho^{-1}\left(J - \frac{v^2k_x^2}{q}\right)\right)\pi_1 = -\frac{1}{\sigma}\left(q + c^2H_\rho^{-1}H_s^{-1} + Dv^2H_\rho^{-1}\left(C\frac{\sigma^2}{q}H_\rho^{-1} - H_B^{-1}\right)\right)\rho_0 u_z\,, \tag{4.43}$$

$$\left(\frac{\mathrm{d}}{\mathrm{d}z} - CH_\rho^{-1}\frac{\sigma^2}{q}\right)u_z = -\frac{\sigma}{q}(k_x^2 + k_y^2)\frac{\pi_1}{\rho_0}\,. \tag{4.44}$$

Hence we can reproduce the fully compressible result (4.40)–(4.41) provided that

$$J \simeq 1\,, \tag{4.45}$$

$$D \simeq 1\,, \tag{4.46}$$

$$C \simeq 1\,. \tag{4.47}$$

The last of these constraints seems at first to be incompatible with what we found previously, i.e. equation (4.34), but in the current asymptotic regime we have $H_s \gg H_\rho$ and $g \simeq c^2/H_\rho$. Therefore (4.47) is actually just a weaker version of the earlier constraint (4.34).

4.3.3 Finite thermal relaxation

We now consider an intermediate case with finite Newtonian Cooling. With a finite value of α, there is no longer a straightforward analogy with thermal diffusion. However, it is still valuable to consider this regime to check that there are no important effects that only take effect in the intermediate α regime. We will assume $\alpha \sim v/H_\rho$ and, as we did in the previous section, we let $(c^2/v^2)H_s^{-1} \sim H_\rho^{-1}$ in order to retain as many terms as possible at leading order. The complete regime is identical to the no thermal relaxation case except our Newtonian cooling coefficient, α is now a comparable size to our growth rate, σ.

$$v \ll c\,, \tag{4.48}$$

$$H_B \sim H_\rho \sim (v^2/c^2)H_s\,, \tag{4.49}$$

$$k_y, \tfrac{\mathrm{d}}{\mathrm{d}z} \gtrsim k_x\,, H_\rho^{-1}\,, \tag{4.50}$$

$$\sigma \sim \alpha \sim v/H_\rho\,, \tag{4.51}$$

As we have done in the previous subsections, we apply this scaling regime to the fully compressible equations (4.1 – 4.7) and keep only the leading order terms. These equations

then reduce to

$$\left(\frac{\mathrm{d}}{\mathrm{d}z}+\left(\frac{\sigma+\gamma\alpha}{\sigma+\alpha}\right)\frac{g}{c^2}\frac{\sigma^2}{q}\right)\pi_1 = -\frac{1}{\sigma}\left(q+\left(\frac{\sigma+\gamma\alpha}{\sigma+\alpha}\right)g\frac{v^2}{c^2}\left(\frac{\sigma^2}{q}H_\rho^{-1}-H_B^{-1}+\frac{\sigma}{\sigma+\gamma\alpha}\frac{c^2}{v^2}H_s^{-1}\right)\right)\rho_0 u_z, \tag{4.52}$$

$$\left(\frac{\mathrm{d}}{\mathrm{d}z}-\frac{\sigma^2}{q}H_\rho^{-1}\right)u_z = -\frac{\sigma}{q}(k_x^2+k_y^2)\frac{\pi_1}{\rho_0}, \tag{4.53}$$

where we have defined $q=\sigma^2+v^2k_x^2$. When we apply the same scaling regime to our sound-proof model (4.9 – 4.14), keeping leading order terms only we arrive at the following coupled differential equations:

$$\left(\frac{\mathrm{d}}{\mathrm{d}z}+\left(\frac{\sigma+\gamma\alpha}{\sigma+\alpha}\right)\frac{g}{c^2}\left(J-\frac{v^2k_x^2}{q}\right)\right)\pi_1 = -\frac{1}{\sigma}\left(q+\left(\frac{\sigma+\gamma\alpha}{\sigma+\alpha}\right)g\frac{v^2}{c^2}\left(C\frac{\sigma^2}{q}H_\rho^{-1}-H_B^{-1}+E\frac{\sigma}{\sigma+\gamma\alpha}\frac{c^2}{v^2}H_s^{-1}\right)\right)\rho_0 u_z\,, \tag{4.54}$$

$$\left(\frac{\mathrm{d}}{\mathrm{d}z}-C\frac{\sigma^2}{q}H_\rho^{-1}\right)u_z = -\frac{\sigma}{q}(k_x^2+k_y^2)\frac{\pi_1}{\rho_0}\,. \tag{4.55}$$

Comparing these equations with (4.52 – 4.53), we find equivalence provided that

$$J\simeq 1\,, \tag{4.56}$$

$$D\simeq 1\,, \tag{4.57}$$

$$G\simeq 1\,, \tag{4.58}$$

$$C\frac{g}{c^2}\simeq H_\rho^{-1}\,. \tag{4.59}$$

These are stronger constraints on D and G than in each of the previous regimes. It should be noted that the previous constraints, for infinite and zero α, are a subset of this set of constraints. We note that the last constraint is in fact compatible with what we saw in Section 4.3.1, but recognising that our background state has $H_s \gg H_\rho$. Note that F does not appear in these constraints since terms involving F vanish due to the scaling assumptions.

So any model that satisfies the constraints

$$J\simeq D\simeq G\simeq 1 \qquad \text{and} \qquad C\frac{g}{c^2}+FH_s^{-1}\simeq H_\rho^{-1} \tag{4.60}$$

will be able to capture the same leading order behaviour as the fully compressible equations in any of the non-rotating regimes discussed so far.

4.4 Rotating case

The growth rate of the magnetic buoyancy instability, for parameters typical of the solar interior, is comparable to or slower than the Sun's rotation rate. We therefore expect the instability to be significantly affected by this rotation. The main interest in this instability is to explain the appearance of active regions in the Sun at low latitudes, where the rotation axis is roughly perpendicular to the direction of gravity, and so in the following we will take $\mathbf{\Omega} = \Omega\widehat{\mathbf{y}}$. We do not present it here, but we have also carried out an identical analysis for a more general axis of rotation; i.e. appropriate for regions at the equator, mid-latitudes, or polar regions. We found that our conclusions, regarding the accuracy of our sound-proof model and the constraints derived upon it, are unchanged. For this reason, we only present this one case which is most appropriate for the Sun. The presence of rotation generally acts to reduce the growth rate of the instability, and to separate the roots of the dispersion relation into "fast" and "slow" modes. In the absence of magnetic diffusion, we expect that the slow (i.e. magnetostrophic) branch is most easily destabilised, so we will only consider that branch here. We focus on the limits of infinite and zero thermal relaxation.

4.4.1 Fast thermal relaxation

As with the non-rotating case, we first consider the limit $\alpha \to \infty$. Where we recall that $Q = \rho c_p \alpha (T_0(z) - T)$. Our complete asymptotic regime is given by

$$\Omega \sim \left(\frac{c}{v}\right)^{1/2} v H_\rho^{-1}\,, \tag{4.61}$$

$$v \ll c\,, \tag{4.62}$$

$$H_B \sim H_\rho \sim H_s\,, \tag{4.63}$$

$$k_y\,, \tfrac{\mathrm{d}}{\mathrm{d}z} \gtrsim k_x\,, H_\rho^{-1}\,, \tag{4.64}$$

$$\sigma \sim \left(\frac{v}{c}\right)^{1/2} v H_\rho^{-1}\,, \tag{4.65}$$

$$\alpha \to \infty\,. \tag{4.66}$$

Note that the growth rate is slower than in the non-rotating case, and is of order $\sigma \sim v^2 k_x^2/\Omega$, characteristic of magnetostrophic dynamics.

We apply these scalings to the fully compressible equations (4.1)–(4.7) and keep only

the leading-order terms, finding that

$$\left(\frac{\mathrm{d}}{\mathrm{d}z}-\frac{2\Omega\sigma}{\mathrm{i}v^2k_x}\right)\pi_1=-\frac{1}{\sigma}\left(v^2k_x^2-g\gamma\frac{v^2}{c^2}\left(H_B^{-1}+\frac{2\Omega\sigma}{\mathrm{i}v^2k_x}\right)-\frac{2\Omega\sigma}{\mathrm{i}k_x}\left(H_\rho^{-1}+\frac{2\Omega\sigma}{\mathrm{i}v^2k_x}\right)\right)\rho_0u_z\,, \tag{4.67}$$

$$\left(\frac{\mathrm{d}}{\mathrm{d}z}+\frac{2\Omega\sigma}{\mathrm{i}v^2k_x}\right)u_z=-\frac{\sigma}{v^2}\left(1+\frac{k_y^2}{k_x^2}\right)\frac{\pi_1}{\rho_0}\,. \tag{4.68}$$

The most unstable modes occur in the limit $k_y\to\infty$, for which we have the local dispersion relation

$$\frac{4\Omega^2\sigma^2}{v^2k_x^2}-\frac{2\Omega\sigma}{\mathrm{i}k_x}\left(H_\rho^{-1}+\gamma\frac{g}{c^2}\right)-g\gamma\frac{v^2}{c^2}H_B^{-1}+v^2k_x^2=0\,. \tag{4.69}$$

We have an (oscillatory) instability if

$$H_B^{-1}>\frac{c^2}{4\gamma g}\left(\gamma\frac{g}{c^2}+H_\rho^{-1}\right)^2\,, \tag{4.70}$$

and the fastest growing mode then has

$$k_x^2=\frac{\gamma}{2}\frac{g}{c^2}H_B^{-1}-\frac{1}{8}\left(\gamma\frac{g}{c^2}+H_\rho^{-1}\right)^2\,. \tag{4.71}$$

Applying the same scaling regime to our sound-proof model (4.9)–(4.14), we obtain

$$\left(\frac{\mathrm{d}}{\mathrm{d}z}+\big(D+G(\gamma-1)\big)\frac{g}{c^2}(J-1)-\frac{2\Omega\sigma}{\mathrm{i}v^2k_x}\right)\pi_1+\frac{1}{\sigma}\Bigg(-\big(D+G(\gamma-1)\big)\frac{g}{c^2}v^2\left(H_B^{-1}+\frac{2\Omega\sigma}{\mathrm{i}v^2k_x}\right)$$
$$+v^2k_x^2-\frac{2\Omega\sigma}{\mathrm{i}k_x}\left(\frac{2\Omega\sigma}{\mathrm{i}v^2k_x}+C\frac{g}{c^2}+FH_s^{-1}\right)\Bigg)\rho_0u_z=0\,, \tag{4.72}$$

$$\left(\frac{\mathrm{d}}{\mathrm{d}z}+\frac{2\Omega\sigma}{\mathrm{i}v^2k_x}\right)u_z=-\frac{\sigma}{v^2}\left(1+\frac{k_y^2}{k_x^2}\right)\frac{\pi_1}{\rho_0}\,. \tag{4.73}$$

Comparing this with the fully compressible result, we recover the same constraints as in the non-rotating case, i.e. equations (4.32)–(4.34), with the same conclusions regarding the applicability of the various sound-proof models in this regime.

4.4.2 No thermal relaxation

As for the non-rotating case, we now consider the ideal limit $\alpha = 0$ and we simultaneously change the scaling of H_s^{-1} accordingly. The regime considered here is given by

$$\Omega \sim \left(\frac{c}{v}\right)^{1/2} v H_\rho^{-1}\,, \tag{4.74}$$

$$v \ll c\,, \tag{4.75}$$

$$H_B \sim H_\rho \sim (v^2/c^2) H_s\,, \tag{4.76}$$

$$k_y\,, \tfrac{\mathrm{d}}{\mathrm{d}z} \gtrsim k_x\,, H_\rho^{-1}\,, \tag{4.77}$$

$$\sigma \sim \left(\frac{v}{c}\right)^{1/2} v H_\rho^{-1}\,, \tag{4.78}$$

$$\alpha = 0\,. \tag{4.79}$$

In this regime the fully compressible equations (4.1)–(4.7) reduce to the following pair of ODEs, where we have only kept the leading-order terms:

$$\left(\frac{\mathrm{d}}{\mathrm{d}z} - \frac{2\Omega\sigma}{\mathrm{i}v^2 k_x}\right)\pi_1 = -\frac{1}{\sigma}\Bigg(v^2k_x^2 + c^2 H_\rho^{-1}H_s^{-1} - \frac{2\Omega\sigma}{\mathrm{i}k_x}\left(H_\rho^{-1} + \frac{2\Omega\sigma}{\mathrm{i}v^2k_x}\right) - v^2 H_\rho^{-1}\left(H_B^{-1} + \frac{2\Omega\sigma}{\mathrm{i}v^2k_x}\right)\Bigg)\rho_0 u_z\,, \tag{4.80}$$

$$\left(\frac{\mathrm{d}}{\mathrm{d}z} + \frac{2\Omega\sigma}{\mathrm{i}v^2 k_x}\right)u_z = -\frac{\sigma}{v^2}\left(1 + \frac{k_y^2}{k_x^2}\right)\frac{\pi_1}{\rho_0}\,. \tag{4.81}$$

Again, the most unstable mode arises in the limit $k_y \to \infty$. In this limit $\pi_1 \to 0$, and we obtain the local dispersion relation

$$\frac{4\Omega^2\sigma^2}{v^2k_x^2} - \frac{4\Omega\sigma}{\mathrm{i}k_x}H_\rho^{-1} - v^2H_\rho^{-1}H_B^{-1} + c^2H_\rho^{-1}H_s^{-1} + v^2k_x^2 = 0\,. \tag{4.82}$$

As in the non-rotating case, we can directly translate the results from the previous section, equation (4.69), by replacing $(c^2/\gamma) \to c^2 = gH_\rho$, and then replacing $H_B^{-1} \to H_B^{-1} - (c^2/v^2)H_s^{-1}$.

Applying the same analysis to our sound-proof model (4.9)–(4.14), we obtain

$$\left(\frac{\mathrm{d}}{\mathrm{d}z} + DH_\rho^{-1}(J-1) - \frac{2\Omega\sigma}{\mathrm{i}v^2k_x}\right)\pi_1 = -\frac{1}{\sigma}\left(c^2H_\rho^{-1}H_s^{-1} - \frac{2\Omega\sigma}{\mathrm{i}k_x}\left(\frac{2\Omega\sigma}{\mathrm{i}v^2k_x} + CH_\rho^{-1}\right)\right.$$
$$\left. - DH_\rho^{-1}v^2\left(H_B^{-1} + \frac{2\Omega\sigma}{\mathrm{i}v^2k_x}\right) + v^2k_x^2\right)\rho_0 u_z\,, \tag{4.83}$$

$$\left(\frac{\mathrm{d}}{\mathrm{d}z} + \frac{2\Omega\sigma}{\mathrm{i}v^2k_x}\right)u_z = -\frac{\sigma}{v^2}\left(1 + \frac{k_y^2}{k_x^2}\right)\frac{\pi_1}{\rho_0}\,. \tag{4.84}$$

Comparing this with the fully compressible result we once again recover the same constraints as in the non-rotating case, i.e. equations (4.45)–(4.47).

4.5 Conclusions

We have introduced a very general sound-proof MHD model, and constrained the coefficients in the model by considering the linear onset of magnetic buoyancy instability under a range of physical conditions. The most general model that satisfies all of these constraints has the form

$$\rho_0\frac{\partial}{\partial t}\mathbf{u} + 2\rho_0\mathbf{\Omega}\times\mathbf{u} = \rho_\mathrm{d}\mathbf{g} - \boldsymbol{\nabla}\pi_1 + \frac{1}{\mu_0}\mathbf{B}_0\cdot\boldsymbol{\nabla}\mathbf{B}_1 + \frac{1}{\mu_0}\mathbf{B}_1\cdot\boldsymbol{\nabla}\mathbf{B}_0\,, \tag{4.85}$$

$$\frac{\partial}{\partial t}\mathbf{B}_1 = \boldsymbol{\nabla}\times(\mathbf{u}\times\mathbf{B}_0)\,, \tag{4.86}$$

$$\frac{\partial}{\partial t}\rho_\mathrm{k} = -\boldsymbol{\nabla}\cdot(\rho_0\mathbf{u})\,, \tag{4.87}$$

$$\frac{\partial}{\partial t}s_1 + \mathbf{u}\cdot\boldsymbol{\nabla}s_0 = \frac{Q_1}{\rho_0 T_0}\,, \tag{4.88}$$

$$\pi_1 = p_1 + \frac{1}{\mu_0}\mathbf{B}_0\cdot\mathbf{B}_1\,, \tag{4.89}$$

where $\rho_\mathrm{d} \equiv (1/c^2)p_1 + (\partial\rho/\partial s)_p\, s_1$ and $\rho_\mathrm{k} \propto s_1$. We call ρ_d the "dynamic density" because it determines the buoyancy force in equation (4.85); it is related to p_1 and s_1 by the usual equation of state. We call ρ_k the "kinematic density" because it satisfies the continuity equation (4.87); it is simply proportional to s_1, with a coefficient that is essentially arbitrary — using the notation introduced in Section 4.2 we have $\rho_\mathrm{k} = F\,(\partial\rho/\partial s)_p\, s_1$ where F remains unconstrained. Since ρ_k is proportional to s_1, equations (4.87) and (4.88) are not independent, and in order for them to both be satisfied we must have

$$\boldsymbol{\nabla}\cdot\mathbf{u} = [H_\rho^{-1} - FH_s^{-1}]u_z - F\left(\frac{\partial\rho}{\partial T}\right)_p\frac{Q_1}{\rho_0^2 c_p}\,, \tag{4.90}$$

which precisely corresponds to our model's velocity constraint (4.12) under the condition that $C(g/c^2) + FH_s^{-1} = H_\rho^{-1}$.

Beyond the specific parameter regimes presented here, a tilted rotation axis, and the fast branch of the rotating dispersion relation have also been considered. In all of these cases, we find that the model given by (4.85)–(4.89) captures the correct leading-order behaviour.

We emphasise that some of the parameter regimes we have considered lie outside the asymptotic regimes in which sound-proof models are usually derived. In particular, the magneto-Boussinesq, anelastic and pseudo-incompressible models are usually derived under the assumption that the fluid has nearly uniform entropy (in the sense that $H_s \gg H_\rho$). As expected, the anelastic and pseudo-incompressible models correctly describe the linear onset of the instability when $H_s \gg H_\rho$, and the magneto-Boussinesq approximation is applicable on small scales (in the directions perpendicular to the magnetic field). These results are consistent with those of Wilczyński *et al.* (2022), who performed a similar analysis of the anelastic model, but restricted attention to regimes in which it is asymptotically valid. Only the GGG anelastic and pseudo-incompressible approximations predict the instability onset correctly in all of the regimes that we have considered, because both can be written in exactly the form of equations (4.85)–(4.89), with $F = 0$ and $F = 1$, respectively.

In this study we have assessed different linearised sound-proof models entirely on the basis of whether they accurately describe the magnetic buoyancy instability. However, there are other important considerations when choosing between the various models. For example, it is known that some (non-magnetic) sound-proof models have a Hamiltonian structure, implying that both the nonlinear and linearized equations conserve a form of energy (Bernardet, 1995; Bannon, 1996; Brown *et al.*, 2012; Vasil *et al.*, 2013). We saw in Section 3.4.1 that the MHD pseudo-incompressible model has a Hamiltonian structure, and therefore also conserves energy. This is a beneficial property for any model, because it can be used to establish stability criteria (Bernstein *et al.*, 1958) and to rule out certain unphysical behaviours (e.g. Jones *et al.*, 2009). A more thorough examination of energy conservation in MHD sound-proof models is presented in Chapter 5.

Another important consideration when comparing numerical models is their computational complexity. The main motivation for using a sound-proof model is the reduced computational burden in comparison with a fully compressible mode. However, within the set of sound-proof models, some are more computationally expensive than others. In particular, as described in Chapter 3, a significant advantage of the LBR anelastic model is that the pressure and temperature perturbations do not need to be calculated explicitly. In the GGG and pseudo-incompressible models, by contrast, the pressure perturbation needs to be calculated explicitly by solving an elliptic equation (Bernardet, 1995; Bannon *et al.*, 2006). Moreover, in the pseudo-incompressible model the velocity field satisfies an

inhomogeneous constraint that must be solved in tandem with the pressure perturbation (Snodin & Wood, 2022). Interestingly, our results show that the models that best reproduce the linear behaviour of the fully compressible system are also the models that are more computationally expensive to solve.

Although we have here only considered the linear instability problem, magnetic buoyancy in the Sun is certainly a nonlinear process, and so full understanding of the formation of active regions can only come from a nonlinear model. However, it seems likely that a necessary condition for accurately describing the full, nonlinear problem would be to accurately describe the linear regime. Hence, the work presented here is a necessary first step towards a nonlinear sound-proof model of magnetic buoyancy. In nonlinear modelling energy budgets are of central importance, and will be considered in subsequent work.

Chapter 5

Self-adjointness of sound-proof models

The majority of this chapter comes from a paper published in Geophysical and Astrophysical Fluid Dynamics, co-written by myself, Toby Wood and Paul Bushby (Moss *et al.*, 2023).

5.1 Introduction

It is well known that the equations of magneto-hydrodynamics (MHD) for an ideal fluid form a Hamiltonian system, i.e. that they are the Euler–Lagrange equations of a suitable action (Newcomb, 1962; Lundgren, 1963). This applies both in the fully compressible and incompressible cases. The existence of such an action implies that the linearised equations, describing perturbations to any nonlinear solution, are themselves the Euler–Lagrange equations of an action that is quadratic in the perturbations, which can be readily obtained from the fully nonlinear action. In particular, if we consider perturbations to a background state that is steady and at rest (in an inertial frame of reference) then the linearised equations are guaranteed to be self-adjoint and to conserve a quadratic quantity that can be called the "external energy" (Eckart & Ferris, 1956). These facts are often useful in proving stability results (e.g. Bernstein *et al.*, 1958), and can rule out certain unphysical behaviours (e.g. Brown *et al.*, 2012).

In astrophysical fluids, it is frequently the case that the dynamics of interest are slow in comparison with acoustic waves, and yet some effects of compressibility (particularly buoyancy and stratification) cannot be neglected. In such situations, it is common to use a "sound-proof" model, such as the Boussinesq, anelastic and pseudo-incompressible models, in which acoustic waves are filtered from the governing equations. As well as simplifying the dynamics, such models are usually also more efficient to solve numerically, because the

timestep is not constrained by the speed of sound. Such sound-proof approximations are usually derived via formal asymptotics, by first assuming a particular set of scalings for all physical quantities. However, this does not guarantee that the Hamiltonian structure of the fully compressible equations will be preserved in the final model. An alternative approach is to make any approximations at the level of the action, in order to ensure that the model retains a Hamiltonian structure (Salmon, 1983, 1988; Morrison, 2005). Indeed, Vasil *et al.* (2013) have shown that a wide family of non-magnetic, sound-proof models — intermediate between the incompressible and fully-compressible models — can be obtained from a suitable action. It is straightforward to generalise their action to include magnetic fields under the MHD approximation. However, this does not guarantee that the resulting equations will closely approximate the solution of the fully compressible MHD equations. In Chapter 4 we have shown that there is one particular sound-proof MHD model — the pseudo-incompressible model — that can be obtained by making physically-motivated approximations to the fully compressible action. The derivation assumes only that the Alfvén speed is much smaller than the sound speed, and that perturbations to the total pressure are small. This result does not, however, rule out the existence of other sound-proof MHD actions derivable under similar approximations.

In the present work we take a complementary approach to that of Chapter 4, and determine which sound-proof model provides the closest approximation to the energy of the fully compressible system under the widest set of physical conditions. Motivated by conditions in the solar tachocline, we consider the linearised equations describing perturbations to a horizontal layer of magnetic field in the presence of gravitational stratification. We introduce a very general sound-proof model, and show that the requirement of self-adjointness greatly constrains the mathematical form of the linearised sound-proof equations. Of all possible self-adjoint and sound-proof models, only the pseudo-incompressible model conserves the same external energy as the fully compressible system.

The plan for this chapter is as follows. In Section 5.2 we present the action for a fully compressible MHD fluid, and derive the equations of motion via Hamilton's principle. We also present the general sound-proof action obtained by Vasil *et al.* (2013). In Section 5.3 we prove that, for any Hamiltonian system, the linearised equations are self-adjoint, and hence have a conserved "external energy". Section 5.4 presents the same general linear sound-proof model introduced in Chapter 4, and derives conditions under which it is self-adjoint. We show that the pseudo-incompressible model is unique in that it conserves the same external energy as the fully compressible system. In Section 5.6 we argue on the basis of this result, and the results of Chapter 4, that this model provides the most reliable sound-proof approximation for magnetic buoyancy.

5.2 Action principles for magneto-hydrodynamics

The governing equations describing a fully compressible fluid under the MHD approximation can be obtained from the action

$$\mathcal{S} = \iint \left[\tfrac{1}{2}\rho|\mathbf{u}|^2 - \rho\Phi - \frac{|\mathbf{B}|^2}{2\mu_0} - \rho U(\rho, s) \right] \mathrm{d}^3\mathbf{x}\,\mathrm{d}t\,, \tag{5.1}$$

where $\mathbf{u}$ is the fluid velocity, ρ is the density, s is the specific entropy, μ_0 is the magnetic permeability, $\Phi(\mathbf{x})$ is the gravitational potential, which we take to be fixed, $\mathbf{B}$ is the magnetic field, and U is the specific internal energy, expressed in terms of its natural variables, ρ and s. We saw in Section 3.4.1 that from this action we can derive the fully compressible equations of motion. For convenience, we will reproduce these equations (3.51 – 3.54) here,

$$\rho\frac{\mathrm{D}\mathbf{u}}{\mathrm{D}t} = -\boldsymbol{\nabla}p - \rho\boldsymbol{\nabla}\Phi + \frac{1}{\mu_0}(\boldsymbol{\nabla}\times\mathbf{B})\times\mathbf{B}\,, \tag{5.2}$$

$$\frac{\partial\mathbf{B}}{\partial t} = \boldsymbol{\nabla}\times(\mathbf{u}\times\mathbf{B})\,, \tag{5.3}$$

$$\frac{\mathrm{D}\rho}{\mathrm{D}t} + \rho\boldsymbol{\nabla}\cdot\mathbf{u} = 0\,, \tag{5.4}$$

$$\frac{\mathrm{D}s}{\mathrm{D}t} = 0\,, \tag{5.5}$$

where $\mathrm{D}/\mathrm{D}t \equiv \partial/\partial t + \mathbf{u}\cdot\boldsymbol{\nabla}$ is the material derivative.

As described by Vasil *et al.* (2013) (see also Durran, 2008), in the absence of magnetic fields a wide family of "sound-proof" models can be derived from an action of the form

$$\mathcal{S} = \iint \left[\tfrac{1}{2}\rho|\mathbf{u}|^2 - \rho\Phi - \rho H(p_0, s) + p_0 + p_1\big(1 - \rho/\rho^\star(p_0, s)\big) \right] \mathrm{d}^3\mathbf{x}\,\mathrm{d}t\,, \tag{5.6}$$

where $H(p, s)$ is the specific enthalpy (introduced by $U = H - p/\rho$), $p_0(\mathbf{x})$ is a fixed "background" pressure field, and p_1 is a Lagrange multiplier that enforces the constraint $\rho = \rho^\star(p_0, s)$, where $\rho^\star$ is any desired function of p_0 and s. The effect of this constraint is to ensure that fluid elements expand or contract instantaneously, rather than oscillating around an equilibrium size and radiating sound waves. This approximation can be justified by assuming an infinitely fast sound speed; i.e. pressure perturbations are instantly carried away by an infinitely fast sound wave. However, we do not make any precise assumption about the sound speed here. Rather, we make the more general, less precise, assumption that pressure perturbations are small without specifying why that may be. If we take p_0 and s to be constant in equation (5.6), so that H and $\rho^\star$ are also constant, then we obtain the action for an incompressible fluid. But allowing for non-constant p_0 and s retains many of the effects of stratification and buoyancy, while still removing sound waves

from the equations. There is considerable freedom in the choice of the function $\rho^\star$, and several well-known sound-proof models can be obtained as special cases. In particular, the anelastic model of Lantz (1992) and Braginsky & Roberts (1995) is recovered by neglecting the dependence of $\rho^\star$ on s, and thus regarding it as a fixed background field, and a pseudo-incompressible model similar to Durran (1989) is recovered by using the equation of state $1/\rho^\star(p_0, s) = \partial H(p_0, s)/\partial p$. We can easily extend this action to include magnetic fields under the MHD approximation, simply by adding $-|\mathbf{B}|^2/2\mu_0$ to the integrand in equation (5.6). This is equivalent to simply adding the Lorentz force into the momentum equation, and solving the induction equation in its usual form (5.3). However, in general there is no reason to expect that the equations derived from such an action would provide a close approximation to the dynamics of the fully compressible MHD system. For example, it is well known that the Boussinesq MHD equations do not describe magnetic buoyancy, unless they are modified to take account of changes in gas pressure produced by the magnetic pressure (Spiegel & Weiss, 1982; Corfield, 1984). Moreover there could be other sound-proof models with a different functional form to equation (5.6). Because there is no way to systematically study all possible nonlinear sound-proof models, in what follows we will confine our attention to the linearised sound-proof equations, describing small perturbations to a prescribed equilibrium state. In place of the functional degrees of freedom present in the nonlinear sound-proof model (5.6), the linearised equations contain only algebraic degrees of freedom, in the form of adjustable coefficients. This allows us to consider all possible linear sound-proof models simultaneously. For reasons described in the next section, the adjointness and energy conserving properties of the linearised equations provide an important test of their fidelity to the fully compressible system.

5.3 Properties of the linearised equations

A convenient property of a Hamiltonian system is that, when we consider linear perturbations to any particular solution, the linearised equations themselves have a Hamiltonian structure. In this section we will prove some important properties of the linearised equations, and for illustration we will consider a particular physical system. Motivated by the solar tachocline, we will consider a steady, static background state with uniform gravity, $\boldsymbol{\nabla}\Phi = -g\widehat{\mathbf{z}}$, containing a horizontal magnetic field whose strength varies with height, $\mathbf{B}_0 = B_0(z)\widehat{\mathbf{x}}$. We express each physical quantity, f say, as $f = f_0(z) + f_1(x, y, z, t)$, where f_0 represents the background state and f_1 is a linear perturbation. The linearised fully

compressible equations are

$$\rho_0 \frac{\partial}{\partial t}\mathbf{u} = -g\rho_1 \widehat{\mathbf{z}} - \boldsymbol{\nabla}\pi_1 + \frac{1}{\mu_0}\mathbf{B}_0 \cdot \boldsymbol{\nabla}\mathbf{B}_1 + \frac{1}{\mu_0}\mathbf{B}_1 \cdot \boldsymbol{\nabla}\mathbf{B}_0, \tag{5.7}$$

$$\frac{\partial}{\partial t}\mathbf{B}_1 = \boldsymbol{\nabla} \times (\mathbf{u} \times \mathbf{B}_0), \tag{5.8}$$

$$\frac{\partial}{\partial t}\rho_1 = -\boldsymbol{\nabla} \cdot (\rho_0 \mathbf{u}), \tag{5.9}$$

$$\frac{\partial}{\partial t}s_1 = -\mathbf{u} \cdot \boldsymbol{\nabla} s_0\,, \tag{5.10}$$

$$\pi_1 = p_1 + \frac{1}{\mu_0}\mathbf{B}_0 \cdot \mathbf{B}_1, \tag{5.11}$$

$$\rho_1 = \left(\frac{\partial \rho}{\partial s}\right)_p s_1 + \left(\frac{\partial \rho}{\partial p}\right)_s p_1, \tag{5.12}$$

where π_1 is the perturbation to the total (i.e. gas plus magnetic) pressure, and where the partial derivatives in equation (5.12) are evaluated in the background state. (Note that we have not assumed a specific equation of state.) The background state must be in magneto-hydrostatic balance, i.e.

$$\frac{\mathrm{d}\pi_0}{\mathrm{d}z} \equiv \frac{\mathrm{d}}{\mathrm{d}z}\left(p_0 + \frac{B_0^2}{2\mu_0}\right) = -g\rho_0\,. \tag{5.13}$$

Because we are considering perturbations to a static background, the resulting linearised equations are guaranteed to be self-adjoint, as we shall now prove.

5.3.1 Self-adjointness of the fully compressible system

The self-adjointness of equations (5.7)–(5.12) was demonstrated by Bernstein *et al.* (1958), and is discussed in further detail by Goedbloed *et al.* (2019), so here we will only summarise the main results. It is convenient to first express all of the perturbations in terms of the (linearised) Lagrangian displacement, $\boldsymbol{\xi}$. This can be achieved using the linearised version of equation (3.49):

$$\rho_1 = -\boldsymbol{\nabla} \cdot (\rho_0 \boldsymbol{\xi})\,, \quad s_1 = -\boldsymbol{\xi} \cdot \boldsymbol{\nabla} s_0\,, \quad \mathbf{u} = \frac{\partial \boldsymbol{\xi}}{\partial t}\,, \quad \mathbf{B}_1 = \boldsymbol{\nabla} \times (\boldsymbol{\xi} \times \mathbf{B}_0)\,. \tag{5.14}$$

With some straightforward but lengthy algebra, the linear system can be written in the form of a single vector equation,

$$\rho_0 \frac{\partial^2 \boldsymbol{\xi}}{\partial t^2} = \mathbf{F}[\boldsymbol{\xi}], \tag{5.15}$$

where $\mathbf{F}$ is a linear differential operator, given by (Bernstein *et al.*, 1958)

$$\mathbf{F}[\boldsymbol{\xi}] = \boldsymbol{\nabla}\left(\rho_0(c^2+v^2)\boldsymbol{\nabla}\cdot\boldsymbol{\xi} - \rho_0 v^2\frac{\partial \xi_x}{\partial x} - g\rho_0\xi_z\right) + \rho_0 v^2\frac{\partial^2\boldsymbol{\xi}}{\partial x^2} - \rho_0 v^2\frac{\partial}{\partial x}(\boldsymbol{\nabla}\cdot\boldsymbol{\xi})\widehat{\mathbf{x}} + g\boldsymbol{\nabla}\cdot(\rho_0\boldsymbol{\xi})\,\widehat{\mathbf{z}}\,. \tag{5.16}$$

Here, c is the sound speed and v is the Alfvén speed in the background state; these are defined as

$$c^2 \equiv \left(\frac{\partial p}{\partial \rho}\right)_s \qquad \text{and} \qquad v^2 \equiv \frac{B_0^2}{\mu_0\rho_0}\,. \tag{5.17}$$

The operator $\mathbf{F}[\boldsymbol{\xi}]$ is self-adjoint with respect to the usual inner product $\langle\cdot,\cdot\rangle$ defined as

$$\langle\boldsymbol{\xi}_1,\boldsymbol{\xi}_2\rangle \equiv \int \boldsymbol{\xi}_1\cdot\boldsymbol{\xi}_2\,\mathrm{d}^3\mathbf{x}\,, \tag{5.18}$$

i.e. we have that

$$\langle\boldsymbol{\xi}_1,\mathbf{F}[\boldsymbol{\xi}_2]\rangle = \langle\mathbf{F}[\boldsymbol{\xi}_1],\boldsymbol{\xi}_2\rangle \tag{5.19}$$

for arbitrary vectors $\boldsymbol{\xi}_1$ and $\boldsymbol{\xi}_2$. In order to derive this result we use integration by parts. That is, we evoke the divergence theorem on a product of an arbitrary scalar, A, and vector, $\boldsymbol{\xi}$, in a volume V bounded by surface S;

$$\int_V \boldsymbol{\nabla}\cdot(A\boldsymbol{\xi})\;\mathrm{d}V = \int_S A\boldsymbol{\xi}\cdot\widehat{\mathbf{n}}\,\mathrm{d}S \tag{5.20}$$

where $\widehat{\mathbf{n}}$ is the normal unit vector to S. We recognise that the left hand side can be re-written as

$$\int_V \boldsymbol{\nabla}\cdot(A\boldsymbol{\xi})\;\mathrm{d}V = \int_V A\,(\boldsymbol{\nabla}\cdot\boldsymbol{\xi})\;\mathrm{d}V + \int_V \boldsymbol{\xi}\cdot\boldsymbol{\nabla}A\,\mathrm{d}V\,. \tag{5.21}$$

If we were in such a system with boundary conditions such that the right hand-side of (5.20) were zero, i.e. $\boldsymbol{\xi}\cdot\widehat{\mathbf{n}} = 0$ on S, then we can use

$$\int_V A\,(\boldsymbol{\nabla}\cdot\boldsymbol{\xi})\;\mathrm{d}V = -\int_V \boldsymbol{\xi}\cdot\boldsymbol{\nabla}A\,\mathrm{d}V\,. \tag{5.22}$$

Since we are concerned here with buoyancy instability — rather than any surface instabilities, such as the Kruskal-Schwarzchild instability — that develop within the body of the fluid we choose boundary conditions that satisfy $\boldsymbol{\xi}\cdot\widehat{\mathbf{n}} = 0$, i.e. displacements that do not move the boundary (Newcomb, 1961). Using this method, neglecting surface terms, we can write $\langle\boldsymbol{\xi}_1,\mathbf{F}[\boldsymbol{\xi}_2]\rangle$ in the symmetric form

$$\langle\boldsymbol{\xi}_1,\mathbf{F}[\boldsymbol{\xi}_2]\rangle = -\int W[\boldsymbol{\xi}_1,\boldsymbol{\xi}_2]\,\mathrm{d}^3\mathbf{x}, \tag{5.23}$$

where $W[\boldsymbol{\xi}_1, \boldsymbol{\xi}_2]$ is the symmetric bilinear operator

$$W[\boldsymbol{\xi}_1, \boldsymbol{\xi}_2] \equiv -g\rho_0\xi_{1z}(\boldsymbol{\nabla}\cdot\boldsymbol{\xi}_2) - g\rho_0\xi_{2z}(\boldsymbol{\nabla}\cdot\boldsymbol{\xi}_1) - \rho_0 v^2\frac{\partial\xi_{2x}}{\partial x}(\boldsymbol{\nabla}\cdot\boldsymbol{\xi}_1) - \rho_0 v^2\frac{\partial\xi_{1x}}{\partial x}(\boldsymbol{\nabla}\cdot\boldsymbol{\xi}_2)$$
$$- g\frac{\mathrm{d}\rho_0}{\mathrm{d}z}\xi_{2z}\xi_{1z} + \rho_0(c^2+v^2)(\boldsymbol{\nabla}\cdot\boldsymbol{\xi}_2)(\boldsymbol{\nabla}\cdot\boldsymbol{\xi}_1) + \rho_0 v^2\frac{\partial\boldsymbol{\xi}_1}{\partial x}\cdot\frac{\partial\boldsymbol{\xi}_2}{\partial x}\,. \tag{5.24}$$

From this symmetry, and the definition (5.18), we see immediately that

$$\langle\boldsymbol{\xi}_1, \mathbf{F}[\boldsymbol{\xi}_2]\rangle = -\int W[\boldsymbol{\xi}_1, \boldsymbol{\xi}_2]\,\mathrm{d}^3\mathbf{x} = -\int W[\boldsymbol{\xi}_2, \boldsymbol{\xi}_1]\,\mathrm{d}^3\mathbf{x} = \langle\mathbf{F}[\boldsymbol{\xi}_1], \boldsymbol{\xi}_2\rangle\,, \tag{5.25}$$

as required.

The proof just presented adopted a relatively simple background state, with a unidirectional magnetic field, $\mathbf{B}_0 = B_0(z)\widehat{\mathbf{x}}$, but with effort it can be generalised to an arbitrary background state, provided only that it is a steady solution of the governing equations in an inertial frame. However, this general result can be arrived at with less effort by considering the action (3.48). Because the nonlinear equations of motion (5.2)–(5.5) are the Euler–Lagrange equations for the functional (3.48), it follows that the linearised equations of motion (5.7)–(5.12) are the Euler–Lagrange equations for an action that can be obtained by taking the second variation of (3.48), i.e. by expanding each variable as $f = f_0 + f_1$ and isolating the terms that are of second order in the perturbations (Newcomb, 1962). The linearised Euler–Lagrange equations are sometimes referred to as Jacobi equations, by analogy with the equations defining Jacobi fields in Riemannian geometry (Taub, 1969). Given that the action (3.48) only depends on the square of the velocity, when we consider perturbations to a background state at rest, it is clear that the second variation, expressed in terms of $\boldsymbol{\xi}$, will have the form

$$\delta^{(2)}\mathcal{S} = \iint\left[\tfrac{1}{2}\rho_0\left|\frac{\partial\boldsymbol{\xi}}{\partial t}\right|^2 - \tfrac{1}{2}W[\boldsymbol{\xi},\boldsymbol{\xi}]\right]\mathrm{d}^3\mathbf{x}\,\mathrm{d}t, \tag{5.26}$$

where $W[\boldsymbol{\xi},\boldsymbol{\xi}]$ is a bilinear operator, which can be taken to be symmetric without loss of generality. If we work in a rotating frame, or if the Hall effect is present, then the action contains terms that are linear in the velocity. In that case the argument presented here fails, and the linearised equations are generally not self-adjoint. This lack of self-adjointness can also be interpreted as a lack of time-reversibility of the governing equations. With a rotating system, it would be possible only to derive necessary conditions for stability — proof of sufficiency relies on self-adjointness. For this reason, we choose to neglect rotation for the entirety of this chapter. While this may seem like a major restriction, especially given that our intended application is to the Sun, or other rotating astrophysical bodies, it is no more of a limitation than the necessary neglect of non-Hamiltonian processes like diffusion or viscosity (which, of course, would be present

in the Sun).

Regarding $\delta^{(2)}\mathcal{S}$ as the action for the perturbations, and applying Hamilton's principle, we find the equation of motion to be precisely (5.15), where the operator $\mathbf{F}$ is defined so that

$$-\int W[\boldsymbol{\xi}, \delta\boldsymbol{\xi}]\,\mathrm{d}^3\mathbf{x} = \int \mathbf{F}[\boldsymbol{\xi}]\cdot\delta\boldsymbol{\xi}\,\mathrm{d}^3\mathbf{x}\,. \tag{5.27}$$

In other words, the operator $\mathbf{F}$ is defined by the functional derivative

$$\mathbf{F}[\boldsymbol{\xi}] = -\frac{\delta\mathcal{W}}{\delta\boldsymbol{\xi}}, \tag{5.28}$$

where $\mathcal{W}$ is the functional

$$\mathcal{W} = \int \tfrac{1}{2}W[\boldsymbol{\xi}, \boldsymbol{\xi}]\,\mathrm{d}^3\mathbf{x}. \tag{5.29}$$

Equation (5.27) applies for arbitrary vectors $\boldsymbol{\xi}$ and $\delta\boldsymbol{\xi}$ (indeed the arbitrariness of $\delta\boldsymbol{\xi}$, and its independence from $\boldsymbol{\xi}$, is built into the definition of the functional derivative in equation (5.28)), demonstrating that the operator $\mathbf{F}$ is self-adjoint with respect to the inner product defined in equation (5.18). The earlier results for the fully compressible MHD system can now be seen as a particular case of this general result, and the operators $\mathbf{F}$ and W defined in equations (5.16) and (5.24) are particular cases of the operators appearing in equations (5.26) and (5.28).

From the above results, it is easily shown that the quantity $(1/2)\rho_0\,|\partial\boldsymbol{\xi}/\partial t|^2+(1/2)W[\boldsymbol{\xi}, \boldsymbol{\xi}]$ is conserved in the linearised equations; following Eckart & Ferris (1956) we will refer to this as the "external energy" density of the perturbed system, and following Bernstein *et al.* (1958) we refer to $\mathcal{W}$ as the "potential energy" of the perturbations. (In fact, conservation of external energy is just an example of Noether's theorem applied to the action $\delta^{(2)}\mathcal{S}$.) Bernstein *et al.* (1958) proved that the converse is also true, i.e. any system of linear equations that have a conserved external energy in this form, and an equation of motion of the form (5.15), must also have an action of the form (5.26), and must therefore be self-adjoint.

The self-adjointness of the linearised equations allows necessary and sufficient stability conditions to be derived in many cases without explicitly solving the equations, simply by considering the potential energy, $\mathcal{W}$. Indeed, the system is linearly unstable if and only if there exists a displacement, $\boldsymbol{\xi}$, that makes the potential energy negative (Laval *et al.*, 1965); this is known as the energy principle (Bernstein *et al.*, 1958). The energy principle has previously been used to determine the stability of magnetostatic states in many physical systems, including stellar magnetic fields (Tayler, 1973) and interstellar clouds (Zweibel & Kulsrud, 1975), and theoretical systems, such as the system considered by (Hughes & Cattaneo, 1987) to study the stability of a vertically stratified horizontal magnetic field.

In the above derivation, the Lagrangian displacement $\boldsymbol{\xi}$ was regarded as an arbitrary vector field, since there is no restriction on the allowed displacements in a fully compressible fluid. In what follows, however, we will consider sound-proof models in which the velocity (and therefore $\boldsymbol{\xi}$) is subject to a constraint. In that context, self-adjointness can be established only over the space of vectors that satisfy this constraint; these ideas are, of course, familiar from studies of incompressible fluids (e.g. Newcomb, 1962).

5.4 Sound-proof models

As described in the introduction, and in Chapter 3, there are many situations in astrophysical (and geophysical) fluid dynamics in which it is advantageous to use a sound-proof model. The choice of which model to use generally comes down to a trade-off between simplicity and accuracy. For reasons already mentioned, energy conservation of the nonlinear equations, and self-adjointness of the linearised equations, are desirable properties for any model. In particular, self-adjointness can be used to rule out certain unphysical behaviours (e.g. Jones *et al.*, 2009; Brown *et al.*, 2012) associated with violations of energy conservation or wave-action conservation. Our goal here is first to find the most general sound-proof MHD model that is also self-adjoint, and then compare its conserved energy with that of the fully compressible system to assess the accuracy of the approximation. As we did in Chapter 4 (and Moss *et al.* (2022)), we start by introducing the following general linearised sound-proof model:

$$\rho_0 \frac{\partial}{\partial t}\mathbf{u} = -\left[\frac{D}{c^2}p_1 + \left(\frac{\partial \rho}{\partial s}\right)_p s_1\right] g\hat{\mathbf{z}} - \boldsymbol{\nabla}\pi_1 + \frac{1}{\mu_0}\mathbf{B}_0\cdot\boldsymbol{\nabla}\mathbf{B}_1 + \frac{1}{\mu_0}\mathbf{B}_1\cdot\boldsymbol{\nabla}\mathbf{B}_0\,, \tag{5.30}$$

$$\frac{\partial}{\partial t}\mathbf{B}_1 = \boldsymbol{\nabla}\times(\mathbf{u}\times\mathbf{B}_0)\,, \tag{5.31}$$

$$\frac{\partial}{\partial t}s_1 = -\frac{\mathrm{d}s_0}{\mathrm{d}z}u_z\,, \tag{5.32}$$

$$\boldsymbol{\nabla}\cdot\mathbf{u} = C\frac{g}{c^2}u_z\,, \tag{5.33}$$

$$J\pi_1 = p_1 + \frac{B_0}{\mu_0}B_{1x}\,. \tag{5.34}$$

(In contrast to Chapter 4, we only consider here the ideal equations, without any dissipative terms.) As previously, we will consider perturbations to a static state that depends only on z, and has $\mathbf{B}_0 = B_0(z)\hat{\mathbf{x}}$. The coefficients C, D, J are assumed to be known functions of z; different choices for these coefficients correspond to different sound-proof approximations. Table 5.1 lists the values of these coefficients that reproduce several commonly-used sound-proof models, where for brevity we have introduced the density scale height, $H_\rho \equiv -\left(\mathrm{d}\ln\rho_0/\mathrm{d}z\right)^{-1}$. The values listed in Table 5.1 were explained in de-

Coefficient \ Model	LBR anelastic	GGG anelastic	Pseudo-incompressible	Magneto-Boussinesq
C	$\frac{c^2}{g}H_\rho^{-1}$	$\frac{c^2}{g}H_\rho^{-1}$	1	$\frac{c^2}{g}H_\rho^{-1}$
D	$\frac{c^2}{g}H_\rho^{-1}$	1	1	1
J	1	1	1	0

Table 5.1: Values for each of the coefficients in our sound-proof model needed to reproduce the models summarised in Section 3. Note that this is a subset of Table 4.1 which is reproduced here for convenience.

tail in Chapters 3 and 4. Each of these models can be rigorously derived under certain assumptions, including that the background state has nearly uniform entropy, and that the sound speed far exceeds the Alfvén speed. It should be acknowledged that, in the solar tachocline — which forms the motivation for this work — the first of these assumptions is not strictly valid. In particular, in the lower, stably stratified part of the tachocline, the entropy scale height (defined as $H_s \equiv g/N^2$, where N is the buoyancy frequency) exceeds the density scale height by only one order of magnitude (e.g. Gough, 2007), whereas each of the sound-proof models listed in Table 5.1 formally assumes that $H_s \gg H_\rho$. On the other hand, the assumption that $v \ll c$ is certainly satisfied in the tachocline, provided that the field is much weaker than 10^7 gauss. A detailed discussion of the assumptions under which different sound-proof models can be rigorously derived can be found in Chapter 3. In what follows, we will make no assumptions about the relative magnitudes of H_s and H_ρ, and we will appeal to energy conservation rather than formal asymptotics to obtain constraints on the values of C, D and J. In this way we will generalise previous results by Fan (2001) and Wilczyński *et al.* (2022), who showed that the linearised anelastic equations are self-adjoint in the asymptotic limit $H_s/H_\rho \to \infty$ for which they are formally valid.

5.4.1 Self-adjointness as a constraint

As mentioned in Section 5.2, there is a wide family of sound-proof MHD models that can be obtained from an action. In Chapter 4 we showed that one such model — the pseudo-incompressible model — captures the linear behaviour of the magnetic buoyancy instability in several asymptotic regimes relevant to the solar tachocline. This leads us to ask if there might exist other sound-proof models, also obtainable from an action, that describe magnetic buoyancy equally well. If such an action did exist then the resulting set of linearised equations would necessarily be self-adjoint, with respect to some choice of inner product. We will therefore determine the conditions under which our general sound-proof model (5.30)–(5.34) is self-adjoint. We define the inner product in the most

general way possible:

$$\langle \boldsymbol{\xi}_1, \boldsymbol{\xi}_2 \rangle \equiv \int w\, \boldsymbol{\xi}_1 \cdot \boldsymbol{\xi}_2 \, \mathrm{d}^3\mathbf{x}, \tag{5.35}$$

where w represents a weight function, which must be positive but is otherwise arbitrary at this stage.

We now follow the same method as in Section 5.3.1, i.e. we reduce equations (5.30)–(5.34) to a single equation describing the acceleration of a linear displacement, $\boldsymbol{\xi}$. However, an important difference here is that, for any sound-proof model, the velocity (and hence $\boldsymbol{\xi}$) is subject to a constraint, given in our case by equation (5.33). The equations must therefore also include a variable that is independent of $\boldsymbol{\xi}$, which in our case we can take to be π_1, that serves to impose this constraint. Hence we arrive at an equation of motion of the form $\rho_0(\partial^2\boldsymbol{\xi}/\partial t^2) = \mathbf{F}[\boldsymbol{\xi}, \pi_1]$, where the operator $\mathbf{F}$ in our case is given by

$$\begin{aligned}\mathbf{F}[\boldsymbol{\xi}, \pi_1] = &- \left(\boldsymbol{\nabla} + DJ\frac{g}{c^2}\widehat{\mathbf{z}}\right)\pi_1 + D\frac{g}{c^2}\rho_0 v^2 \left(\frac{\partial \xi_x}{\partial x} + \frac{1}{H_B}\xi_z - \boldsymbol{\nabla}\cdot\boldsymbol{\xi}\right)\widehat{\mathbf{z}} \\ &+ \rho_0 v^2 \frac{\partial^2 \boldsymbol{\xi}}{\partial x^2} - \rho_0 v^2 \frac{\partial}{\partial x}(\boldsymbol{\nabla}\cdot\boldsymbol{\xi})\widehat{\mathbf{x}} - \rho_0 \frac{g}{H_s}\xi_z \widehat{\mathbf{z}}\,,\end{aligned} \tag{5.36}$$

and where $\boldsymbol{\xi}$ must satisfy the constraint

$$\boldsymbol{\nabla}\cdot\boldsymbol{\xi} = C\frac{g}{c^2}\xi_z\,. \tag{5.37}$$

For brevity, in equation (5.36) we have introduced scale heights for the magnetic field, H_B, and specific entropy, H_s, defined as

$$H_B^{-1} = -\frac{1}{B_0}\frac{\mathrm{d}B_0}{\mathrm{d}z}\,, \tag{5.38}$$

$$H_s^{-1} = -\frac{1}{\rho_0}\left(\frac{\partial \rho}{\partial s}\right)_p \frac{\mathrm{d}s_0}{\mathrm{d}z}\,. \tag{5.39}$$

(Equation (5.39) is equivalent to the definition $H_s = g/N^2$ given earlier.) Given that the background state must satisfy magneto-hydrostatic balance, equation (5.13), these can be related to the density scale height, H_ρ, as follows:

$$g = c^2 H_\rho^{-1} - c^2 H_s^{-1} + v^2 H_B^{-1}\,. \tag{5.40}$$

Now, in order for $\mathbf{F}$ to be self-adjoint, with respect to our general inner product (5.35), the terms involving π_1 in the integral $\int w\, \boldsymbol{\xi}_2 \cdot \mathbf{F}[\boldsymbol{\xi}_1, \pi_1]\, \mathrm{d}^3\mathbf{x}$ must vanish for all possible functions

π_1, and all functions $\boldsymbol{\xi}_2$ that satisfy the constraint (5.37). We therefore require that

$$\begin{aligned} 0 &= -\int w\left[\boldsymbol{\xi}_2\cdot\boldsymbol{\nabla}\pi_1 + DJ\frac{g}{c^2}\xi_{2z}\pi_1\right]\,\mathrm{d}^3\mathbf{x} \\ &= \int \pi_1\left[\boldsymbol{\xi}_2\cdot\boldsymbol{\nabla}w + w(C-DJ)\frac{g}{c^2}\xi_{2z}\right]\,\mathrm{d}^3\mathbf{x}\,, \end{aligned} \tag{5.41}$$

where we have used integration by parts, as well as equation (5.37). As before, in using integration by parts we are neglecting surface terms, this is justified by choosing boundary conditions for which $\boldsymbol{\xi}\cdot\widehat{\mathbf{n}} = 0$ on the boundary, where $\widehat{\mathbf{n}}$ is the normal to the boundary surface. We therefore require that the weight function w depends only on z, and satisfies

$$\frac{1}{w}\frac{\mathrm{d}w}{\mathrm{d}z} = (DJ - C)\frac{g}{c^2}. \tag{5.42}$$

Provided that this is the case, we then find that

$$\begin{aligned} \langle\boldsymbol{\xi}_2, \mathbf{F}[\boldsymbol{\xi}_1,\pi_1]\rangle = \int w\Bigg[&\rho_0\frac{g}{c^2}\left(Dv^2\left(\frac{1}{H_B} - \frac{Cg}{c^2}\right) - \frac{c^2}{H_s}\right)\xi_{2z}\xi_{1z} - \rho_0 v^2\frac{\partial\boldsymbol{\xi}_2}{\partial x}\cdot\frac{\partial\boldsymbol{\xi}_1}{\partial x} \\ &+ \frac{g}{c^2}\rho_0 v^2\left(D\xi_{2z}\frac{\partial\xi_{1x}}{\partial x} + C\frac{\partial\xi_{2x}}{\partial x}\xi_{1z}\right)\Bigg]\,\mathrm{d}^3\mathbf{x}\,. \end{aligned} \tag{5.43}$$

We conclude that our sound-proof model is self-adjoint if and only if $C = D$, because only in that case is equation (5.43) symmetric with respect to $\boldsymbol{\xi}_1$ and $\boldsymbol{\xi}_2$.

Comparing with Table 5.1, we see that the LBR anelastic and pseudo-incompressible models satisfy this condition. We emphasise that this condition only arises in the presence of a magnetic field; in the non-magnetic case ($v = 0$) the sound-proof equations can always be made self-adjoint by judiciously choosing the weight function w to satisfy equation (5.42). This implies that the linearised non-magnetic equations have the following conserved quantity:

$$\int \tfrac{1}{2}w\left(\rho_0\left|\frac{\partial\boldsymbol{\xi}}{\partial t}\right|^2 - \boldsymbol{\xi}\cdot\mathbf{F}[\boldsymbol{\xi},\pi]\right)\,\mathrm{d}^3\mathbf{x} = \int \tfrac{1}{2}w\rho_0\left(\left|\frac{\partial\boldsymbol{\xi}}{\partial t}\right|^2 + \frac{g}{H_s}\xi_z^2\right)\,\mathrm{d}^3\mathbf{x}\,, \tag{5.44}$$

which Brown *et al.* (2012) have called the "pseudo energy".

In the more general case, including a magnetic field, self-adjointness requires $C = D$, and therefore the weight function w must satisfy

$$\frac{1}{w}\frac{\mathrm{d}w}{\mathrm{d}z} = C(J-1)\frac{g}{c^2}. \tag{5.45}$$

In that case, the model conserves the following pseudo energy:

$$\int \tfrac{1}{2} w\rho_0 \left(\left| \frac{\partial \boldsymbol{\xi}}{\partial t} \right|^2 + g \left(\frac{1}{H_s} + C\frac{v^2}{c^2} \left(C\frac{g}{c^2} - \frac{1}{H_B} \right) \right) \xi_z^2 + v^2 \left| \frac{\partial \boldsymbol{\xi}}{\partial x} \right|^2 - 2Cg\frac{v^2}{c^2}\xi_z \frac{\partial \xi_x}{\partial x} \right) \mathrm{d}^3\mathbf{x} \,. \tag{5.46}$$

To determine the optimal choice for the remaining parameters C and J we can directly compare this pseudo energy to the true external energy of the fully compressible system; we do this in the following section.

5.4.2 Comparison with fully compressible external energy

We have shown in Section 5.3.1 that the linearised, fully compressible system conserves the following external energy

$$\int \left(\tfrac{1}{2}\rho_0 \left| \frac{\partial \boldsymbol{\xi}}{\partial t} \right|^2 + \tfrac{1}{2} W[\boldsymbol{\xi}, \boldsymbol{\xi}] \right) \mathrm{d}^3\mathbf{x} =$$

$$\int \tfrac{1}{2}\rho_0 \left(\left| \frac{\partial \boldsymbol{\xi}}{\partial t} \right|^2 + \frac{g}{H_\rho}\xi_z^2 - 2g\xi_z(\boldsymbol{\nabla}\cdot\boldsymbol{\xi}) + (c^2+v^2)(\boldsymbol{\nabla}\cdot\boldsymbol{\xi})^2 + v^2 \left| \frac{\partial \boldsymbol{\xi}}{\partial x} \right|^2 - 2v^2 \frac{\partial \xi_x}{\partial x}(\boldsymbol{\nabla}\cdot\boldsymbol{\xi}) \right) \mathrm{d}^3\mathbf{x} \,, \tag{5.47}$$

where W is given by equation (5.24). On first inspection, this appears quite different to the conserved quantity (5.46) of the sound-proof system. However, if we only consider displacements $\boldsymbol{\xi}$ that satisfy the divergence constraint (5.37) then the compressible external energy reduces to

$$\int \tfrac{1}{2}\rho_0 \left(\left| \frac{\partial \boldsymbol{\xi}}{\partial t} \right|^2 + g \left(\frac{1}{H_\rho} - 2C\frac{g}{c^2} + (c^2+v^2)C^2\frac{g}{c^4} \right) \xi_z^2 + v^2 \left| \frac{\partial \boldsymbol{\xi}}{\partial x} \right|^2 - 2Cg\frac{v^2}{c^2}\xi_z \frac{\partial \xi_x}{\partial x} \right) \mathrm{d}^3\mathbf{x} \,, \tag{5.48}$$

which can now be directly compared with equation (5.46). We first note that, for these two conserved quantities to be comparable, the weight function in equation (5.46) must be constant, and therefore we must have either $J = 1$ or $C = 0$. The latter option is easily ruled out by considering the rest of the integrands. Indeed, requiring the ξ_z^2 terms to be identical yields a quadratic equation for the remaining coefficient C, implying that there are two values for which the two conserved quantities match. Using the relation (5.40), these are found to be

$$C = 1 \qquad \text{and} \qquad C = 1 - \frac{v^2}{gH_B} = \frac{\mathrm{d}p_0/\mathrm{d}z}{\mathrm{d}\pi_0/\mathrm{d}z} \,. \tag{5.49}$$

The latter choice would not be practical in any computational model, since it would imply a divergence constraint on the velocity that also depends on the magnetic field, whose

strength and geometry would generally not be known in advance. Furthermore, in most sound-proof MHD models the background state is assumed to be essentially non-magnetic, in the sense that $\frac{\mathrm{d}\pi_0}{\mathrm{d}z} \simeq \frac{\mathrm{d}p_0}{\mathrm{d}z}$, and so the only sensible choice for the parameter C is $C = 1$.

In summary, in order for the sound-proof model to conserve the same external energy as the fully compressible model, under the widest range of conditions, we must take the coefficients in equations (5.30)–(5.34) to be $C = D = J = 1$. This singles out the pseudo-incompressible model.

However, we note that, if the background state is assumed to be both non-magnetic and close to isentropic, so that both the H_B and H_s terms in equation (2.20) are negligible, then we have $g \simeq c^2/H_\rho$. This is the regime in which the LBR anelastic model is formally valid, and we see from Table 5.1 that in this regime that model has $C = D \simeq 1$. Therefore the LBR model is self-adjoint in all parameter regimes, but only conserves the correct external energy when the background state is essentially non-magnetic and isentropic. This is consistent with the results of Fan (2001) and Wilczyński *et al.* (2022).

5.5 Energy stability method

Above, in Section 5.4.2, we have shown that the pseudo-incompressible model conserves the same energy as the fully compressible equations. However, this does not guarantee that the two systems have identical stability properties, but rather that the pseudo-incompressible is "at least as stable" as the fully compressible system in the sense that any perturbation that grows in the pseudo-incompressible model must also grow in the fully compressible system. The converse, however, is not true since there could be an unstable solution of the fully compressible equations that violates the pseudo-incompressible velocity constraint. In this section we will use the energy stability method (Bernstein *et al.*, 1958) to derive an instability criteria for our general sound-proof model and determine the constraints on the model such that the stability properties match that of the fully compressible system.

We have shown that our sound-proof equations (5.30)–(5.34) are self-adjoint if $C = D$ and if the weight function is chosen to satisfy equation (5.45). In that case, they have the following potential energy:

$$\mathcal{W} = \int \tfrac{1}{2} w \rho_0 \left(g \left(\frac{1}{H_s} + C\frac{v^2}{c^2}(C\frac{g}{c^2} - \frac{1}{H_B}) \right) \xi_z^2 + v^2 \left| \frac{\partial \boldsymbol{\xi}}{\partial x} \right|^2 - 2Cg\frac{v^2}{c^2}\xi_z \frac{\partial \xi_x}{\partial x} \right) \mathrm{d}^3\mathbf{x} \,. \quad (5.50)$$

The system is then stable if and only if $\mathcal{W}$ is positive for all displacements $\boldsymbol{\xi}$ that satisfy the constraint

$$\boldsymbol{\nabla}\cdot\boldsymbol{\xi} = C\frac{g}{c^2}\xi_z \,. \quad (5.51)$$

We first consider interchange modes, i.e. displacements with $\partial\boldsymbol{\xi}/\partial x = \mathbf{0}$. For such modes,

we see immediately from equation (5.50) that the condition for instability is

$$C\frac{v^2}{H_B} > \frac{c^2}{H_s} + C^2 g\frac{v^2}{c^2}\,. \tag{5.52}$$

If this condition is satisfied for any range of z, then there are displacements for which $\mathcal{W}$ is negative, and therefore the system is unstable.

For the more general case of undular modes, that is modes with $\partial/\partial x \neq 0$, we can first eliminate ξ_x from the potential energy using the constraint (5.51). The potential energy then becomes

$$\mathcal{W} = \int \tfrac{1}{2} w\rho_0 \left(g\left(\frac{1}{H_s} - \frac{v^2}{c^2}\frac{C}{H_B}\right)\xi_z^2 + v^2\left(\left(\frac{\partial \xi_y}{\partial x}\right)^2 + \left(\frac{\partial \xi_z}{\partial x}\right)^2 + \left(\frac{\partial \xi_y}{\partial y} + \frac{\partial \xi_z}{\partial z}\right)^2\right)\right) \mathrm{d}^3\mathbf{x}\,. \tag{5.53}$$

As per Hughes & Cattaneo (1987) (see also; Section 2.3), without loss of generality we can consider displacements with $\xi_y = \hat{\xi}_y(z)\sin(lx)\sin(my)$ and $\xi_z = \hat{\xi}_z(z)\sin(lx)\cos(my)$. These forms are chosen to simplify the algebra as best we can; here, we ensure that the final terms have common factors; i.e. $\partial\xi_y/\partial y$ and $\partial\xi_z/\partial z$ will have the same x and y dependence. When you carry out the integration over $\mathrm{d}^3\mathbf{x}$, the factors of sin and cos integrate to a constant; and so do not effect the stability criteria that we are interested in here. Minimising with respect to $\hat{\xi}_y$, we find that

$$\hat{\xi}_y = -\frac{m\hat{\xi}_z'}{l^2+m^2}\,, \tag{5.54}$$

and then the potential energy becomes

$$\mathcal{W} = \int \tfrac{1}{8} w\rho_0 \left(g\left(\frac{1}{H_s} - \frac{v^2}{c^2}\frac{C}{H_B}\right)\hat{\xi}_z^2 + v^2 l^2\left(\hat{\xi}_z^2 + \frac{\hat{\xi}_z'^2}{l^2+m^2}\right)\right) \mathrm{d}z\,. \tag{5.55}$$

Instability is then most easily achieved in the limit of small l, and so we have the instability condition

$$C\frac{v^2}{H_B} > \frac{c^2}{H_s}\,. \tag{5.56}$$

Equations (5.52) and (5.56) match the instability criteria for the fully compressible system if and only if $C = 1$.

5.6 Discussion

We have shown that the (linearised) LBR anelastic and pseudo-incompressible models are both self-adjoint, with respect to the same inner product as the fully compressible equations. This is consistent with the fact, mentioned in Section 5.2, that both of these

models can be derived from an action. However, only the pseudo-incompressible model conserves the same energy as the fully compressible system when the background state has a significant entropy gradient.

Not only is energy conservation a desirable property for any model, it can also be used to establish stability results. The fact that the pseudo-incompressible model conserves the same energy as the fully compressible model guarantees that it is "at least as stable". However, there could still be unstable solutions of the fully compressible system that are not permitted by the pseudo-incompressible velocity constraint. To rule out this possibility, in Section 5.5 we used the energy stability method to obtain an instability criterion for our general sound-proof model, demonstrating that the pseudo-incompressible model has the same stability criteria as the fully compressible system. This is consistent with the results of Chapter 4, where we showed that this model also correctly reproduces the growth rate of the instability under a range of parameter conditions, provided that the Alfvén speed, v, is much smaller than the sound speed, c. This is a condition that is assumed in the rigorous derivation of all of the sound-proof models mentioned in Section 5.4. However, it should be emphasized that the results of the present chapter were obtained without making any explicit scaling assumptions. It is perhaps remarkable that we have arrived at a single sound-proof model simply by requiring conservation of the correct external energy, without any additional physical assumptions about length scales (of the perturbations and scale heights), time scales, or the magnitude of v/c. On the one hand, this gives us confidence that the accuracy of the pseudo-incompressible model is not limited to some specific asymptotic parameter regime. On the other hand, we cannot provide an exhaustive set of conditions under which this model is rigorously valid. Nevertheless, the results in Chapter 4 demonstrate that this model is indeed asymptotically valid in a number of regimes of relevance to magnetic buoyancy in the solar interior.

The conclusions here, coupled with those of Chapter 4, demonstrate that the pseudo-incompressible model describes magnetic buoyancy instability for the widest parameter range, and is therefore the "best" sound-proof approximation in this sense. However, as noted in Chapter 4, its numerical implementation is non-trivial when compared with other sound-proof models and so it may not always be the most practical choice. In particular, for atmospheres that are nearly adiabatically stratified, it may be preferable to use an anelastic model. Such a choice may be less appropriate for the lower part of the solar tachocline, where the departure from adiabatic stratification becomes more significant. However, we demonstrated in Chapter 4 that the GGG anelastic model (despite its lack of self-adjointness) describes magnetic buoyancy instability just as accurately as the pseudo-incompressible model in this regime. If one is prepared to sacrifice energy conservation in order to achieve a more numerically tractable model, then this may be the logical choice.

We must acknowledge that all of the analysis presented here (and in Chapter 4) con-

siders only the linear regime of magnetic buoyancy. We would argue that an accurate description of the linear dynamics is essential for any model. However, the extent to which any of these sound-proof models accurately describes the nonlinear dynamics remains an important and open question.

Chapter 6

Double-diffusive instability

Throughout the majority of the thesis thus far the effects of diffusion have been neglected. In Chapter 2.4 we discussed the effect of thermal diffusion, as considered by Gilman (1970), in the limit of extremely fast diffusion. We also considered the limit of fast thermal diffusion in Chapter 4. However, we have yet to consider the effects of including viscosity and magnetic diffusivity. In this chapter we will include thermal diffusivity, κ, but will not necessarily assume that κ is fast. We will also include magnetic diffusivity, η, and viscosity, ν. When these diffusivities are included a new instability emerges, a so-called double-diffusive instability. We explore this instability analytically and numerically, initially in the magneto-Boussinesq regime and then extending to parameters which no longer approximate the magneto-Boussinesq case. We begin in the magneto-Boussinesq regime to enable comparison with previous analyses, which allows us to verify our results, before then exploring further in parameter space. Throughout this chapter we omit rotation. With this in mind, this chapter is not entirely intended to accurately model the Sun (or other astrophysical bodies), but rather allow us to study the double-diffusive instability in a simplified system. Whilst it is beyond the scope of the current analysis, comparisons of the results of this chapter with similar obtained from a general sound-proof model could derive further constraints on the general sound-proof model and would be a logical next-step.

6.1 Double-diffusive instability in the magneto-Boussinesq approximation

Following the work of Schubert (1968), Acheson (1979) and Hughes (1985), we will derive conditions for instability under the magneto-Boussinesq approximation. As such, we begin with the linearised magneto-Boussinesq equations (equations (3.16)– 3.20)). When we add

in the appropriate diffusivities, and neglect rotation, we arrive at

$$\rho_0 \frac{\partial}{\partial t}\mathbf{u} = -g\rho_1 \widehat{\mathbf{z}} - \boldsymbol{\nabla}_\perp \pi_1 + \frac{1}{\mu_0}\mathbf{B}_0 \cdot \boldsymbol{\nabla}\mathbf{B}_1 - \frac{1}{\mu_0} H_B^{-1} B_{1z}\mathbf{B}_0 + \rho_0 \nu \nabla^2 \mathbf{u}\,, \tag{6.1}$$

$$\frac{\partial}{\partial t}\mathbf{B}_1 = (\mathbf{B}_0 \cdot \boldsymbol{\nabla})\mathbf{u} + (H_B^{-1} - H_\rho^{-1}) u_z \mathbf{B}_0 + \eta \nabla^2 \mathbf{B}_1\,, \tag{6.2}$$

$$\boldsymbol{\nabla}_\perp \cdot \mathbf{u} = 0\,, \tag{6.3}$$

$$\frac{\partial}{\partial t} s_1 + \mathbf{u} \cdot \boldsymbol{\nabla} s_0 = \frac{Q_1}{\rho_0 T_0}, \tag{6.4}$$

$$p_1 + \frac{1}{\mu_0}\mathbf{B}_0 \cdot \mathbf{B}_1 = 0\,, \tag{6.5}$$

(Spiegel & Weiss, 1982) where, as before, the subscript $\perp$ indicates only the components perpendicular to the background field, $\mathbf{B}_0$. We take $Q_1 = \rho_0 c_p \bar{\kappa} \nabla^2 T_1$ where T_1 is given by equation (2.30), $c_p = T_0 \left(\partial s/\partial T\right)_p$ is the specific heat capacity at constant pressure and $\bar{\kappa}$ is the thermal diffusivity (the bar here is used to differentiate from a similar quantity defined later). We then can replace equation (6.4) with

$$\left(\frac{\partial \rho}{\partial s}\right)_p \frac{\partial}{\partial t} s_1 = \rho_0 H_s^{-1} u_z + \left(\frac{\partial \rho}{\partial T}\right)_p \bar{\kappa} \nabla^2 T_1\,, \tag{6.6}$$

$$\left(\frac{\partial \rho}{\partial T}\right)_p T_1 = \left(\frac{\partial \rho}{\partial s}\right)_p s_1 - \frac{\gamma - 1}{c^2} p_1\,, \tag{6.7}$$

where the latter is exactly equation (2.30) which we reproduce here for ease of reference. We recall that under the magneto-Boussinesq assumptions, ρ_0, T_0, $\mathbf{B}_0$ and $\boldsymbol{\nabla} s_0$ are taken to be constant. As we did in Chapter 4, we have assumed our background has a horizontal magnetic field i.e. $\mathbf{B}_0 = B_0 \widehat{\mathbf{x}}$. We will assume that each perturbation variable, say f, varies as $f(\mathbf{x}, t) = \tilde{f} \exp\left(\sigma t + i k_x x + i k_y y + i k_z z\right)$, where $\tilde{f}$ is constant. Note that we will routinely omit tildes in our notation. In accordance with the magneto-Boussinesq approximation, we assume that we are a regime such that $H_\rho^{-1} \sim k_x \ll k_y \sim k_z$. Under

these approximations, all components of equations (6.1 – 6.5) become,

$$\rho_0\sigma^{(\nu)}u_x = \frac{B_0}{\mu_0}ik_xB_{1x} - \frac{1}{\mu_0}H_B^{-1}B_0B_{1z}\,, \tag{6.8}$$

$$\rho_0\sigma^{(\nu)}u_y = -ik_y\pi_1 + \frac{B_0}{\mu_0}ik_xB_{1y}\,, \tag{6.9}$$

$$\rho_0\sigma^{(\nu)}u_z = -g\left[\left(\frac{\partial\rho}{\partial s}\right)_p s_1 + \frac{1}{c^2}p_1\right] - ik_z\pi_1 + \frac{B_0}{\mu_0}ik_xB_{1z}\,, \tag{6.10}$$

$$\sigma^{(\eta)}B_{1x} = B_0ik_xu_x + (H_B^{-1} - H_\rho^{-1})B_0u_z\,, \tag{6.11}$$

$$\sigma^{(\eta)}B_{1y} = B_0ik_xu_y\,, \tag{6.12}$$

$$\sigma^{(\eta)}B_{1z} = B_0ik_xu_z\,, \tag{6.13}$$

$$ik_yu_y + ik_zu_z = 0\,, \tag{6.14}$$

$$p_1 + \frac{1}{\mu_0}B_0B_{1x} = 0\,, \tag{6.15}$$

$$\left(\frac{\partial\rho}{\partial s}\right)_p \sigma s_1 - \rho_0H_s^{-1}u_z = -\left(\frac{\partial\rho}{\partial T}\right)_p \bar{\kappa}k^2T_1\,, \tag{6.16}$$

$$\left(\frac{\partial\rho}{\partial T}\right)_p T_1 = \left(\frac{\partial\rho}{\partial s}\right)_p s_1 - \frac{\gamma-1}{c^2}p_1\,, \tag{6.17}$$

where we have already eliminated ρ_1 by $\rho_1 = (\partial\rho/\partial s)_p\, s_1 + (1/c^2)p_1$ and introduced notation $\sigma^{(a)} = \sigma + ak^2$ for any a where $k^2 = k_x^2 + k_y^2 + k_z^2$.
After some simple but lengthy algebra we can arrive at

$$\rho_0\sigma^{(\nu)}u_x = \frac{B_0}{\mu_0}ik_xB_{1x} - \frac{B_0^2}{\mu_0}H_B^{-1}\frac{ik_x}{\sigma^{(\eta)}}u_z\,, \tag{6.18}$$

$$-\rho_0\left(\sigma^{(\nu)} + v^2\frac{k_x^2}{\sigma^{(\eta)}}\right)\frac{k_z}{k_y}u_z = -ik_y\pi_1\,, \tag{6.19}$$

$$\rho_0\left(\sigma^{(\nu)} + g\frac{H_s^{-1}}{\sigma^{(\bar{\kappa})}} + v^2\frac{k_x^2}{\sigma^{(\eta)}}\right)u_z = g\frac{B_0}{\mu_0}\frac{(\gamma-1)}{c^2\sigma^{(\bar{\kappa})}}\bar{\kappa}k^2B_{1x} + g\frac{1}{c^2}\frac{B_0}{\mu_0}B_{1x} - ik_z\pi_1\,, \tag{6.20}$$

$$\sigma^{(\eta)}B_{1x} = B_0ik_xu_x + (H_B^{-1} - H_\rho^{-1})B_0u_z\,, \tag{6.21}$$

where we recall $v^2 = B_0^2/(\mu_0\rho_0)$. One could eliminate π_1 from equations (6.19) and (6.20), but since this would not greatly simplify the equations we have chosen not to here. We now restrict our focus to interchange modes, in which case we let $k_x = 0$. With a little more algebra we can now arrive at the dispersion relation,

$$\sigma^{(\nu)}\sigma^{(\eta)}\sigma^{(\bar{\kappa})}\left(1 + \frac{k_z^2}{k_y^2}\right) + gH_s^{-1}\sigma^{(\eta)} = v^2\frac{g}{c^2}\sigma^{(\gamma\bar{\kappa})}(H_B^{-1} - H_\rho^{-1})\,. \tag{6.22}$$

Initially we restrict our focus to the onset of purely *direct* modes of instability, and set

$\sigma = 0$. We can now derive the following instability condition:

$$-v^2 H_\rho^{-1} \frac{\mathrm{d}}{\mathrm{d}z} \ln\left(\frac{B_0}{\rho_0}\right) > \frac{\nu\eta}{\gamma}\frac{k^6}{k_y^2} + \frac{\eta}{\bar{\kappa}\gamma} c^2 H_\rho^{-1} H_s^{-1}\,, \tag{6.23}$$

where now $k^2 = k_y^2 + k_z^2$ and we recall that, in this regime, $g \approx c^2 H_\rho^{-1}$. Inequality (6.23) is consistent with results found in Hughes (1985) (see also, Hughes & Proctor (1988); Hughes & Weiss (1995)) . Similarly, we can look for the stability boundary for oscillatory instability by letting $\sigma = i\sigma_i$ (where $\sigma_i \in \mathbb{R}$), to yield a complex equation (equivalently, two real equations) for σ_i,

$$\begin{aligned}\frac{k^2}{k_y^2}(i\sigma_i + \nu k^2)(i\sigma_i + \eta k^2)(i\sigma_i + \bar{\kappa}k^2) + gH_s^{-1}(i\sigma_i + \eta k^2) = \\ v^2 \frac{g}{c^2}\left(i\sigma_i + \gamma\bar{\kappa}k^2\right)\left(H_B^{-1} - H_\rho^{-1}\right).\end{aligned} \tag{6.24}$$

Taking the real part only, we get the following expression for the frequency, σ_i,

$$\sigma_i^2(\nu + \eta + \bar{\kappa})\frac{k^4}{k_y^2} = gH_s^{-1}\eta k^2 + \nu\eta\bar{\kappa}\frac{k^8}{k_y^2} - \frac{gv^2\gamma\bar{\kappa}k^2}{c^2}(H_B^{-1} - H_\rho^{-1})\,. \tag{6.25}$$

It is simple enough to take the real and imaginary parts of equation (6.24) separately, combine to eliminate σ_i and derive the following marginal stability criterion

$$-(\nu + \eta - \bar{\kappa}(\gamma - 1))\frac{v^2}{c^2}\frac{\mathrm{d}}{\mathrm{d}z}\ln\left(\frac{B_0}{\rho_0}\right) = (\nu + \bar{\kappa})H_s^{-1} + \frac{1}{g}(\bar{\kappa} + \nu)(\bar{\kappa} + \eta)(\nu + \eta)\frac{k^6}{k_y^2}\,. \tag{6.26}$$

This matches the result of Hughes (1985) (see also, Hughes & Weiss (1995)) for oscillatory instability. Equation (6.26) tells us there are two distinct regions of instability depending on the sign of $\eta+\nu-\bar{\kappa}(\gamma-1)$. If $\eta+\nu-\bar{\kappa}(\gamma-1) < 0$; then there is instability for sufficiently positive gradient in B/ρ, on the other hand, if $\eta + \nu - \bar{\kappa}(\gamma - 1) > 0$; then there is instability for sufficiently negative gradient in B/ρ. The former circumstance is particularly interesting. For stellar interiors, it would not be uncommon for $\eta + \nu - \bar{\kappa}(\gamma - 1) < 0$ to be satisfied. Then we can have a situation whereby both the magnetic field gradient and thermodynamic gradient have a stabilising effect (in equation 6.23), but contrive to produce a system that produces oscillatory instability (in equation 6.26). This instability is often referred to as a double-diffusive instability since the instability requires disparate rates of diffusion of two different quantities that affect the density — here they are the diffusion of magnetic field and temperature field. It is most easily understood by comparison to a more well known double-diffusive instability, namely the thermohaline instability whereby density of water is affected by diffusion of both heat and salt. Hughes & Weiss (1995) (see also, Spiegel & Weiss (1982); Hughes & Proctor (1988); Hughes & Brummell (2021))

demonstrated that, with careful translation, the mathematical system of thermohaline instability can be made equivalent to the magnetohydrodynamic system we are considering here. However, this analogy only holds for 2D modes and cannot be extended to 3D. The reason for this is that while both thermohaline and MHD systems have two properties affecting density, the magnetic field in the MHD system is not a scalar and hence its effect is anisotropic. Indeed, in the salt-water system there cannot be instability when both the heat and solute (salt) gradients are stabilising. In the MHD setup we have seen above that this is possible. The reason lies in the compressibility of fluid by the magnetic field. In this situation, of stabilising gradients of both magnetic field and temperature, Hughes (1985) and Hughes & Proctor (1988) describe how double-diffusive magnetic buoyancy oscillatory instability can occur. Consider a flux tube vertically displaced upwards, since both stratifications are stabilising, it will naturally return back to its original position. The instability arises in the action of the thermal diffusivity which acts to remove heat from the risen tube to its cooler surroundings. Therefore, when the tube returns to its original position it will be cooler than it was originally and will continue to fall. Magnetic diffusion on the other hand has a stabilising effect. The stronger external field acts to squash, and hence heat, the tube. Magnetic diffusion somewhat erodes this effect. Indeed, as per $\eta+\nu-\bar{\kappa}(\gamma-1)<0$, sufficiently large magnetic diffusion will not allow overstability in this stable-stable regime. Hughes & Brummell (2021) study magnetic buoyancy double-diffusive instability, through analogy with thermosolutal convection, to demonstrate how magnetic layering can occur in regimes relevant to the solar interior.

There has not been extensive research on the double-diffusive instability outside of the magneto-Boussinesq limit. In this chapter we will extend our previous investigations to include all three diffusivities and the double-diffusive instability.

6.2 Double-diffusive instability with fully compressible equations

There has been limited work done to explore the double-diffusive instability outside the magneto-Boussinesq regime. Here we will numerically solve the linearised fully compressible equations with all three diffusivities present and a uniform horizontal background magnetic field. Initially, we do this in a parameter regime that approximates the Boussinesq regime. This will allow us to compare our results to that of Hughes (1985). We will then explore how the onset of this instability changes as we leave the Boussinesq regime. We solve the equations using a Newton-Raphson-Kantorovich method. More information on the numerical method is provided in Section 6.2.2.

6.2.1 Geometry and governing equations

First, we will spend some time deriving the governing equations. We begin with the fully compressible equations (2.13 – 2.15), but we omit rotation and replace equation (2.16) with the temperature equation,

$$\rho\frac{\mathrm{D}\mathbf{u}}{\mathrm{D}t} = -\boldsymbol{\nabla}p + g\rho\widehat{\mathbf{z}} + \frac{1}{\mu_0}(\boldsymbol{\nabla}\times\mathbf{B})\times\mathbf{B} + \mu\boldsymbol{\nabla}\cdot\tau\,, \tag{6.27}$$

$$\frac{\partial\mathbf{B}}{\partial t} = \boldsymbol{\nabla}\times(\mathbf{u}\times\mathbf{B}) + \eta\nabla^2\mathbf{B}\,, \tag{6.28}$$

$$\frac{\mathrm{D}\rho}{\mathrm{D}t} + \rho\boldsymbol{\nabla}\cdot\mathbf{u} = 0\,, \tag{6.29}$$

$$\rho c_V\frac{\partial T}{\partial t} + \rho c_V(\mathbf{u}\cdot\boldsymbol{\nabla})T = -p\boldsymbol{\nabla}\cdot\mathbf{u} + \boldsymbol{\nabla}\cdot(K\boldsymbol{\nabla}T) + \frac{\eta}{\mu_0}|\boldsymbol{\nabla}\times\mathbf{B}|^2 + \frac{\mu}{2}\|\tau\|^2\,, \tag{6.30}$$

where τ is the symmetric deviatoric rate-of-strain tensor, given by

$$\tau_{ij} = (\partial u_i/\partial x_j) + (\partial u_j/\partial x_i) - (2/3)\delta_{ij}\boldsymbol{\nabla}\cdot\mathbf{u} \tag{6.31}$$

and $K = \rho_0 c_p\bar{\kappa}$. The final two terms in equation (6.30) represent ohmic and viscous heating respectively, but will not play a significant role in the linear analysis to come. We assume a constant dynamic viscosity μ given by $\mu = \nu\rho$ where ν is the kinematic viscosity. Note that the sign in front of g has changed here due to a change in geometry — our z-direction is now oriented downwards, in the same direction as gravity (see Figure 6.1). This change in geometry has been adopted for later numerical convenience

As per Figure 6.1, we will consider a box of depth d, which is heated from below and cooled from above, with a uniform horizontal magnetic field (in the x-direction).

We make the following substitutions to non-dimensionalise the equations, where tildes denote the dimensionless-version of the variable:

$$\mathbf{B} = B_0\tilde{\mathbf{B}}\,, \qquad t \sim \frac{d}{\sqrt{RT_0}}\tilde{t}\,, \qquad \mathbf{x} = d\tilde{\mathbf{x}} \implies \boldsymbol{\nabla} = \frac{1}{d}\tilde{\boldsymbol{\nabla}}\,, \qquad \mathbf{u} = \sqrt{RT_0}\tilde{\mathbf{u}}\,,$$
$$\rho = \rho_0\tilde{\rho}\,, \qquad T = T_0\tilde{T}\,, \qquad p = RT_0\rho_0\tilde{p}\,, \qquad \tau = \frac{\sqrt{RT_0}}{d}\tilde{\tau}\,. \tag{6.32}$$

Here, d is the depth of our domain and our characteristic velocity is the isothermal sound speed, $\sqrt{RT_0}$ (see (Matthews *et al.*, 1995)).

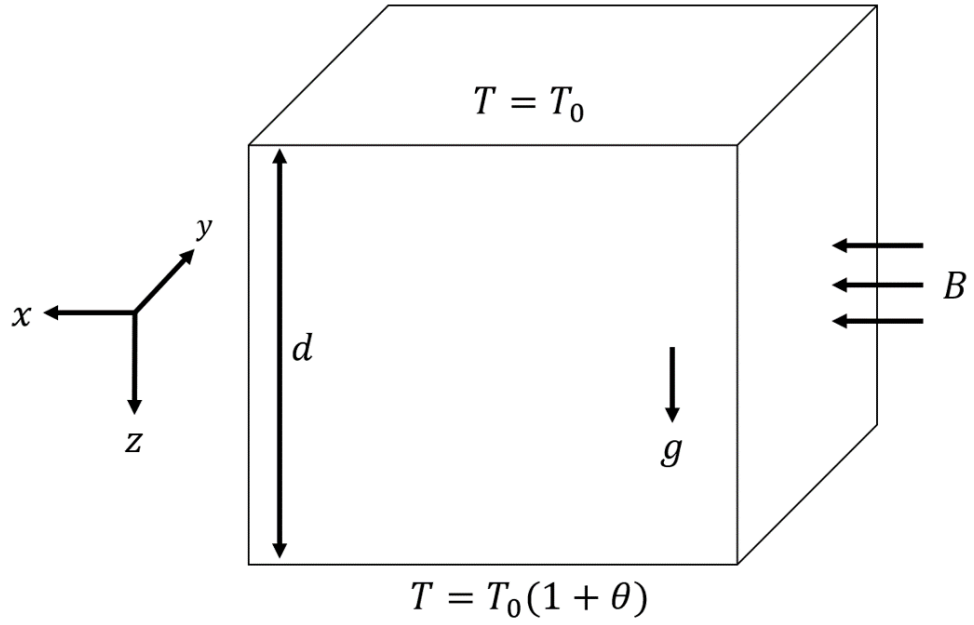

Figure 6.1: Sketch of the geometry of our problem. We consider a box of depth d which is heated from below and cooled from above with a horizontal, uniform magnetic field.

Substituting into our equations, we get

$$\rho_0\tilde{\rho}\frac{RT_0}{d}\left(\frac{\partial\tilde{\mathbf{u}}}{\partial\tilde{t}}+(\tilde{\mathbf{u}}\cdot\tilde{\boldsymbol{\nabla}})\tilde{\mathbf{u}}\right)=-\frac{RT_0\rho_0}{d}\tilde{\boldsymbol{\nabla}}\tilde{p}+g\rho_0\tilde{\rho}\,\hat{\mathbf{z}}+\frac{B_0^2}{d\mu_0}(\tilde{\boldsymbol{\nabla}}\times\tilde{\mathbf{B}})\times\tilde{\mathbf{B}}+\frac{1}{d}\frac{\sqrt{RT_0}}{d}\rho_0\nu\tilde{\boldsymbol{\nabla}}\cdot\tilde{\tau}\,, \tag{6.33}$$

$$B_0\frac{\sqrt{RT_0}}{d}\frac{\partial\tilde{\mathbf{B}}}{\partial\tilde{t}}=\frac{\sqrt{RT_0}B_0}{d}\tilde{\boldsymbol{\nabla}}\times(\tilde{\mathbf{u}}\times\tilde{\mathbf{B}})+\frac{B_0}{d^2}\eta\tilde{\nabla}^2\tilde{\mathbf{B}}\,, \tag{6.34}$$

$$\frac{\sqrt{RT_0}\rho_0}{d}\frac{\partial\tilde{\rho}}{\partial\tilde{t}}+\frac{\sqrt{RT_0}\rho_0}{d}(\tilde{\mathbf{u}}\cdot\tilde{\boldsymbol{\nabla}})\tilde{\rho}+\frac{\sqrt{RT_0}\rho_0}{d}\tilde{\rho}\tilde{\boldsymbol{\nabla}}\cdot\tilde{\mathbf{u}}=0\,, \tag{6.35}$$

$$\begin{aligned}\tilde{\rho}c_V\frac{\sqrt{RT_0}\rho_0T_0}{d}\frac{\partial\tilde{T}}{\partial\tilde{t}}+\frac{\sqrt{RT_0}\rho_0T_0}{d}\tilde{\rho}c_V(\tilde{\mathbf{u}}\cdot\tilde{\boldsymbol{\nabla}})\tilde{T}+\frac{\sqrt{RT_0}}{d}RT_0\rho_0\tilde{p}\tilde{\boldsymbol{\nabla}}\cdot\tilde{\mathbf{u}}\\ =\frac{T_0}{d^2}\tilde{\boldsymbol{\nabla}}\cdot(K\tilde{\boldsymbol{\nabla}}\tilde{T})+\frac{\eta B_0^2}{\mu_0d^2}|\tilde{\boldsymbol{\nabla}}\times\tilde{\mathbf{B}}|^2+\frac{RT_0\rho_0}{d^2}\frac{\tilde{\rho}\nu}{2}\tilde{\tau}^2\,.\end{aligned} \tag{6.36}$$

This can be simplified to get

$$\tilde{\rho}\left(\frac{\partial\tilde{\mathbf{u}}}{\partial\tilde{t}}+(\tilde{\mathbf{u}}\cdot\tilde{\boldsymbol{\nabla}})\tilde{\mathbf{u}}\right)=-\tilde{\boldsymbol{\nabla}}\tilde{p}+\frac{gd}{RT_0}\tilde{\rho}\,\widehat{\mathbf{z}}+\frac{B_0^2}{RT_0\rho_0\mu_0}(\tilde{\boldsymbol{\nabla}}\times\tilde{\mathbf{B}})\times\tilde{\mathbf{B}}+\frac{\nu}{d\sqrt{RT_0}}\tilde{\boldsymbol{\nabla}}\cdot\tilde{\tau}\,, \tag{6.37}$$

$$\frac{\partial\tilde{\mathbf{B}}}{\partial\tilde{t}}=\tilde{\boldsymbol{\nabla}}\times(\tilde{\mathbf{u}}\times\tilde{\mathbf{B}})+\frac{\eta}{d\sqrt{RT_0}}\tilde{\nabla}^2\tilde{\mathbf{B}}\,, \tag{6.38}$$

$$\frac{\partial\tilde{\rho}}{\partial\tilde{t}}+(\tilde{\mathbf{u}}\cdot\tilde{\boldsymbol{\nabla}})\tilde{\rho}+\tilde{\rho}\tilde{\boldsymbol{\nabla}}\cdot\tilde{\mathbf{u}}=0\,, \tag{6.39}$$

$$\begin{aligned}\tilde{\rho}c_V\frac{\partial\tilde{T}}{\partial\tilde{t}}+\tilde{\rho}c_V(\tilde{\mathbf{u}}\cdot\tilde{\boldsymbol{\nabla}})\tilde{T}=&-R\tilde{p}\tilde{\boldsymbol{\nabla}}\cdot\tilde{\mathbf{u}}+\frac{1}{d\sqrt{RT_0}\rho_0}\tilde{\boldsymbol{\nabla}}\cdot(K\tilde{\boldsymbol{\nabla}}\tilde{T})\\&+\frac{B_0^2}{\mu_0\rho_0}\frac{\eta}{d\sqrt{RT_0}T_0}|\tilde{\boldsymbol{\nabla}}\times\tilde{\mathbf{B}}|^2+\frac{R\nu}{d\sqrt{RT_0}}\frac{\tilde{\rho}}{2}\tilde{\tau}^2\,.\end{aligned} \tag{6.40}$$

We then introduce the following parameters (see Matthews *et al.* (1995))

$$\begin{aligned}&\zeta_0=\frac{\eta c_P\rho_0}{K}\,,\qquad\kappa=\frac{K}{d\rho_0c_P\sqrt{RT_0}}\,,\qquad\sigma=\frac{\rho_0\nu c_P}{K}\,,\qquad\theta=\frac{\Delta T}{T_0}\,,\\&m=\frac{gd}{R\Delta T}-1\implies m+1=\frac{gd}{RT_0\theta}\,,\qquad F=\frac{B_0^2}{\mu_0\rho_0RT_0}\,.\end{aligned} \tag{6.41}$$

Here, θ measures the stratification of our background state which, in order to closely approximate the magneto-Boussinesq regime, will need to be small (i.e. $\theta\ll1$). F is proportional to v^2/c^2 so, as per previous chapters, will need to be small if we expect a sound-proof model to be applicable to the regime. The Prandtl number is given by σ, ζ_0 is the ratio of magnetic to thermal diffusivity, κ is a dimensionless thermal diffusivity, and m is the polytropic index.

When we substitute for parameters (6.41), and use $R=c_P-c_V=(\gamma-1)c_V$, we get

$$\tilde{\rho}\frac{\mathrm{D}\tilde{\mathbf{u}}}{\mathrm{D}\tilde{t}}=-\tilde{\boldsymbol{\nabla}}\tilde{p}+\theta(m+1)\tilde{\rho}\,\widehat{\mathbf{z}}+F(\tilde{\boldsymbol{\nabla}}\times\tilde{\mathbf{B}})\times\tilde{\mathbf{B}}+\sigma\kappa\tilde{\boldsymbol{\nabla}}\cdot\tilde{\tau}\,, \tag{6.42}$$

$$\frac{\partial\tilde{\mathbf{B}}}{\partial\tilde{t}}=\tilde{\boldsymbol{\nabla}}\times(\tilde{\mathbf{u}}\times\tilde{\mathbf{B}})+\zeta_0\kappa\tilde{\nabla}^2\tilde{\mathbf{B}}\,, \tag{6.43}$$

$$\frac{\mathrm{D}\tilde{\rho}}{\mathrm{D}\tilde{t}}=-\tilde{\rho}\tilde{\boldsymbol{\nabla}}\cdot\tilde{\mathbf{u}}\,, \tag{6.44}$$

$$\tilde{\rho}\frac{\mathrm{D}\tilde{T}}{\mathrm{D}\tilde{t}}=-(\gamma-1)\tilde{p}\tilde{\boldsymbol{\nabla}}\cdot\tilde{\mathbf{u}}+\tilde{\boldsymbol{\nabla}}\cdot(\gamma\kappa\tilde{\boldsymbol{\nabla}}\tilde{T})+F(\gamma-1)\zeta_0\kappa|\tilde{\boldsymbol{\nabla}}\times\tilde{\mathbf{B}}|^2+(\gamma-1)\sigma\kappa\frac{\tilde{\rho}}{2}\tilde{\tau}^2\,. \tag{6.45}$$

6.2.2 Numerical method, boundary conditions and initial conditions

Our numerical method will utilise a Newton-Raphson-Kantorovich (NRK) algorithm. This is a relaxation method using an eighth-order finite difference scheme. Our code has been amended from one originally written to study convective instability (Gough *et al.*, 1976).

Our NRK algorithm begins with finite difference equations; that is, equations in the form of

$$\frac{\partial}{\partial z}A = B\,, \tag{6.46}$$

for each variable A, where B is some expression of the other variables. Roughly speaking, our NRK method then works to produce a matrix equation to be solved, but one involving an easily-invertible matrix in block-diagonal form. The implementation works over a grid of N points, and couples points together to allow incrementation from one solution to the next. An initial guess is provided, from which successive iterations refine the trial "solution" to an improved "solution". This process is repeated until the trial solution is within a specified threshold of the true solution; i.e. the solution has converged. For more general discussion about the principles of NRK methods see, for example, Garaud & Garaud (2008) who use a similar (though not identical) approach.

Our background state is chosen to be a static polytrope — which is an equilibrium solution of the governing equations. That is, we have

$$\tilde{\rho}_0 = (1+\theta\tilde{z})^m\,, \tag{6.47}$$

$$\tilde{T}_0 = 1+\theta\tilde{z}\,, \tag{6.48}$$

$$\tilde{p}_0 = \tilde{T}_0\tilde{\rho}_0 = (1+\theta\tilde{z})^{m+1}\,, \tag{6.49}$$

$$\tilde{\mathbf{u}} = \mathbf{0}\,, \tag{6.50}$$

and a horizontal uniform background magnetic field in the x-direction, i.e. $\tilde{\mathbf{B}}_0 = \widehat{\mathbf{x}}$. By assuming the background magnetic field is uniform we eliminate ohmic heating which enables a simple linear temperature gradient that is independent of F. With this set-up the only possible instability is an oscillatory doubly diffusive instability. The value of m can determine the convective stability of the system. Specifically, for an ideal gas, i.e. $\gamma = 5/3$, a value of $m > 1.5$ implies convective stability, in the absence of other effects. This can be easily proved by applying the Schwarzchild criterion here (and translating into our notation).

We consider simple boundary conditions, which allow for comparisons with previous work. All variables will be periodic over boundaries in the horizontal directions. We will use fixed temperature boundary conditions at the top and bottom of the domain to simulate constant heating from the deep solar interior. Also, at both the top and bottom of the domain, we will be using stress-free and vertical field boundary conditions.

6.2.3 Linear theory

We linearise the equations by expressing each variable as $\tilde{f} = \tilde{f}_0(z) + \tilde{f}_1(z)\exp[i\tilde{k}_x x + i\tilde{k}_y y + st]$ with respect to the polytropic background described in the previous section.

Note that, compared to previous chapters, our symbol for the growth rate has changed from σ to s. The Prandtl number is now represented by σ. For this background, and ignoring non-linear terms,

$$(\tilde{\boldsymbol{\nabla}} \times \tilde{\mathbf{B}}) \times \tilde{\mathbf{B}} = \left(i\tilde{k}_x \tilde{B}_y - i\tilde{k}_y \tilde{B}_x \right) \widehat{\mathbf{y}} - \left(\frac{\partial \tilde{B}_x}{\partial \tilde{z}} - i\tilde{k}_x \tilde{B}_z \right) \widehat{\mathbf{z}} \tag{6.51}$$

and $|\tilde{\boldsymbol{\nabla}} \times \tilde{\mathbf{B}}|^2 = 0$. The resulting equations are then

$$\tilde{\rho}_0 s\tilde{u}_x = -i\tilde{k}_x \tilde{p}_1 + \sigma\kappa[\tilde{\boldsymbol{\nabla}} \cdot \tilde{\tau}]_x \,, \tag{6.52}$$

$$\tilde{\rho}_0 s\tilde{u}_y = -i\tilde{k}_y \tilde{p}_1 + F\left(i\tilde{k}_x \tilde{B}_y - i\tilde{k}_y \tilde{B}_x \right) + \sigma\kappa[\tilde{\boldsymbol{\nabla}} \cdot \tilde{\tau}]_y \,, \tag{6.53}$$

$$\tilde{\rho}_0 s\tilde{u}_z = -\frac{\partial \tilde{p}_1}{\partial \tilde{z}} + \theta(m+1)\tilde{\rho}_1 - F\left(\frac{\partial \tilde{B}_x}{\partial \tilde{z}} - i\tilde{k}_x \tilde{B}_z \right) + \sigma\kappa[\tilde{\boldsymbol{\nabla}} \cdot \tilde{\tau}]_z \,, \tag{6.54}$$

$$s\tilde{B}_x = -i\tilde{k}_y \tilde{u}_y - \frac{\partial \tilde{u}_z}{\partial \tilde{z}} + \zeta_0\kappa\left(-\tilde{k}_H^2 + \frac{\partial^2}{\partial \tilde{z}^2} \right) \tilde{B}_x \,, \tag{6.55}$$

$$s\tilde{B}_y = i\tilde{k}_x \tilde{u}_y + \zeta_0\kappa\left(-\tilde{k}_H^2 + \frac{\partial^2}{\partial \tilde{z}^2} \right) \tilde{B}_y \,, \tag{6.56}$$

$$s\tilde{B}_z = i\tilde{k}_x \tilde{u}_z + \zeta_0\kappa\left(-\tilde{k}_H^2 + \frac{\partial^2}{\partial \tilde{z}^2} \right) \tilde{B}_z \,, \tag{6.57}$$

$$s\tilde{\rho}_1 = -\tilde{u}_z \frac{\mathrm{d}\tilde{\rho}_0}{\mathrm{d}\tilde{z}} - \tilde{\rho}_0\left(i\tilde{k}_x \tilde{u}_x + i\tilde{k}_y \tilde{u}_y + \frac{\partial \tilde{u}_z}{\partial \tilde{z}} \right) \,, \tag{6.58}$$

$$\tilde{\rho}_0\left(s\tilde{T}_1 + \tilde{u}_z \frac{\mathrm{d}\tilde{T}_0}{\mathrm{d}\tilde{z}} \right) = -(\gamma-1)\tilde{p}_0\left(i\tilde{k}_x \tilde{u}_x + i\tilde{k}_y \tilde{u}_y + \frac{\partial \tilde{u}_z}{\partial \tilde{z}} \right) + \gamma\kappa\left(-\tilde{k}_H^2 + \frac{\partial^2}{\partial \tilde{z}^2} \right) \tilde{T}_1 \,, \tag{6.59}$$

where $\tilde{k}_H^2 = \tilde{k}_x^2 + \tilde{k}_y^2$.

We now evaluate the viscous terms,

$$\begin{aligned}
\sigma\kappa[\boldsymbol{\nabla} \cdot \tau]_i &= \sigma\kappa \frac{\partial}{\partial x_j} \tau_{ij} \\
&= \sigma\kappa \frac{\partial}{\partial x_j}\left(\frac{\partial u_i}{\partial x_j} + \frac{\partial u_j}{\partial x_i} - \frac{2}{3}\delta_{ij} \boldsymbol{\nabla} \cdot \mathbf{u} \right) \\
&= \sigma\kappa\left(\frac{\partial^2 u_i}{\partial x_j^2} + \frac{\partial u_j}{\partial x_j \partial x_i} - \frac{2}{3}\frac{\partial}{\partial x_i} \boldsymbol{\nabla} \cdot \mathbf{u} \right) \\
&= \sigma\kappa\left(\frac{\partial^2 u_i}{\partial x_j^2} + \frac{\partial}{\partial x_i}\frac{\partial u_j}{\partial x_j} - \frac{2}{3}\frac{\partial}{\partial x_i} \boldsymbol{\nabla} \cdot \mathbf{u} \right) \\
&= \sigma\kappa\left[\nabla^2 \mathbf{u} + \frac{1}{3}\boldsymbol{\nabla}(\boldsymbol{\nabla} \cdot \mathbf{u}) \right]_i \,,
\end{aligned} \tag{6.60}$$

where we have omitted tildes. Our numerical solver uses a finite-difference scheme and

therefore we require the equations to be in a format where each equation is written in the form of equation (6.46). Therefore, we will now manipulate our equations to force them into this form. We will now input the viscous terms above and rearrange the three components of the momentum equation to get

$$\frac{\partial^2 u_x}{\partial z^2} = \frac{1}{\sigma\kappa}\left(\left(\rho_0 s + \sigma\kappa\tilde{k}_H^2\right)u_x + i\tilde{k}_x(T_0\rho_1 + \rho_0 T_1) - \frac{\sigma\kappa i\tilde{k}_x}{3}\left(i\tilde{k}_x u_x + i\tilde{k}_y u_y + \frac{\partial u_z}{\partial z}\right)\right), \tag{6.61}$$

$$\begin{aligned}\frac{\partial^2 u_y}{\partial z^2} =& \frac{1}{\sigma\kappa}\Bigg(\left(\rho_0 s + \sigma\kappa\tilde{k}_H^2\right)u_y + i\tilde{k}_y(T_0\rho_1 + \rho_0 T_1) - F\left(i\tilde{k}_x B_y - i\tilde{k}_y B_x\right) \\ &- \frac{\sigma\kappa i\tilde{k}_y}{3}\left(i\tilde{k}_x u_x + i\tilde{k}_y u_y + \frac{\partial u_z}{\partial z}\right)\Bigg),\end{aligned} \tag{6.62}$$

$$\begin{aligned}\frac{4}{3}\frac{\partial^2 u_z}{\partial z^2} =& \frac{1}{\sigma\kappa}\Bigg(\frac{\partial}{\partial z}(T_0\rho_1 + \rho_0 T_1) - \theta(m+1)\rho_1 - F\left(i\tilde{k}_x B_z - \frac{\partial B_x}{\partial z}\right) \\ &+ \left(\rho_0 s + \sigma\kappa\tilde{k}_H^2\right)u_z - \frac{\sigma\kappa}{3}\frac{\partial}{\partial z}\left(i\tilde{k}_x u_x + i\tilde{k}_y u_y\right)\Bigg),\end{aligned} \tag{6.63}$$

where we have eliminated p_1 by the linearised equation of state $p_1 = T_0\rho_1 + \rho_0 T_1$ and removed tildes from all variables. The first two components can be input into our numerical solver. However, the third (z) component we will instead use to combine with the continuity equation to derive an expression for $\partial\rho_1/\partial z$. To do this, we take the z-derivative of the continuity equation (6.58) and rearrange as;

$$\begin{aligned} s\frac{\partial\rho_1}{\partial z} =& -\frac{\partial}{\partial z}\left(u_z\frac{\mathrm{d}\rho_0}{\mathrm{d}z}\right) - \frac{\partial}{\partial z}\left(\rho_0\left(i\tilde{k}_x u_x + i\tilde{k}_y u_y + \frac{\partial u_z}{\partial z}\right)\right), \\ \implies \frac{\partial^2 u_z}{\partial z^2} =& -i\tilde{k}_x\frac{\partial u_x}{\partial z} - i\tilde{k}_y\frac{\partial u_y}{\partial z} - \frac{1}{\rho_0}\frac{\partial^2\rho_0}{\partial z^2}u_z - \frac{1}{\rho_0}\frac{\partial\rho_0}{\partial z}\frac{\partial u_z}{\partial z} + \frac{1}{\rho_0^2}\left(\frac{\partial\rho_0}{\partial z}\right)^2 u_z \\ &+ \frac{1}{\rho_0^2}\frac{\partial\rho_0}{\partial z}s\rho_1 - \frac{1}{\rho_0}s\frac{\partial\rho_1}{\partial z}.\end{aligned} \tag{6.64}$$

Combining equations (6.63) and (6.64) gives

$$\begin{aligned}(4s\sigma\kappa + 3\rho_0 T_0)\frac{\partial\rho_1}{\partial z} = 3\rho_0\Bigg[&-(\rho_0 s + \sigma\kappa\tilde{k}_H^2)u_z - \rho_0\frac{\partial T_1}{\partial z} - \frac{\partial\rho_0}{\partial z}T_1 - \frac{\partial T_0}{\partial z}\rho_1 \\ &+ \theta(m+1)\rho_1 + F\left(i\tilde{k}_x B_z - \frac{\partial B_x}{\partial z}\right) + \sigma\kappa\Bigg(-i\tilde{k}_x\frac{\partial u_x}{\partial z} - i\tilde{k}_y\frac{\partial u_y}{\partial z} \\ &- \left(4\frac{\partial^2\rho_0}{\partial z^2}u_z + 4\frac{\partial\rho_0}{\partial z}\left(\frac{\partial u_z}{\partial z} - \frac{1}{\rho_0}\frac{\partial\rho_0}{\partial z}u_z - \frac{1}{\rho_0}s\rho_1\right)\right)/(3\rho_0)\Bigg)\Bigg],\end{aligned} \tag{6.65}$$

we now use the continuity equation (6.58) again to get

$$\frac{\partial \rho_1}{\partial z} = 3\rho_0 \Bigg[-(\rho_0 s + \sigma\kappa \tilde{k}_H^2) u_z - \rho_0 \frac{\partial T_1}{\partial z} - \frac{\partial \rho_0}{\partial z} T_1 - \frac{\partial T_0}{\partial z}\rho_1 + \theta(m+1)\rho_1 + F\left(i\tilde{k}_x B_z - \frac{\partial B_x}{\partial z}\right) + \sigma\kappa\Bigg(- i\tilde{k}_x \frac{\partial u_x}{\partial z} - i\tilde{k}_y \frac{\partial u_y}{\partial z} - \left(4\frac{\partial^2 \rho_0}{\partial z^2} u_z + 4\frac{\partial \rho_0}{\partial z}\left(i\tilde{k}_x u_x + i\tilde{k}_y u_y + 2\frac{\partial u_z}{\partial z}\right)\right)/(3\rho_0)\Bigg)\Bigg] / \left(4s\sigma\kappa + 3\rho_0 T_0\right) . \quad (6.66)$$

In our numerical system we will therefore input equations (6.61, 6.62, 6.66) as well as

$$\frac{\partial^2 B_x}{\partial z^2} = \frac{1}{\zeta_0 \kappa}\left(\left(s + \zeta_0 \kappa \tilde{k}_H^2\right) B_x + i\tilde{k}_y u_y + \frac{\partial u_z}{\partial z}\right) , \quad (6.67)$$

$$\frac{\partial^2 B_z}{\partial z^2} = \frac{1}{\zeta_0 \kappa}\left((s + \zeta_0 \kappa \tilde{k}_H^2) B_z - i\tilde{k}_x u_z\right) , \quad (6.68)$$

$$\frac{\partial u_z}{\partial z} = - i\tilde{k}_x u_x - i\tilde{k}_y u_y - \frac{1}{\rho_0}\frac{\mathrm{d}\rho_0}{\mathrm{d}z} u_z - s\frac{\rho_1}{\rho_0} , \quad (6.69)$$

$$\frac{\partial^2 T_1}{\partial z^2} = \frac{\rho_0}{\gamma\kappa}\left(\left(s + \frac{\gamma\kappa\tilde{k}_H^2}{\rho_0}\right) T_1 + u_z \frac{\mathrm{d}T_0}{\mathrm{d}z} + (\gamma - 1) T_0 \left(i\tilde{k}_x u_x + i\tilde{k}_y u_y + \frac{\partial u_z}{\partial z}\right)\right) \quad (6.70)$$

which are rearrangements of (6.55, 6.57, 6.58, 6.59) respectively. Rather than input a rearrangment of (6.56), we instead make use of the solenoidal condition on $\mathbf{B}$ and define B_y as $B_y = (1/i\tilde{k}_y)(i\tilde{k}_x B_x + \partial B_z/\partial z)$ and therefore will only consider non-zero values of $\tilde{k}_y$ (as appropriate for wavelike disturbances to the background state).

6.3 Results

Equations (6.61, 6.62, 6.66 – 6.70) are solved numerically to find the onset of oscillatory instability. The results from Section 6.1 will inform our search and initially we will look for results with parameters approximating the magneto-Boussinesq regime (but with the fully compressible equations) to verify our code and to ensure the solution does indeed exist as expected. To do this, we need to translate condition (6.26) into the notation used in our code.

Firstly, we note the change in geometry (with the z-direction oppositely oriented), so we alter equation (6.26) by replacing $z \to -z$ (via $\mathrm{d}/\mathrm{d}z \to -\mathrm{d}/\mathrm{d}z$), to get

$$(\nu + \eta - \bar{\kappa}(\gamma - 1))\frac{v^2}{c^2}\frac{\mathrm{d}}{\mathrm{d}z}\ln\left(\frac{B_0}{\rho_0}\right) = (\nu + \bar{\kappa}) H_s^{-1} + \frac{1}{g}\left(\bar{\kappa} + \nu\right)\left(\bar{\kappa} + \eta\right)\left(\nu + \eta\right)\frac{k^6}{k_y^2} . \quad (6.71)$$

For our background state (see Section 6.2.2) we can evaluate, and non-dimensionalise by

$z \to d\tilde{z}$, the z-derivatives as

$$H_s^{-1} = \frac{-1}{d\gamma}\frac{\mathrm{d}}{\mathrm{d}\tilde{z}}\ln\left(\frac{\tilde{p}_0}{\tilde{\rho}_0^{\gamma}}\right) = \frac{-\theta}{d\gamma(1+\theta\tilde{z})}[m+1-m\gamma] \approx \frac{-\theta}{d\gamma}(m+1-m\gamma)\,, \quad (6.72)$$

$$\frac{\mathrm{d}}{\mathrm{d}z}\ln\left(\frac{B_0}{\rho_0}\right) = \frac{1}{d}\frac{\mathrm{d}}{\mathrm{d}\tilde{z}}\ln\left(\frac{\tilde{B}_0}{\tilde{\rho}_0}\right) = \frac{-m\theta}{d(1+\theta\tilde{z})} \approx \frac{-m\theta}{d}\,, \quad (6.73)$$

where we have assumed $\theta \ll 1$ — since we are looking in the Boussinesq regime. Note that we have introduced a minus sign into our definition of H_s^{-1} to reflect our change in orientation. We also non-dimensionalise, as we did before, by introducing the following parameters

$$k^2 = \frac{\tilde{k}^2}{d^2}\,, \qquad k_y^2 = \frac{\tilde{k}_y^2}{d^2}\,, \qquad g = (m+1)\frac{RT_0\theta}{d}\,,$$
$$\eta = \frac{\zeta_0 K}{c_p\rho_0}\,, \qquad \nu = \frac{\sigma K}{c_p\rho_0}\,, \qquad \kappa = \frac{K}{d\rho_0 c_P\sqrt{RT_0}}\,, \qquad F = \gamma\frac{v^2}{c^2}\,. \quad (6.74)$$

where we recall $K = \rho_0 c_p \bar{\kappa}$, and have re-introduced $\tilde{k_y}$ and $\tilde{k}$ as the dimensionless equivalents of k_y and $k = \sqrt{k_y^2 + k_z^2}$ respectively. The other parameters were introduced in equations (6.41). Substituting in these parameters, as well as equations (6.72) and (6.73), gives

$$-(\sigma+\zeta_0-(\gamma-1))\frac{F}{\gamma}\theta^2 m(m+1) = -(\sigma+1)\frac{\theta^2}{\gamma}(m+1)(m+1-m\gamma)$$
$$+\kappa^2(1+\sigma)(1+\zeta_0)(\sigma+\zeta_0)\frac{\tilde{k}^6}{\tilde{k}_y^2}\,. \quad (6.75)$$

We can rearrange to give

$$\frac{\theta^2(m+1)}{\gamma\kappa^2}(m+1-m\gamma) = \frac{(\sigma+\zeta_0-(\gamma-1))}{\gamma(1+\sigma)}\frac{F\theta^2 m(m+1)}{\kappa^2} + (1+\zeta_0)(\sigma+\zeta_0)\frac{\tilde{k}^6}{\tilde{k}_y^2}\,. \quad (6.76)$$

We can now introduce the Rayleigh and magnetic Rayleigh numbers

$$Ra = (1+\theta\tilde{z})^{m-1}\frac{\theta^2(m+1)}{\gamma\sigma\kappa^2}(m+1-m\gamma) \approx \frac{\theta^2(m+1)}{\gamma\sigma\kappa^2}[m+1-m\gamma]\,, \quad (6.77)$$

$$R_b = \frac{F\theta^2 m(m+1)}{\sigma\kappa^2}\,, \quad (6.78)$$

as per Matthews *et al.* (1995) and Hughes & Weiss (1995), where we have approximated

$1 + \theta\tilde{z} \approx 1$ since we assume $\theta \ll 1$. Our stability criterion can then be written as

$$Ra = \frac{(1+\sigma+\zeta_0-\gamma)}{\gamma(1+\sigma)} R_b + \frac{(1+\zeta_0)(\sigma+\zeta_0)}{\sigma} \frac{\tilde{k}^6}{\tilde{k}_y^2}, \tag{6.79}$$

which is precisely the result found in Hughes & Weiss (1995).

Maximising equation (6.79) with respect to $\tilde{k}_y$, we find the optimum value of $\tilde{k}_y = \pi/\sqrt{2}$ is for a value of $\tilde{k}_z = \pi$. Hence, the critical value of Ra is given by

$$Ra_{\text{crit}} = \frac{(1+\sigma+\zeta_0-\gamma)}{\gamma(1+\sigma)} R_b + \frac{(1+\zeta_0)(\sigma+\zeta_0)}{\sigma} \frac{27\pi^4}{4}. \tag{6.80}$$

or, replacing R_b by (6.78),

$$Ra_{\text{crit}} = \frac{(1+\sigma+\zeta_0-\gamma)}{\gamma(1+\sigma)} \frac{F\theta^2 m(m+1)}{\sigma\kappa^2} + \frac{(1+\zeta_0)(\sigma+\zeta_0)}{\sigma} \frac{27\pi^4}{4}. \tag{6.81}$$

Clearly the final term is positive, therefore in order to have an instability we must have

$$\begin{aligned} Ra = (1+\theta\tilde{z})^{m-1} \frac{\theta^2(m+1)}{\gamma\sigma\kappa^2}[m+1-m\gamma] &> \frac{(1+\sigma+\zeta_0-\gamma)}{\gamma(1+\sigma)} \frac{F\theta^2 m(m+1)}{\sigma\kappa^2} \\ \implies \qquad (1+\theta\tilde{z})^{m-1}[m+1-m\gamma] &> \frac{(1+\sigma+\zeta_0-\gamma)}{(1+\sigma)} Fm \\ \implies \qquad \frac{(1+\sigma)(\gamma-1)\left[m-\frac{1}{(\gamma-1)}\right]}{m(\gamma-1-\sigma-\zeta_0)} &< F\,. \end{aligned} \tag{6.82}$$

We use this inequality to inform our choices of parameters for our numerical solver. Firstly, F must be positive therefore the left hand side must also be positive. We are assuming an ideal gas here, so we take $\gamma = 5/3$. Therefore we require $m > 1/(\gamma-1) = 3/2$ whilst also having $\sigma + \zeta_0 < \gamma - 1 = 2/3$. However, if we are expecting this to closely mimic the Boussinesq results we will require $F \ll 1$ (and also $\theta \ll 1$).

To derive an expression for the expected value of the frequency at the onset of oscillatory instability, we can convert equation (6.25) into our numerical notation. We begin by taking equation (6.25) which we reproduce here for convenience, where we recall that our z-direction has changed,

$$\sigma_i^2 \frac{k^2}{k_y^2} = -gH_s^{-1} \frac{\eta}{(\nu+\eta+\bar{\kappa})} + \frac{\nu\eta\bar{\kappa}}{(\nu+\eta+\bar{\kappa})} \frac{k^6}{k_y^2} + \frac{gv^2\gamma\bar{\kappa}}{c^2(\nu+\eta+\bar{\kappa})}(H_B^{-1} - H_\rho^{-1}). \tag{6.83}$$

We then non-dimensionalise by making the substitutions in (6.74), coupled with

$$\sigma_i = (\sqrt{RT_0}/d)\omega, \tag{6.84}$$

for the dimensionless frequency ω. We evaluate the scale heights as we did in equations (6.72) and (6.73) to yield

$$H_s^{-1} \approx \frac{-\theta}{d\gamma}(m+1-m\gamma)\,, \tag{6.85}$$

$$H_\rho^{-1} \approx \frac{m\theta}{d}\,, \tag{6.86}$$

$$H_B^{-1} = 0\,. \tag{6.87}$$

Making these substitutions and rearranging we get

$$\omega^2 \frac{\tilde{k}^2}{\tilde{k}_y^2} = -Ra\frac{\sigma\kappa^2\zeta_0}{(\sigma+\zeta_0+1)} + \frac{\sigma\zeta_0\kappa^2}{(\sigma+\zeta_0+1)}\frac{\tilde{k}^6}{\tilde{k}_y^2} + \frac{F\theta^2 m(m+1)}{(\sigma+\zeta_0+1)}\,. \tag{6.88}$$

where we have introduced Ra by equation (6.77). We now substitute $\tilde{k}$, $\tilde{k}_y$ and Ra for their values at the onset of instability. That is, $\tilde{k}^2 = 3\pi^2/2$, $\tilde{k}_y^2 = \pi^2/2$, and $Ra_{\rm crit}$ given by equation (6.81). Inputting these gives us

$$\omega^2 = \frac{F\theta^2 m(m+1)}{3(1+\sigma)}\left(1-\frac{\zeta_0}{\gamma}\right) - \zeta_0^2\kappa^2\frac{9\pi^4}{4}\,. \tag{6.89}$$

We also need the value of κ, so we can rearrange (6.81) for κ^2, where we use (6.77) (and set $(1+\theta z)\approx 1$), to get

$$\kappa^2 = \frac{\theta^2(m+1)}{\gamma}\left([m+1-m\gamma] - \frac{Fm(1+\sigma+\zeta_0-\gamma)}{(1+\sigma)}\right)\frac{4}{27\pi^4(1+\zeta_0)(\sigma+\zeta_0)}\,. \tag{6.90}$$

We initially use the following parameters

$$F = \sigma = \zeta_0 = \theta = 0.01\,, \qquad m = 1.51\,, \qquad \gamma = \tfrac{5}{3}\,. \tag{6.91}$$

Our numerical solver will then run to find the critical Rayleigh number, and associated frequency of the instability. We use an eighth-order finite difference method with an NRK algorithm. Roughly speaking, the solver will find a solution to the equations (i.e. will find the Rayleigh number where the real growth rate is 0 and non-zero imaginary growth rate corresponding to oscillatory instability.) for given values of $\tilde{k}_x$ and $\tilde{k}_y$. It will then loop over both $\tilde{k}_x$ and $\tilde{k}_y$ (or, for the 2D case, only $\tilde{k}_y$) to find the smallest value of the Rayleigh number, keeping all other parameters constant. For the most part, we study the 2D instability (with $\tilde{k}_x = 0$) and the increment between successive values of $\tilde{k}_y$ is 0.001. When we move to 3D, we reduce the increment in $\tilde{k}_y$ to 0.01 and later to 0.1, at the same time the increment in $\tilde{k}_x$ is 0.01 and 0.0005 respectively. In this way, it tells you, for each value of $\tilde{k}_x$, what the critical Rayleigh number is and the associated wavenumber $\tilde{k}_y$

where it occurs. Note that we describe our results in terms of the Rayleigh number, but it does not appear in the governing equations. An initial guess for the Rayleigh number is provided to the algorithm, which then translates it into a value for κ and effectively iterates for a critical value of κ, before translating that back to give us a critical Rayleigh number. The code will also output the imaginary growth rate and the frequency for each critical Rayleigh number. When we are in the Boussinesq regime of parameter space (i.e $\theta \ll 1$, $F \ll 1$) we would expect good agreement with equation (6.81). Plugging our parameter values (6.91) into (6.81), (6.89) and (6.90) tells us we would expect our numerical solver to approximately give

$$Ra_{\text{crit}} \approx -2950.2\,, \qquad \omega \approx 0.0011\,. \tag{6.92}$$

Recall that these values are derived, using our parameters, from existing results with the magneto-Boussinesq equations from Hughes (1985) and Hughes & Weiss (1995). Note that we expect the Rayleigh number to be negative, since we are interested in a situation where both thermal and magnetic stratifications are stable (i.e. the "stable-stable" fourth quadrant, as per Hughes & Weiss (1995); see also Hughes (1985)).

When we run our Newton-Raphson-Kantorovich code, in the 2D case with $\tilde{k}_x = 0$, we find an oscillatory instability with a similar frequency and critical Rayleigh number to these values. Specifically we find

$$Ra_{\text{crit}} = -3206.1\,, \qquad \omega = 0.0011\,. \tag{6.93}$$

Clearly the frequency is in good agreement, the critical Rayleigh number differs by about 10%. Some discrepancy is of course expected, seeing as we are using different equations (and have neglected several factors of $1 + \theta z$). Results of the next section (specifically Figure 6.2) suggest that agreement would improve for smaller values of θ.

6.3.1 Results further from the magneto-Boussinesq limit

Above, we have restricted ourselves to the Boussinesq regime and found that our results approximately match those of Hughes (1985) (and Hughes & Weiss (1995)). We will now extend our analysis by considering non-Boussinesq regimes by increasing θ (recall that θ measures the stratification of the system). As we repeat the run with increasing values of θ the agreement breaks down (see Figures 6.2, 6.3, 6.4). In addition to the change in critical Rayleigh number, the frequency of the oscillation also increases with θ. This is to be expected: as θ is increased we move out of the Boussinesq regime and therefore cannot expect the results to be maintained.

Figure 6.2 shows good agreement for the critical Rayleigh number with the Boussinesq value for small θ, and even suggests that there would be even better agreement for $\theta < 0.01$.

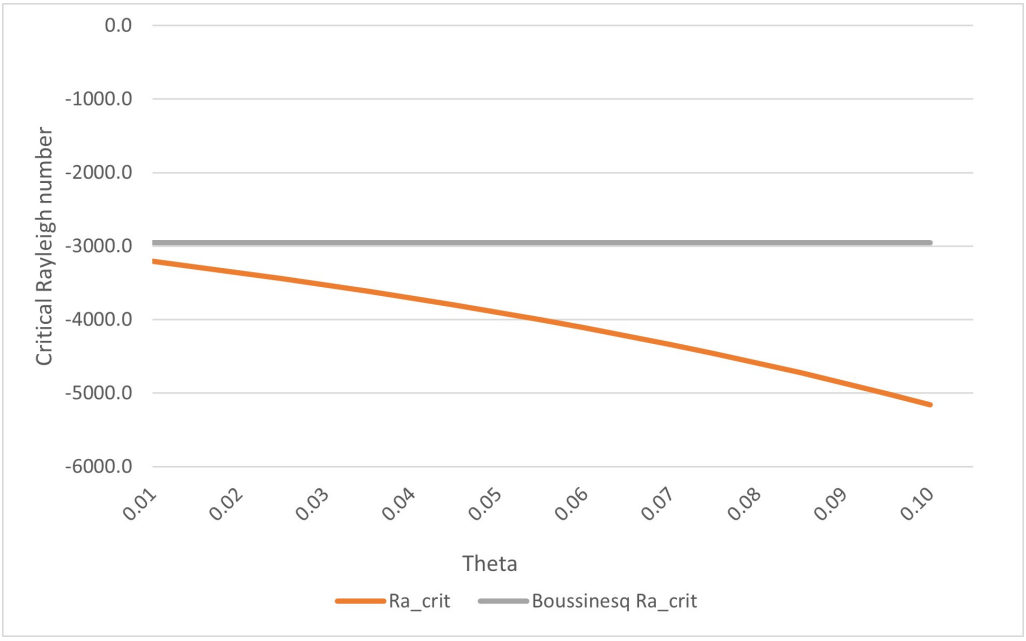

Figure 6.2: Change in critical Rayleigh number as θ increases. Here we used the following parameter values: $F = \zeta_0 = \sigma = 0.01$, $m = 1.51$, $\gamma = 5/3$.

If one were to plot a polynomial to fit the curve in Figure 6.2, and extrapolate to $\theta = 0$, then the curve would intercept at a critical Rayleigh number of approximately -3063 (depending slightly on the order of the fitted polynomial). This differs from the Boussinesq prediction of -2950.2 by approximately 4%. Here, we were unable to explore the $\theta < 0.01$ regime because of computational limitations. When θ is smaller, increased numerical precision is required to adequately resolve the problem. As θ increases, as expected, the critical Rayleigh number departs from the Boussinesq value. The decreasing critical Rayleigh number shows that in non-Boussinesq regimes this double-diffusive instability is less easily induced. It is not immediately obvious why this is the case — it would have been difficult to predict beforehand whether increasing the temperature difference (θ) would have made the instability more or less easily induced. It is worth noting however, that our diffusivities of momentum and temperature are chosen such that they scale as $1/\rho$. If instead, they had been chosen to be uniform then how the instability responds to changes in θ could have been different.

Figure 6.3 shows that as θ is increased, the frequency of the oscillations, ω, increases proportionally. From Figure 6.3, we see that there is good agreement between our frequency with $\theta = 0.01$ and the Boussinesq frequency. However, based on the trend presented in Figure 6.3, it looks as though for even smaller values of θ (i.e. $\theta < 0.01$) our frequency (from the fully compressible equations) would begin to diverge from the Boussinesq approximation. Note that this is not necessarily what we would expect; we would

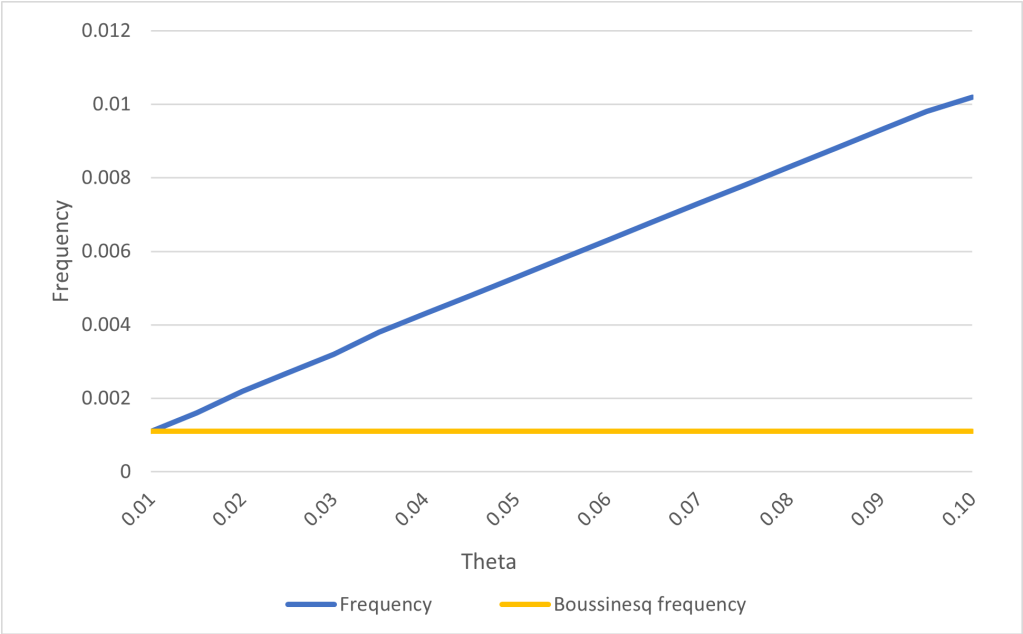

Figure 6.3: Change in frequency as θ increases. Here we used the following parameter values: $F = \zeta_0 = \sigma = 0.01$, $m = 1.51$, $\gamma = 5/3$.

expect the frequency to asymptote toward the Boussinesq value; much like the critical Rayleigh number appears to asymptote toward the Boussinesq approximation for the critical Rayleigh number in Figure 6.2. It is not clear why Figure 6.3 seems to suggest that the fully compressible frequency best approximates the Boussinesq value at a finite, rather than zero, value of θ; this could be that there are hidden errors in the plot, or perhaps the plot would change shape for smaller values of θ. Therefore, exploration of the $\theta < 0.01$ regime is recommend. This exploration has not been carried out here due to computational limitations. The values of ω presented in Table 6.1 shows that, for our parameters and non-dimensionalisation and with $\tilde{k}_x = 0$, $\omega \approx \theta/10$, i.e. we can approximate equation (6.89) by $\omega^2 \approx F\theta^2$ (at least for this set of parameters).

The fact that the critical wavenumber, $\tilde{k}_y$, stays roughly constant as you increase θ, as shown in Figure 6.4, confirms that as we change θ we are indeed still seeing modes of the same instability — i.e. our numerical solver hasn't jumped onto a different instability entirely. Note that in our runs that produced Figure 6.4 we are looping over $\tilde{k}_y$ with an interval of 0.001, which explains the discrete jumps in wavenumber. Much like the decrease in critical Rayleigh number with increasing θ, the increase in preferred $\tilde{k}_y$ with θ would have been difficult to predict beforehand. We would, however, have expected to see some departure from the Boussinesq prediction as we left the small θ regime.

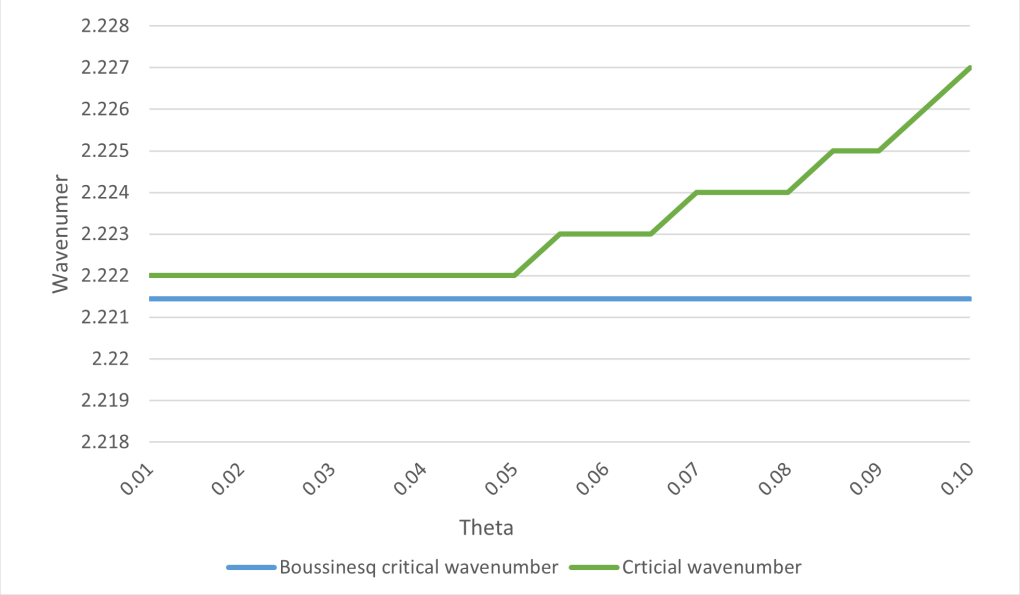

Figure 6.4: Change in critical wavenumber as θ increases. Here we used the following parameter values: $F = \zeta_0 = \sigma = 0.01$, $m = 1.51$, $\gamma = 5/3$.

3D case

Thus far in this chapter we have only considered purely interchange modes (with $\tilde{k}_x = 0$, where $\tilde{k}_x$ is the dimensionless wavenumber in the x-direction). Here we will present results for small but non-zero values of $\tilde{k}_x$, i.e. for perturbations with very long wavelengths in the direction of the field. The results are presented in Tables 6.1 and 6.2. In Table 6.1, we see that for each value of θ, as k_x is increased the critical Rayleigh number increases (becomes less negative). This tells us that, for these cases, the 3D cases are more easily destabilised — i.e. instability ensues for a smaller (in magnitude) Rayleigh number. Therefore, there is not a regime where we have a 2D instability without a 3D one. Table 6.1 also clearly shows the effects of increasing θ presented in Figures 6.2, 6.3, 6.4. Namely, as θ increases, ω increases proportionally, Ra_{crit} decreases (the rate of this decrease increases with θ) and k_y slowly increases (again, the rate of this increase increases with θ).

In Table 6.2 we show the minimum values of the modulus of Ra_{crit} for each value of θ and the wavenumber $\tilde{k}_x$ at which they occur. For each value of θ, the optimisation proceeds in the following way. For each value of k_x, we find Ra_{crit} and the value of k_y at which it occurs (by solving over a range of k_y and selecting the smallest Rayleigh number). We then increment over k_x to find the value of k_x at which Ra_{crit} is smallest, and the corresponding value of k_y. This process is repeated for each value of θ. That is to say that the wavenumbers presented in Table 6.2 are the optimum values for this instability (for our choice of parameters). Specifically, we see that the instability favours a small, but non-zero, wavenumber in the x-direction — i.e. the direction of the background magnetic

field. This means a very long lengthscale in the field parallel direction, compared to the field perpendicular direction. Therefore, for these cases, the 2D case is not the dominant mode as there will always be a faster-growing 3D mode. Table 6.2 also shows how the instability prefers Boussinesq-like regimes (i.e. shallow temperature gradients and low values of θ).

For studying the Sun, these results demonstrate that provided you are in a regime where you anticipate a very shallow temperature gradient, the magneto-Boussinesq equations will produce a similar critical Rayleigh number as the fully compressible equations. As you increase θ, or in the context of the solar interior, as you study regimes with steeper temperature gradients, this correspondence breaks down as the instability becomes less easily induced. This is not surprising given the assumptions of the magneto-Boussinesq model. Furthermore, it is demonstrated that the preferred mode for this instability is undular, but with very small wavenumber in the direction of the field; i.e. where the magnetic field lines bend slightly with a long wavelength. In fact, as demonstrated by Table 6.2, the preferred mode has increased wavenumber in the field direction as you increase θ. That is to say that, a 2D analysis will more closely capture the dominant modes in regimes closer to that of the magneto-Boussinesq approximation (with small θ). It should however be noted that we have chosen our diffusivities of momentum and temperature such that they scale as $1/\rho$, rather than being uniform. This choice may have an impact on how the instability responds to changes in θ.

θ	$\tilde{k}_x$	$\tilde{k}_y$	ω	Ra_{crit}
0.02	0	2.22	0.0022	-3360.1
	0.01	2.33	0.0026	-3123.2
	0.02	2.44	0.0034	-2703.8
	0.03	2.55	0.0043	-2384.6
	0.04	2.66	0.0053	-2172.4
	0.05	2.78	0.0063	-2035.3
0.04	0	2.22	0.0043	-3705.3
	0.01	2.26	0.0045	-3610.6
	0.02	2.33	0.0051	-3380.2
	0.03	2.39	0.0059	-3118.8
	0.04	2.44	0.0067	-2883.7
	0.05	2.50	0.0076	-2688.7
0.06	0	2.22	0.0063	-4109.8
	0.01	2.24	0.0065	-4046.1
	0.02	2.28	0.0069	-3881.6
	0.03	2.32	0.0076	-3671.1
	0.04	2.37	0.0083	-3457.0
	0.05	2.41	0.0091	-3259.8
0.08	0	2.22	0.0083	-4588.5
	0.01	2.23	0.0084	-4535.4
	0.02	2.26	0.0088	-4394.7
	0.03	2.29	0.0093	-4205.4
	0.04	2.32	0.0099	-4001.8
	0.05	2.35	0.0107	-3804.3
0.10	0	2.23	0.0102	-5161.6
	0.01	2.23	0.0103	-5112.0
	0.02	2.24	0.0106	-4978.0
	0.03	2.26	0.0110	-4792.0
	0.04	2.29	0.0116	-4585.6
	0.05	2.31	0.0122	-4379.5

Table 6.1: Critical wavenumber, frequency, and Rayleigh number for varying values of θ and $\tilde{k}_x$. Here we used the following parameter values: $F = \zeta_0 = \sigma = 0.01$, $m = 1.51$, $\gamma = 5/3$.

θ	$\tilde{k}_x$	$\tilde{k}_y$	ω	Ra_{crit}
0.02	0.0825	3.2	0.0095	-1883.4
0.04	0.1515	3.2	0.0175	-2045.4
0.06	0.2040	3.1	0.0237	-2251.7
0.08	0.2385	3.0	0.0281	-2499.0
0.10	0.2715	3.0	0.0324	-2783.4

Table 6.2: The minimum values of $|Ra_{\text{crit}}|$ as a function of $\tilde{k}_x$. Critical wavenumbers, frequencies, and Rayleigh numbers for varying values of θ and $\tilde{k}_x$ are displayed. Note that here we have looped over $\tilde{k}_y$ in increments of 0.1, where previously the increment was 0.01. Here we used the following parameter values: $F = \zeta_0 = \sigma = 0.01$, $m = 1.51$, $\gamma = 5/3$.

Chapter 7

Discussion

7.1 Summary

Our work was primarily motivated by magnetic buoyancy in the solar interior, specifically the solar tachocline. In this region, there is strong toroidal magnetic field, which is transported to the solar surface where it appears to form sunspots and other surface phenomena. The transportation process in this description is not well understood, but it is believed that magnetic buoyancy will play a crucial role. When modelling the solar tachocline, the presence of sound waves make using the fully compressible equations too computationally expensive. However, properties of the tachocline mean that it falls outside the regime of validity for existing sound-proof models. Therefore, we have performed analysis to determine which, if any, sound-proof models produce "accurate" results for regimes applicable to magnetic buoyancy in the solar tachocline.

In Chapter 4, we introduced a general sound-proof model which can be used to assess any sound-proof model which fits into the form of the model. Specifically, we compared four existing models: magneto-Boussinesq, pseudo-incompressible and two formulations of the anelastic model which we refer to as GGG and LBR, (after Gough (1969); Gilman & Glatzmaier (1981) and Lantz (1992); Braginsky & Roberts (1995) respectively). By comparing the dispersion relations garnered from the linearised equations and the general model in a number of asymptotic regimes we were able to make conclusions about the accuracy of these existing models. We looked at regimes with and without rotation and thermal relaxation (a proxy for thermal diffusion), and found that the only models which reproduce the same dispersion relation as the compressible equations, in the linear regime, are the pseudo-incompressible model and GGG anelastic. Moreover, we showed that any model of the form of equations (4.85)-(4.89) would satisfy all the constraints of each of the regimes. This resulting set of equations contains one degree of freedom.

While it is certainly desirable that a sound-proof model reproduces the same dispersion

relation as the fully compressible equations, it is not the only thing to consider when selecting a sound-proof model. Other desirable properties are self-adjointness and energy conservation. A model that is self-adjoint will necessarily conserve *some* energy. When models do not have this conservation, they can produce some unphysical behaviour. In the absence of diffusion, we derive constraints on our general sound proof model if it is to be self-adjoint. We then go on to compare it to the compressible system to see under what conditions it will conserve the same energy as the compressible system. We found that both LBR anelastic and pseudo-incompressible models are self-adjoint — this is not surprising since they can both be derived from an action. Furthermore, only the pseudo-incompressible model conserves the same energy as the fully compressible system (for a general background). Therefore, as shown in Section 5.5, the pseudo-incompressible model will reproduce the same stability criteria. However, for a background state with nearly-uniform entropy gradient — i.e. in the regime of validity of the anelastic approximation — LBR anelastic also conserves the same energy as the fully compressible system.

The conclusions drawn in Chapters 4 and 5 recommend using the pseudo-incompressible model for magnetic buoyancy simulations in the Sun. However, there are other factors than just accuracy of a model that are worthy of consideration. Specifically, there are numerical complexities associated with implementing the pseudo-incompressible model that are not present in, for example, anelastic models. In the tachocline specifically, the motivation for this study, Chapter 4 demonstrates that despite the anelastic approximation requiring nearly uniform entropy, the GGG anelastic can reproduce the leading order results of the fully compressible equations for asymptotic regimes relevant to the tachocline; i.e. in regimes that violate the nearly uniform entropy assumption of the anelastic model. Chapter 5 however, shows that only the pseudo-incompressible model conserves the same energy as the fully compressible system when the background state has a significant entropy gradient; which we would expect in the tachocline. With these conclusions in mind, our work therefore recommends using pseudo-incompressible model for modelling the tachocline, or, if you are willing to forego energy conservation, the GGG anelastic model may be suitable.

In the majority of this thesis we do not account for magnetic diffusion or viscosity; we justify this by the fact that these are slow processes for parameters relevant to the solar interior. However, the inclusion of these terms allows for a new type of instability that does not appear in their absence. This instability is a double-diffusive instability. Double-diffusive instability relies on the diffusion of two variables that both affect density at different rates. In Chapter 6, following Acheson (1979), we derive an instability criterion for oscillatory double-diffusive instability in the magneto-Boussinesq regime. We note that, for parameters relevant to the solar tachocline; i.e. with $\eta + \nu - \kappa(\gamma - 1) < 0$, one could find a situation where both magnetic and temperature gradients are stabilising

but, in the presence of diffusion, allow for instability. Informed by the results obtained analytically in the magneto-Boussinesq regime, we then numerically solve the fully compressible equations to find the onset of instability for interchange modes for parameter regimes relevant to solar tachocline. Initially, we do this in the Boussinesq regime, but with the fully compressible equations, to enable comparison between our analytical and numerical work. We then extend our numerical work to non-Boussinesq regimes by considering steeper background temperature gradients. We find that as you move outside of the Boussinesq regime, the oscillatory doubly-diffusive instability is less easily induced. The assumption of 2D perturbations is then dropped as we consider undular modes, with long wavelengths in the direction of the background field. We find that the instability has a preferred wavelength that is small, but finite. That is, that 3D modes are more easily destabilised.

7.2 Future work

There is plenty of scope to extend the work of Chapter 6. In Chapter 6, we compare the linear fully compressible result to that of the magneto-Boussinesq equations. We then extend our analysis by considering non-Boussinesq regimes by increasing the stratification (i.e. the temperature gradient). Firstly, it would be interesting to see if a decrease in θ (the stratification — see Chapter 6) would produce even better agreement of the fully compressible result with the Boussinesq — Figure 6.2 suggests it may. Secondly, we have only considered a relatively narrow range of θ from 0.01 to 0.1. Further work could encompass a wider exploration for larger θ. For larger θ we would expect further departure from the Boussinesq solution, plotting the solutions could be instructive to see the (expected) departures from the symmetric solutions of the Boussinesq equations (which will be minimal for the cases considered here). Furthermore, a different way of violating the Boussinesq assumptions would be to consider larger values of F (which is proportional to v^2/c^2 — the ratio of Alfvén speed to sound speed).

In the spirit of Chapters 4 and 5, another avenue for potential future work would be to assess how well our general sound-proof model captures the double-diffusive instability of Chapter 6. This would involve repeating the numerical work in Chapter 6 but replacing the linear fully compressible equations with our linear sound-proof model and comparing the results. With this analysis, we could determine if there are any further constraints on our general sound proof model such that it still captures the leading order behaviour of the compressible equations.

All the results in this thesis have been derived from linear analysis. Clearly, a necessary condition for a model to correctly describe the full non-linear problem would be that it handles the linear problem accurately. With this in mind, we consider the work done here

to be the first step to the larger problem of finding a sound-proof model to describe the compressible system. Therefore, a potential avenue for future work would be to continue this work into the non-linear regime. This would need to be numerical work — very little progress can be made analytically in the non-linear regime.

Appendix A

Derivation of linear temperature and density equations

Here, we will briefly derive equations (2.28), (2.30), (2.31). These had been written in a slightly non-standard form in order to simplify the subsequent analysis. We consider density, ρ, as a function of pressure, p, and specific entropy, s, i.e. $\rho = \rho(s, p)$. We can then write

$$\begin{aligned} \mathrm{d}\rho &= \left(\frac{\partial \rho}{\partial s}\right)_p \mathrm{d}s + \left(\frac{\partial \rho}{\partial p}\right)_s \mathrm{d}p \\ &= \left(\frac{\partial \rho}{\partial s}\right)_p \mathrm{d}s + \frac{1}{c^2}\mathrm{d}p\,, \end{aligned} \tag{A.1}$$

where, as before, $c^2 = \left(\frac{\partial p}{\partial \rho}\right)_s$. Equation (A.1) justifies the form of equation (2.31).

Similarly, considering pressure as a function of density and temperature, T, i.e. $p = p(\rho, T)$, and temperature as a function of specific entropy and density, i.e. $T = T(s, \rho)$ we can write

$$\begin{aligned} \mathrm{d}p &= \left(\frac{\partial p}{\partial \rho}\right)_T \mathrm{d}\rho + \left(\frac{\partial p}{\partial T}\right)_\rho \mathrm{d}T\,, \\ \mathrm{d}T &= \left(\frac{\partial T}{\partial s}\right)_\rho \mathrm{d}s + \left(\frac{\partial T}{\partial \rho}\right)_s \mathrm{d}\rho\,. \end{aligned}$$

Combining these equations by eliminating $\mathrm{d}T$, we get

$$\mathrm{d}p = \left[\left(\frac{\partial p}{\partial \rho}\right)_T + \left(\frac{\partial p}{\partial T}\right)_\rho \left(\frac{\partial T}{\partial \rho}\right)_s\right] \mathrm{d}\rho + \left(\frac{\partial p}{\partial T}\right)_\rho \left(\frac{\partial T}{\partial s}\right)_\rho \mathrm{d}s\,.$$

Therefore,

$$\begin{aligned} c^2 = \left(\frac{\partial p}{\partial \rho}\right)_s &= \left(\frac{\partial p}{\partial \rho}\right)_T + \left(\frac{\partial p}{\partial T}\right)_\rho \left(\frac{\partial T}{\partial \rho}\right)_s , \\ \implies \frac{c^2}{\left(\frac{\partial p}{\partial \rho}\right)_T} &= 1 + \left(\frac{\partial \rho}{\partial p}\right)_T \left(\frac{\partial p}{\partial T}\right)_\rho \left(\frac{\partial T}{\partial \rho}\right)_s , \\ &= 1 - \left(\frac{\partial \rho}{\partial T}\right)_p \left(\frac{\partial T}{\partial \rho}\right)_s . \end{aligned} \tag{A.2}$$

We can do something similar to get an expression for $\left(\frac{\partial s}{\partial T}\right)_p / \left(\frac{\partial s}{\partial T}\right)_\rho$. Let $s = s(\rho, T)$ and $\rho = \rho(T, p)$, hence

$$\begin{aligned} \mathrm{d}s &= \left(\frac{\partial s}{\partial \rho}\right)_T \mathrm{d}\rho + \left(\frac{\partial s}{\partial T}\right)_\rho \mathrm{d}T , \\ \mathrm{d}\rho &= \left(\frac{\partial \rho}{\partial T}\right)_p \mathrm{d}T + \left(\frac{\partial \rho}{\partial p}\right)_T \mathrm{d}p . \end{aligned} \tag{A.3}$$

Combining these, we get

$$\mathrm{d}s = \left(\frac{\partial s}{\partial \rho}\right)_T \left(\frac{\partial \rho}{\partial p}\right)_T \mathrm{d}p + \left[\left(\frac{\partial s}{\partial \rho}\right)_T \left(\frac{\partial \rho}{\partial T}\right)_p + \left(\frac{\partial s}{\partial T}\right)_\rho\right] \mathrm{d}T .$$

Therefore, we can write

$$\begin{aligned} \left(\frac{\partial s}{\partial T}\right)_p &= \left(\frac{\partial s}{\partial \rho}\right)_T \left(\frac{\partial \rho}{\partial T}\right)_p + \left(\frac{\partial s}{\partial T}\right)_\rho , \\ \implies \frac{\left(\frac{\partial s}{\partial T}\right)_p}{\left(\frac{\partial s}{\partial T}\right)_\rho} &= \left(\frac{\partial T}{\partial s}\right)_\rho \left(\frac{\partial s}{\partial \rho}\right)_T \left(\frac{\partial \rho}{\partial T}\right)_p + 1 , \\ &= 1 - \left(\frac{\partial T}{\partial \rho}\right)_s \left(\frac{\partial \rho}{\partial T}\right)_p . \end{aligned} \tag{A.4}$$

Combining equations (A.2) and (A.4), we can determine

$$\frac{c^2}{\left(\frac{\partial p}{\partial \rho}\right)_T} = \frac{\left(\frac{\partial s}{\partial T}\right)_p}{\left(\frac{\partial s}{\partial T}\right)_\rho} = \frac{c_p}{c_v} = \gamma , \tag{A.5}$$

where we have introduced the specific heat capacity at constant volume and pressure (c_v and c_p respectively)

$$c_v = T_0 \left(\frac{\partial s}{\partial T}\right)_\rho , \qquad c_p = T_0 \left(\frac{\partial s}{\partial T}\right)_p . \tag{A.6}$$

Rearranging equation (A.5), we get

$$\left(\frac{\partial p}{\partial \rho}\right)_T = \frac{c^2}{\gamma} \qquad \Longrightarrow \qquad \left(\frac{\partial \rho}{\partial p}\right)_T = \frac{\gamma}{c^2}\,. \tag{A.7}$$

We can input result (A.7) into equation (A.3) to get

$$\mathrm{d}\rho = \left(\frac{\partial \rho}{\partial T}\right)_p \mathrm{d}T + \frac{\gamma}{c^2}\mathrm{d}p\,, \tag{A.8}$$

which, when we combine with equation (A.1), by eliminating $\mathrm{d}\rho$, gives

$$\left(\frac{\partial \rho}{\partial T}\right)_p \mathrm{d}T = \left(\frac{\partial \rho}{\partial s}\right)_p \mathrm{d}s + \frac{(1-\gamma)}{c^2}\mathrm{d}p\,. \tag{A.9}$$

This equation (A.9), justifies the form of equation (2.30).

Finally, we derive equation (2.28). Starting from equation (2.16), as we did in Chapter 2, we linearise about a static background (see Chapter 2 for more details and notation) to get

$$\begin{aligned} \rho_0 T_0 \left(\frac{\partial s_1}{\partial t} + \mathbf{u}\cdot\boldsymbol{\nabla} s_0\right) &= Q_1\,, \\ \Longrightarrow\ \frac{\partial s_1}{\partial t} + \mathbf{u}\cdot\boldsymbol{\nabla} s_0 &= \frac{Q_1}{\rho_0 T_0}\,. \end{aligned}$$

We can now multiply through by $\left(\frac{\partial \rho}{\partial s}\right)_p$, and also eliminate T_0 by our definition of c_p (A.6) to get

$$\left(\frac{\partial \rho}{\partial s}\right)_p \frac{\partial s_1}{\partial t} + \left(\frac{\partial \rho}{\partial s}\right)_p \mathbf{u}\cdot\boldsymbol{\nabla} s_0 = \left(\frac{\partial \rho}{\partial s}\right)_p \left(\frac{\partial s}{\partial T}\right)_p \frac{Q_1}{\rho_0 c_p}\,.$$

which, when we recall from Chapter 2 that s_0 depends only on z and

$$H_s^{-1} = -\left(\frac{\partial \ln \rho}{\partial s}\right)_p \frac{\mathrm{d}s_0}{\mathrm{d}z}\,,$$

becomes

$$\left(\frac{\partial \rho}{\partial s}\right)_p \frac{\partial s_1}{\partial t} - \rho_0 H_s^{-1} u_z = \left(\frac{\partial \rho}{\partial T}\right)_p \frac{Q_1}{\rho_0 c_p}\,, \tag{A.10}$$

which is precisely equation (2.16).

Bibliography

Acheson, D. J. 1979 Instability by magnetic buoyancy. *Solar Physics* **62** (1), 23–50.

Acheson, D. J. & Hide, R. 1973 Hydromagnetics of rotating fluids. *Reports on Progress in Physics* **36** (2), 159–221.

Arakawa, A. & Konor, C. S. 2009 Unification of the anelastic and quasi-hydrostatic systems of equations. *Monthly Weather Review* **137** (2), 710–726.

Babcock, H. D. 1959 The Sun's polar magnetic field. *The Astrophysical Journal* **130**, 364.

Babcock, H. W. 1961 The topology of the sun's magnetic field and the 22-year cycle. *The Astrophysical Journal* **133**, 572.

Bannon, P. R. 1995 Potential vorticity conservation, hydrostatic adjustment, and the anelastic approximation. *Journal of the atmospheric sciences* **52** (12), 2302–2312.

Bannon, P. R. 1996 On the anelastic approximation for a compressible atmosphere. *Journal of the Atmospheric Sciences* **53** (23), 3618–3628.

Bannon, P. R., Chagnon, J. M. & James, R. P. 2006 Mass conservation and the anelastic approximation. *Monthly weather review* **134** (10), 2989–3005.

Batchelor, G. K. 1954 The conditions for dynamical similarity of motions of a frictionless perfect-gas atmosphere. *Quarterly Journal of the Royal Meteorological Society* **80** (343), 106–107.

Berkoff, N. A., Kersale, E. & Tobias, S. M. 2010 Comparison of the anelastic approximation with fully compressible equations for linear magnetoconvection and magnetic buoyancy. *Geophysical and Astrophysical Fluid Dynamics* **104** (5), 545–563.

Bernardet, P. 1995 The pressure term in the anelastic model: A symmetric elliptic solver for an Arakawa C-grid in generalized coordinates. *Monthly weather review* **123** (8), 2474–2490.

Bernstein, I. B., Frieman, E. A., Kruskal, M. D. & Kulsrud, R. M. 1958 An energy principle for hydromagnetic stability problems. *Proceedings of the Royal Society of London Series A* **244**, 17–40.

Boussinesq, J. 1903 *Théorie analytique de la chaleur mise en harmonic avec la thermodynamique et avec la théorie mécanique de la lumière: Tome I-[II]...*, , vol. 2. Gauthier-Villars.

Braginsky, S. I. & Roberts, P. H. 1995 Equations governing convection in earth's core and the geodynamo. *Geophysical and Astrophysical Fluid Dynamics* **79** (1), 1–97.

Braginsky, S. I. & Roberts, P. H. 2007 *Anelastic and Boussinesq approximations: Encyclopedia of Geomagnetism and Paleomagnetism*. Heidelberg: Springer.

Brown, B. P., Vasil, G. M. & Zweibel, E. G. 2012 Energy conservation and gravity waves in sound-proof treatments of stellar interiors. Part I. Anelastic approximations. *The Astrophysical Journal* **756** (2), 109.

Charbonneau, P. 2010 Dynamo models of the solar cycle. *Living Reviews in Solar Physics* **7** (1), 1–91.

Choudhuri, A. R. 1998 *The physics of fluids and plasmas: an introduction for astrophysicists*. Cambridge University Press.

Corfield, C. N. 1984 The magneto-Boussinesq approximation by scale analysis. *Geophysical and Astrophysical Fluid Dynamics* **29** (1), 19–28.

Cowling, T. G. 1933 The magnetic field of sunspots. *Monthly Notices of the Royal Astronomical Society* **94**, 39–48.

Davidson, P. A. 2001 *An Introduction to Magnetohydrodynamics*. Cambridge University Press.

Davies, T., Staniforth, A., Wood, N. & Thuburn, J. 2003 Validity of anelastic and other equation sets as inferred from normal-mode analysis. *Quarterly Journal of the Royal Meteorological Society: A journal of the atmospheric sciences, applied meteorology and physical oceanography* **129** (593), 2761–2775.

Dubos, T. & Voitus, F. 2014 A semihydrostatic theory of gravity-dominated compressible flow. *Journal of the Atmospheric Sciences* **71** (12), 4621–4638.

Durran, D. R. 1989 Improving the anelastic approximation. *Journal of Atmospheric Sciences* **46** (11), 1453–1461.

Durran, D. R. 2008 A physically motivated approach for filtering acoustic waves from the equations governing compressible stratified flow. *Journal of Fluid Mechanics* **601**, 365–379.

Eckart, C. & Ferris, H. G. 1956 Equations of motion of the ocean and atmosphere. *Reviews of Modern Physics* **28** (1), 48.

Fan, Y. 2001 Nonlinear growth of the three-dimensional undular instability of a horizontal magnetic layer and the formation of arching flux tubes. *The Astrophysical Journal* **546** (1), 509–527.

Garaud, P. & Garaud, J.-D. 2008 Dynamics of the solar tachocline–II. The stratified case. *Monthly Notices of the Royal Astronomical Society* **391** (3), 1239–1258.

Gay-Balmaz, F. 2019 A variational derivation of the thermodynamics of a moist atmosphere with rain process and its pseudoincompressible approximation. *Geophysical & Astrophysical Fluid Dynamics* **113** (5-6), 428–465.

Gilman, P. A. 1970 Instability of magnetohydrostatic stellar interiors from magnetic buoyancy. I. *The Astrophysical Journal* **162**, 1019.

Gilman, P. A. & Glatzmaier, G. A. 1981 Compressible convection in a rotating spherical shell. I - Anelastic equations. II - A linear anelastic model. III - Analytic model for compressible vorticity waves. *Astrophysical Journal Supplement Series* **45**, 335–388.

Glatzmaier, G. A. 1984 Numerical simulations of stellar convective dynamos. I. The model and method. *Journal of Computational Physics* **55**, 461–484.

Goedbloed, H., Keppens, R. & Poedts, S. 2019 *Magnetohydrodynamics of Laboratory and Astrophysical Plasmas*. Cambridge University Press.

Goffrey, T., Pratt, J., Viallet, M., Baraffe, I., Popov, M. V., Walder, R., Folini, D., Geroux, C. & Constantino, T. 2017 Benchmarking the multidimensional stellar implicit code music. *Astronomy & Astrophysics* **600**, A7.

Gough, D. O. 1969 The anelastic approximation for thermal convection. *Journal of Atmospheric Sciences* **26** (3), 448–456.

Gough, D. O. 2007 An introduction to the solar tachocline. In Hughes *et al.* (2007), pp. 3–31.

Gough, D. O., Moore, D. R., Spiegel, E. A. & Weiss, N. O. 1976 Convective instability in a compressible atmosphere, II. *The Astrophysical Journal* **206**, 536–542.

Gray, D. D. & Giorgini, A. 1976 The validity of the Boussinesq approximation for liquids and gases. *International Journal of Heat and Mass Transfer* **19** (5), 545–551.

Hale, G. E. 1908 On the probable existence of a magnetic field in sun-spots. *The Astrophysical Journal* **28**, 315.

Hale, G. E., Ellerman, F., Nicholson, S. B. & Joy, A. H. 1919 The magnetic polarity of sun-spots. *The Astrophysical Journal* **49**, 153.

Hathaway, D. H. 2010 The solar cycle. *Living Reviews in Solar Physics* **7** (1), 1.

Hughes, D. W. 1985 Magnetic buoyancy instabilities for a static plane layer. *Geophysical and Astrophysical Fluid Dynamics* **32** (3), 273–316.

Hughes, D. W. 2007 Magnetic buoyancy instabilities in the tachocline. In Hughes *et al.* (2007), pp. 275–289.

Hughes, D. W. & Brummell, N. H. 2021 Double-diffusive magnetic layering. *The Astrophysical Journal* **922** (2), 195.

Hughes, D. W. & Cattaneo, F. 1987 A new look at the instability of a stratified horizontal magnetic field. *Geophysical & Astrophysical Fluid Dynamics* **39** (1-2), 65–81.

Hughes, D. W. & Proctor, M. R. E. 1988 Magnetic fields in the solar convection zone: magnetoconvection and magnetic buoyancy. *Annual review of fluid mechanics* **20** (1), 187–223.

Hughes, D. W., Rosner, R. & Weiss, N. O., ed. 2007 *The Solar Tachocline*. Cambridge University Press.

Hughes, D. W. & Weiss, N. O. 1995 Double-diffusive convection with two stabilizing gradients: strange consequences of magnetic buoyancy. *Journal of Fluid Mechanics* **301**, 383–406.

Iijima, H., Hotta, H. & Imada, S. 2019 Semiconservative reduced speed of sound technique for low Mach number flows with large density variations. *Astronomy & Astrophysics* **622**, A157.

Jeffreys, H. 1930 The instability of a compressible fluid heated below. *Proceedings of the Cambridge Philosophical Society* **26** (2), 170.

Jensen, E. 1955 On tubes of magnetic forces embedded in stellar material. *Annales d'Astrophysique, Vol. 18, p. 127* **18**, 127.

Jones, C. A., Boronski, P., Brun, A. S., Glatzmaier, G. A., Gastine, T., Miesch, M. S. & Wicht, J. 2011 Anelastic convection-driven dynamo benchmarks. *Icarus* **216** (1), 120–135.

Jones, C. A., Kuzanyan, K. M. & Mitchell, R. H. 2009 Linear theory of compressible convection in rapidly rotating spherical shells, using the anelastic approximation. *Journal of Fluid Mechanics* **634**, 291.

Klein, R., Achatz, U., Bresch, D., Knio, O. M. & Smolarkiewicz, P. K. 2010 Regime of validity of soundproof atmospheric flow models. *Journal of the Atmospheric Sciences* **67** (10), 3226–3237.

Klein, R. & Pauluis, O. 2012 Thermodynamic consistency of a pseudoincompressible approximation for general equations of state. *Journal of the atmospheric sciences* **69** (3), 961–968.

Lantz, S. R. 1992 Dynamical behavior of magnetic fields in a stratified, convecting fluid layer. PhD thesis, Cornell University.

Laval, G., Mercier, C. & Pellat, R. 1965 Necessity of the energy principles for magnetostatic stability. *Nuclear Fusion* **5** (2), 156.

Lehnert, B. 1954 Magnetohydrodynamic waves under the action of the Coriolis force. *The Astrophysical Journal* **119**, 647.

Leighton, R. B. 1964 Transport of magnetic fields on the sun. *Astrophysical Journal* **140**, 1547.

Leighton, R. B. 1969 A magneto-kinematic model of the solar cycle. *Astrophysical Journal* **156**, 1.

Lilly, D. K. 1996 A comparison of incompressible, anelastic and Boussinesq dynamics. *Atmospheric research* **40** (2-4), 143–151.

Lipps, F. B. & Hemler, R. S. 1982 A scale analysis of deep moist convection and some related numerical calculations. *Journal of Atmospheric Sciences* **39** (10), 2192–2210.

Lundgren, T. S. 1963 Hamilton's variational principle for a perfectly conducting plasma continuum. *The Physics of Fluids* **6** (7), 898–904.

Matthews, P. C., Proctor, M. R. E. & Weiss, N. O. 1995 Compressible magnetoconvection in three dimensions: planforms and nonlinear behaviour. *Journal of Fluid Mechanics* **305**, 281–305.

Mihaljan, J. M. 1962 A rigorous exposition of the Boussinesq approximations applicable to a thin layer of fluid. *The Astrophysical Journal* **136**, 1126.

Miller, M. J. & White, A. A. 1984 On the non-hydrostatic equations in pressure and sigma coordinates. *Quarterly Journal of the Royal Meteorological Society* **110** (464), 515–533.

Mizerski, K. A., Davies, C. R. & Hughes, D. W. 2013 Short-wavelength magnetic buoyancy instability. *The Astrophysical Journal Supplement Series* **205** (2), 16.

Moffatt, K. & Dormy, E. 2019 *Self-exciting fluid dynamos*. Cambridge University Press.

Morrison, P. J. 2005 Hamiltonian and action principle formulations of plasma physics. *Physics of plasmas* **12** (5), 058102.

Moss, J. B., Wood, T. S. & Bushby, P. J. 2022 Validity of sound-proof approximations for magnetic buoyancy. *Physical Review Fluids* **7** (10), 103701.

Moss, J. B., Wood, T. S. & Bushby, P. J. 2023 Self-adjointness of sound-proof models for magnetic buoyancy. *Geophysical and Astrophysical Fluid Dynamics* **117** (4), 263–277.

Newcomb, W. A. 1961 Convective instability induced by gravity in a plasma with a frozen-in magnetic field. *Physics of Fluids* **4**, 391–396.

Newcomb, W. A. 1962 Nuclear fusion: Supplement part 2. *Vienna: International Atomic Energy Agency* **451**.

Oberbeck, A. 1879 Ueber die Wärmeleitung der Flüssigkeiten bei Berücksichtigung der Strömungen infolge von Temperaturdifferenzen. *Annalen der Physik* **243** (6), 271–292.

Ogura, Y. & Phillips, N. A. 1962 Scale analysis of deep and shallow convection in the atmosphere. *Journal of Atmospheric Sciences* **19** (2), 173–179.

Parker, E. N. 1955*a* The formation of sunspots from the solar toroidal field. *The Astrophysical Journal* **121**, 491.

Parker, E. N. 1955*b* Hydromagnetic dynamo models. *Astrophysical Journal, vol. 122, p. 293* **122**, 293.

Parker, E. N. 1993 A solar dynamo surface wave at the interface between convection and nonuniform rotation. *The Astrophysical Journal* **408**, 707–719.

Pauluis, O. 2008 Thermodynamic consistency of the anelastic approximation for a moist atmosphere. *Journal of Atmospheric Sciences* **65** (8), 2719–2729.

Priest, E. R. 2014 *Magnetohydrodynamics of the Sun*. Cambridge University Press.

Priest, E. R. & Forbes, T. G. 2000 *Magnetic Reconnection: MHD Theory and Applications*. Cambridge University Press.

Rehm, R. G. & Baum, H. R. 1978 The equations of motion for thermally driven, buoyant flows. *Journal of Research of the National Bureau of Standards* **83** (297-308), 2.

Rockafellar, R. T. 1970 *Convex Analysis*. Princeton University Press.

Salmon, R. 1983 Practical use of Hamilton's principle. *Journal of Fluid Mechanics* **132**, 431–444.

Salmon, R. 1988 Hamiltonian fluid mechanics. *Annual review of fluid mechanics* **20** (1), 225–256.

Schou, J., Antia, H. M., Basu, S., Bogart, R. S., Bush, R. I., Chitre, S. M., Christensen-Dalsgaard, J., Di Mauro, M. P., Dziembowski, W. A., Eff-Darwich, A. *et al.* 1998 Helioseismic studies of differential rotation in the solar envelope by the solar oscillations investigation using the Michelson Doppler Imager. *The Astrophysical Journal* **505** (1), 390.

Schubert, G. 1968 The stability of toroidal magnetic fields in stellar interiors. *The Astrophysical Journal* **151**, 1099.

Schwabe, H. 1843 Sonnen-Beobachtungen im Jahre 1843 [Observation of the sun in the year 1843]. *Astronomische Nachrichten [Astronomical News]* **21**, 233–236.

Snodin, A. P. & Wood, T. S. 2022 A hybrid pseudo-incompressible–hydrostatic model. *Journal of Fluid Mechanics* **936**.

Spiegel, E. A. & Veronis, G. 1960 On the Boussinesq approximation for a compressible fluid. *The Astrophysical Journal* **131**, 442.

Spiegel, E. A. & Weiss, N. O. 1982 Magnetic buoyancy and the Boussinesq approximation. *Geophysical and Astrophysical Fluid Dynamics* **22** (3), 219–234.

Spiegel, E. A. & Zahn, J. P. 1992 The solar tachocline. *Astronomy and Astrophysics* **265**, 106–114.

Steenbeck, M. & Krause, F. 1969 Zur dynamotheorie stellarer und planetarer magnetfelder I. berechnung sonnenähnlicher wechselfeldgeneratoren. *Astronomische Nachrichten* **291** (2), 49–84.

Steenbeck, M., Krause, F. & Rädler, K.-H. 1966 A calculation of the mean electromutive force in an electrically conducting fluid in turbulent motion, under the influence of Coriolis forces. *Zeitschrift für Naturforschung A* **21** (4), 369–376.

Taub, A. H. 1969 Stability of general relativistic gaseous masses and variational principles. *Communications in Mathematical Physics* **15** (3), 235–254.

Tayler, R. J. 1973 The adiabatic stability of stars containing magnetic fields — I: Toroidal fields. *Monthly Notices of the Royal Astronomical Society* **161** (4), 365–380.

Thomas, J. H. & Nye, A. H. 1975 Convective instability in the presence of a nonuniform horizontal magnetic field. *Physics of Fluids* **18**, 490.

Thomas, J. H., Weiss, N. O., Tobias, S. M. & Brummell, N. H. 2002 Downward pumping of magnetic flux as the cause of filamentary structures in sunspot penumbrae. *Nature* **420** (6914), 390–393.

Tobias, S. M. 1996 Diffusivity quenching as a mechanism for Parker's surface dynamo. *The Astrophysical Journal* **467**, 870.

Tobias, S. M., Brummell, N. H., Clune, T. L. & Toomre, J. 2001 Transport and storage of magnetic field by overshooting turbulent compressible convection. *The Astrophysical Journal* **549** (2), 1183.

Vasil, G. M., Lecoanet, D., Brown, B. P., Wood, T. S. & Zweibel, E. G. 2013 Energy conservation and gravity waves in sound-proof treatments of stellar interiors. II. Lagrangian constrained analysis. *The Astrophysical Journal* **773** (2), 169.

Weiss, N. O. & Proctor, M. R. E. 2014 *Magnetoconvection*. Cambridge University Press.

Wilczyński, F., Hughes, D. W. & Kersalé, E. 2022 Magnetic buoyancy instability and the anelastic approximation: regime of validity and relationship with compressible and Boussinesq descriptions. *Journal of Fluid Mechanics* **942**.

Wood, T. S. & Bushby, P. J. 2016 Oscillatory convection and limitations of the Boussinesq approximation. *Journal of Fluid Mechanics* **803**, 502–515.

Zweibel, E. G. & Kulsrud, R. M. 1975 The stabilizing effects of cloud reacceleration; microturbulence, and rotation on Parker's instability. *The Astrophysical Journal* **201**, 63–73.